

Single- and Multiphoton Ionization Processes in Molecules

by

Richard Leslie Dubs

**In Partial Fulfillment of the Requirements
for the Degree of
Doctor of Philosophy**

California Institute of Technology

Pasadena, California

1988

(Submitted May 19, 1988)

Acknowledgements

Many years ago, someone told me that choosing a research advisor would be the most important decision of my career. I didn't take the advice lightly, and I've come to realize over the past five years that I made a wonderful choice. Professor B. Vincent McKoy is a master at what he does - he is both a consummate scientist and a great politician. An important part of my education here at Caltech has been just sitting back and watching him at work. I hope some of his wisdom has rubbed off on me. At the same time, I sincerely appreciate his genuine regard for my interests and well-being. I am especially grateful to him for giving me the freedom in my research endeavors to march to the beat of that different drummer. It has been an honor to work under his guidance.

Truly the most important decision of my life was to marry my best friend. Lois has put up with more than should be expected from anyone these last five years. She held many conversations with me while my head was in outer space, and I am grateful to her for always being there when I returned to earth and for helping me keep my research in a proper perspective. Her love and support were my main staple during these graduate years; the success of my research here would not have happened without her, nor been worth it, could I not have shared it with her.

As always, I am grateful to my parents Carol and Joe for bestowing upon me a good heart and providing me with such an enriched and carefree life.

Of all the people in the McKoy group with whom I've enjoyed working, I would especially like to thank Drs. Sham Dixit and Diane Lynch for holding my hand the first few years here. I miss working with both of them. In addition, I am very grateful to the National Science Foundation for supporting me those first years.

Finally I would like to thank Dr. Michael G. White who believed in our work and continues to put CDAD on the map with his efforts.

Abstract

This dissertation is theoretical in nature and can be separated into two main areas: 1) single- and multiphoton ionization studies of a novel photoelectron effect, and 2) single-photon ionization studies of simple clusters as models for adsorbate photoemission. The first area centers on the phenomenon of circular dichroism in photoelectron angular distributions (CDAD). CDAD is shown to exist from oriented linear molecules, adsorbed atoms, and aligned atoms and molecules in the gas phase. The calculations presented here are the first to demonstrate the experimental feasibility of CDAD studies. CDAD is shown to be a measurable effect which exists because the photoelectron collection direction can break the symmetry of these otherwise highly symmetric systems. As a direct result of the work presented here, CDAD has now been observed experimentally. Coupled with resonantly enhanced multiphoton ionization (REMPI), CDAD is shown to be a powerful probe of unknown alignment in gas phase atomic and molecular samples. The second area of research focuses on the simple oriented molecules NiCO and NiN₂ as models for the corresponding adsorbate systems. These simple models provide insight into features observed in the experimental angle-resolved photoemission spectra.

Table of Contents

Acknowledgments	ii
Abstract	iv
Introduction	1
Chapter 1: Circular Dichroism in Photoelectron Angular Distributions from Oriented Linear Molecules	9
Chapter 2: Circular Dichroism in Photoelectron Angular Distributions from Adsorbed Atoms	13
Chapter 3: Circular Dichroism in Photoelectron Angular Distributions as a Probe of Atomic and Molecular Alignment	17
Chapter 4: Extraction of Alignment Parameters from Circular Dichroic Photoelectron Angular Distribution (CDAD) Measurements	26
Chapter 5: Circular Dichroism in Photoelectron Angular Distributions from Two-Color (1+1) REMPI of NO	30

Chapter 6:	(1+1) CDAD: A New Technique for Studying Photo-fragment Alignment	38
Chapter 7:	Atomic and Molecular Alignment from Photoelectron Angular Distributions in (n+1) Resonantly Enhanced Multiphoton Ionization	41
Chapter 8:	Studies of Angle-Resolved Photoelectron Spectra from Oriented NiCO: A Model for Adsorbed CO	49
Chapter 9:	Studies of NiN ₂ as a Model for Photoemission from N ₂ Adsorbed on Nickel	58

Introduction

Atomic and molecular physics has been revitalized in the last decade with recent developments in both synchrotron radiation sources and lasers. Synchrotron sources provide intense, polarized light over a continuously tunable spectral range, from the ultraviolet to the x-ray. Fixed wavelength, gas discharge lamps are no longer limitations for photoelectron spectroscopists.¹ Lasers, with their high intensity and extremely small bandwidth, enable scientists to study spectra at a resolution never realized only a decade ago. The high intensities attainable from laser sources have made possible a detailed investigation of a variety of nonlinear phenomena.² These developments have enabled scientists to explore atoms and molecules at a very detailed level, and to rekindle the idea that much about these systems remains to be understood. One of the most important techniques underlying the recent developments in this field has been resonantly enhanced multiphoton ionization (REMPI). This technique is a highly selective probe of excited states of atoms and molecules, with a resolution not achievable in single-photon ionization studies of ground states.³

This dissertation is a study of atomic and molecular photoionization processes. The work presented here is theoretical in nature and can be separated into two main areas 1) single- and multiphoton ionization studies of a novel photoelectron effect, and 2) single-photon ionization studies of simple clusters as models for adsorbate photoemission.

The first area of research centers on the phenomenon of circular dichroism in photoelectron angular distributions (CDAD). CDAD is defined as the difference between two angular distributions, one obtained with left circularly-polarized light and one obtained with right polarized light. CDAD is shown to exist from a variety of systems, from oriented linear molecules and adsorbed atoms, to aligned atoms and molecules in the gas phase. While in photoabsorption circular dichroism is normally associated with chiral molecules, CDAD can exist from the previously mentioned systems because the photoelectron collection direction can be used to break the symmetry of the system. (See Figure 1 of chapter seven and the accompanying discussion.)

In chapter one, CDAD from oriented linear molecules is considered. CDAD in this case is shown to be a large effect of the same order of magnitude as the left or right photoelectron spectrum. It should be emphasized that this result could not have been predicted without a detailed calculation, as CDAD is shown to arise solely from a delicate interference effect. Therefore, although the existence of CDAD for this particular case was first predicted independently by Cherepkov,⁴ he was not able to predict the magnitude of the effect nor stimulate experimental interest in this phenomenon. The work presented in chapter one thus strongly emphasizes the importance of theoretical methods which provide accurate differential photoionization cross sections such as those developed by McKoy and coworkers.⁵

In chapter two, the ideas of chapter one are extended to adsorbed

atoms. CDAD in this case is a direct consequence of the atom-surface interaction. When an atom adsorbs to a surface, its p orbitals are no longer necessarily degenerate.⁶ For example, when an atom adsorbs at a fourfold site, the energy of the p_z orbital (perpendicular to the surface) will be, in general, different from that of the p_x , p_y pair. These orbitals can be resolved spectroscopically.⁷ The p_z orbital can then be considered an experimentally-accessible atomic orbital of fixed spatial orientation. In chapter two, a calculation of CDAD from an oriented oxygen p orbital is presented. Once again CDAD is shown to be a large effect. In the same spirit, CDAD from dangling surface bonds should be observable.

In chapter three a completely new idea is proposed. It is the seed for the most important contributions of this dissertation. Clearly if linear molecules are randomly oriented in the gas phase, CDAD must vanish for symmetry reasons. However, if the molecules are not randomly oriented, but rather found in certain orientations preferentially to others, CDAD should be expected to exist, though the effect would not be as large as for a molecule fixed in space. In chapter three this idea is explored and the magnitude of the CDAD effect is predicted. This work stimulated the very first experimental observation of CDAD in 1986 (Figure 1).⁸ The experimental results were found to be in excellent agreement with the theoretical predictions. The question which remains, namely, "Is CDAD useful for anything?" forms the basis for the work presented in chapters four through seven.

Traditionally, the spatial distribution or "alignment" of molecules in the gas phase is described by alignment parameters, A_0 ,

A_2 , A_4 , etc.⁹ These alignment parameters are conventionally determined by fluorescence or laser-induced fluorescence techniques.⁹ On the other hand, angle-resolved photoionization techniques are not commonly used to probe state alignment. The bound-free nature of the ionization step, coupled with the anisotropy associated with photon absorption, causes the alignment information to be intimately entangled with the photoionization dynamics. Even angle-integrated cross sections suffer from this problem.¹⁰ Nevertheless, in chapter four it is shown theoretically that alignment information presents itself in a very straightforward way in CDAD spectra. Experimental verification of this fact is presented in chapter five. (Examine the relationship between Figures 3 and 5 of that chapter, for example). In these experiments, one photon absorption was used to prepare NO molecules with a known alignment.

Gas phase atomic and molecular alignment occurs in a variety of important physical situations such as photoabsorption,¹¹ photodissociation,¹² particle excitation,¹³ surface scattering¹⁴ or desorption,¹⁵ interaction with external fields,¹⁶ etc. A complete determination of alignment effects on chemical reactions is essential to our understanding of elementary processes. Therefore, to be of practical use, CDAD must offer the ability to determine quantitatively the unknown alignment of a sample. Simple recipes for this determination are presented in chapters six and seven. Because it is not always possible to photoionize a molecule with one photon (and for other reasons which are made apparent in the chapters), these CDAD techniques are based on $(n+1)$ multiphoton schemes. Chapter seven

includes many of the details of CDAD theory in addition to a physically-motivated discussion of the basis for CDAD. In addition, that chapter includes the introduction of a new multiphoton technique called PINDAD which uses linearly-polarized light, rather than circularly-polarized light, to obtain alignment information from photoelectron angular distributions. To serve as the first example of the use of these techniques for the determination of unknown molecular alignment, studies of NO photofragmented from methylnitrite (CH_3ONO) at 226nm are near completion.¹⁷

The second part of this dissertation (chapters eight and nine) addresses the question, "How well do simple cluster models such as oriented NiCO or NiN_2 simulate adsorbate molecules with respect to photoemission?" Calculations with these simple cluster models suggest that for adsorbate orbitals pointing toward the surface, backscattering of ejected photoelectrons off the surface cannot be ignored. The NiN_2 results are particularly interesting. For gas phase N_2 , total cross section measurements as a function of energy lack a feature in the spectrum¹⁸ which is present in the isoelectronic CO spectrum¹⁹ because N_2 is homonuclear. However, this feature appears in the adsorbate (N_2 on Ni) spectrum.²⁰ Our calculations support the proposition that the feature could be a result of symmetry breaking by the Ni-N interaction.²⁰

References

- ¹ D. A. Shirley, J. Stöhr, P. S. Wehner, R. S. Williams and G. Apai, *Phys. Scrip.* **16**, 398 (1977).
- ² W. Demtröder, *Laser Spectroscopy*, 2nd ed. (Springer-Verlag, Heidelberg, 1982).
- ³ K. Kimura, *Adv. Chem. Phys.* **60**, 161 (1985).
- ⁴ N. A. Cherepkov, *Chem. Phys. Lett.* **87**, 344 (1982).
- ⁵ R. R. Lucchese, K. Takatsuka and V. McKoy, *Phys. Rep.* **131**, 147 (1986).
- ⁶ P. V. S. Rao and J. T. Waber, *Surf. Sci.* **28**, 299 (1971); T. B. Grimley, *Disc. Faraday Soc.* **58**, 7 (1974); J. F. Herbst, *Phys. Rev.* **B15**, 3720 (1976).
- ⁷ K. Jacobi, M. Scheffler, K. Kambe and F. Forstmann, *Solid State Comm.* **22**, 17 (1977).
- ⁸ J. R. Appling, M. G. White, T. M. Orlando and S. L. Anderson, *J. Chem. Phys.* **85**, 6803 (1986).
- ⁹ C. H. Greene and R. N. Zare, *Ann. Rev. Phys. Chem.* **33**, 119 (1982); *J. Chem. Phys.* **78**, 6741 (1983); A. C. Kummel, G. O. Sitz and R. N. Zare, *J. Chem. Phys.* **85**, 6874 (1986).
- ¹⁰ See D. C. Jacobs and R. N. Zare, *J. Chem. Phys.* **85**, 5457 (1986) and D. C. Jacobs, R. N. Madix and R. N. Zare, *J. Chem. Phys.* **85**, 5469 (1986) for a method to extract alignment information from angle-integrated cross sections.
- ¹¹ R. E. Drullinger and R. N. Zare, *J. Chem. Phys.* **51**, 5532 (1969); R. N. Zare, *Ber. Bunsenges. Phys. Chem.* **86**, 422 (1982); W. J. Kessler and E. D. Poliakov, *J. Chem. Phys.* **84**, 3647 (1986).
- ¹² M. T. Macpherson, J. P. Simons and R. N. Zare, *Mol. Phys.* **38**, 2049 (1979); G. W. Loge and J. R. Wiesenfeld, *J. Chem. Phys.* **75**, 2795 (1981); R. Vasudev, R. N. Zare and R. N. Dixon, *J. Chem. Phys.* **80**, 4863 (1984); G. E. Hall, N. Sivakumar and P. L. Houston, *J. Chem. Phys.* **84**, 2120 (1986); M. Dubs, U. Bruhlmann and J. R. Huber, *J. Chem. Phys.* **84**, 3106 (1986); F. Lahmani, C. Lardeux and D. Solgadi, *Chem. Phys. Lett.* **129**, 24 (1986); U. Bruhlmann, M. Dubs and J. R. Huber, *J. Chem. Phys.* **86**, 1249 (1987); M. R. S. McCoustra, J. A. Dyet and J. Pfab, *Chem. Phys. Lett.* **136**, 231 (1987); J. A. Guest and F. Webster, *J. Chem. Phys.* **86**, 5479 (1987); M. A. O'Halloran, H. Joswig and R. N. Zare, *J. Chem. Phys.* **87**, 303 (1987).

- ¹³ R. Bersohn and S. H. Lin, *Adv. Chem. Phys.* **16**, 67 (1969).
- ¹⁴ a) M. C. Lin and G. Ertl, *Ann. Rev. Phys. Chem.* **37**, 587 (1986) and references therein. b) T. R. Proctor, D. J. Kouri and R. B. Gerber, *J. Chem. Phys.* **80**, 3845 (1984); J. G. Lauderdale, J. F. McNutt and C. W. McCurdy, *Chem. Phys. Lett.* **107**, 43 (1984); R. J. Wolf, D. C. Collins, Jr. and H. R. Mayne, *Chem. Phys. Lett.* **119**, 533 (1985); C.-Y. Kuan, H. R. Mayne and R. J. Wolf, *Chem. Phys. Lett.* **133**, 415 (1987); G. O. Sitz, A. C. Kummel and R. N. Zare, *J. Vac. Sci. Technol.* **A5**, 513 (1987); G. C. Corey and M. H. Alexander, *J. Chem. Phys.* **87**, 4937 (1987); A. C. Luntz, A. W. Kleyn and D. J. Auerbach, *Phys. Rev.* **B25**, 4273 (1982); A. W. Kleyn, A. C. Luntz and D. J. Auerbach, *Surf. Sci.* **117**, 33 (1982); G. O. Sitz, A. C. Kummel and R. N. Zare, *J. Chem. Phys.* **87**, 3247 (1987).
- ¹⁵ D. C. Jacobs, K. W. Kolasinski, R. J. Madix and R. N. Zare, *J. Chem. Phys.* **87**, 5038 (1987).
- ¹⁶ J. Reuss, *Adv. Chem. Phys.* **30**, 389 (1975); P. R. Brooks, *Science* **193**, 11 (1976); D. H. Parker, K. K. Chakrovorty and R. B. Bernstein, *Chem. Phys. Lett.* **86**, 113 (1982) and references therein.
- ¹⁷ J. Winniczek, R. L. Dubs, J. R. Appling, V. McKoy, and M. G. White, in preparation.
- ¹⁸ R. R. Lucchese, G. Raseev and V. McKoy, *Phys. Rev.* **A25**, 2572 (1982).
- ¹⁹ M. E. Smith, D. L. Lynch and V. McKoy, *J. Chem. Phys.* **85**, 6455 (1986); D. L. Lynch, unpublished work.
- ²⁰ K. Horn, J. DiNardo, W. Eberhardt, H.-J. Freund and E. W. Plummer, *Surf. Sci.* **118**, 465 (1982).

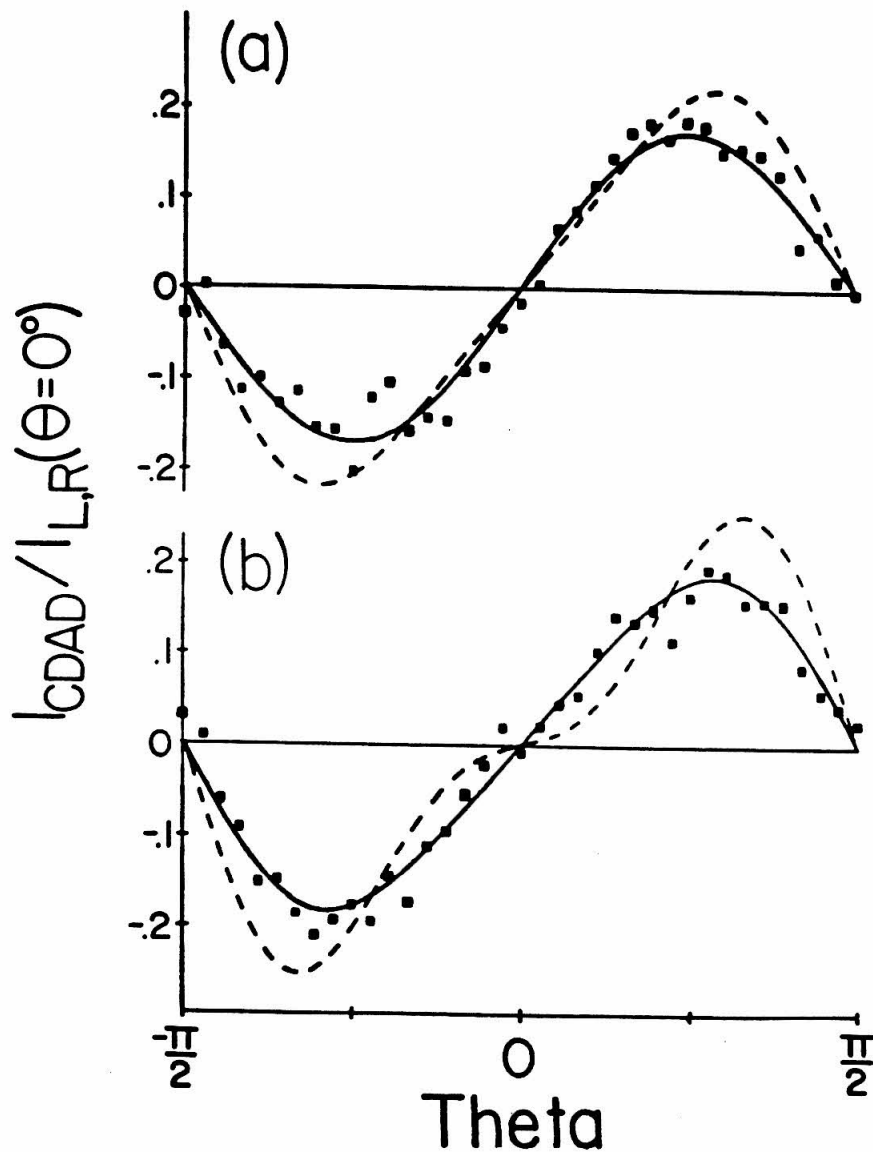


Figure 1. First experimentally observed CDAD spectra (Reference 6). Alignment created by two photon excitation to the $A^2\Sigma$ state of NO: (a) $R_{2,1} + S_{1,1}(1/2)$ rotational branch and (b) $S_{2,1}(1/2)$ rotational branch. (\blacksquare \blacksquare \blacksquare) experimental data; (—) best fit to data; (---) theoretical prediction. See Reference 6 for details.

**Chapter 1: Circular Dichroism in Photoelectron Angular
Distributions from Oriented Linear Molecules**

[The text of this chapter appeared in: R. L. Dubs, S. N. Dixit and V. McKoy, Phys. Rev. Lett. **54**, 1249 (1985).]

Circular Dichroism in Photoelectron Angular Distributions from Oriented Linear Molecules

Richard L. Dubs, S. N. Dixit, and V. McKoy

Arthur Amos Noyes Laboratory of Chemical Physics, California Institute of Technology,
Pasadena, California 91125

(Received 25 January 1985)

We show that circular dichroism exists in the photoelectron angular distributions from oriented linear molecules in the electric dipole approximation. Contributions to the dichroism arise solely from interferences between degenerate photoelectron continua with m values differing by ± 1 . We identify specific photon-propagation, electron-detection configurations where circular dichroism will be observable. Finally, we illustrate the magnitude of this effect through *ab initio* calculations for photoionization out of the 4σ orbital of an oriented CO molecule.

PACS numbers: 33.60.Cv, 33.55.Ad, 33.80.Eh

Circular dichroism (CD) is a phenomenon in which the responses of a system to left and right circularly polarized light are different. Traditionally, CD has been observed in solutions of chiral molecules through the rotation of the plane of polarization of linearly polarized light (optical rotary dispersion), or through the conversion of linearly polarized light to elliptically polarized light.¹ Several recent theoretical analyses²⁻⁷ have predicted CD in photoelectron angular distributions (CDAD). These studies either assumed a chiral molecule, included spin-orbit interaction, or went beyond the electric dipole approximation. In this Letter we demonstrate CDAD from *oriented linear molecules within the electric dipole approximation*. This CDAD appears in the absence of any spin-orbit interaction. We show that only interference terms between degenerate photoelectron continua with the m values differing by ± 1 contribute to CDAD. This feature gives better resolved information than is available from linear-polarization studies and hence can be a useful tool in the study of oriented molecules. We also identify the photon-propagation and electron-detection geometrics in which CDAD can be observed. Finally, we illustrate the magnitude of this effect by calculating the CDAD in the photoionization of the 4σ orbital of CO oriented normal to a surface. In a recent paper focusing on CD from chiral molecules, Cherepkov⁷ alluded to the existence of CDAD in linear molecules. In our paper, we carry out the analysis in greater detail stressing the importance of this phenomenon.

The doubly differential photoionization cross section, in the molecular frame, is defined as⁸

$$\partial^2\sigma/\partial\Omega_{\hat{k}}\partial\Omega_{\hat{e}} = (4\pi^2E/c)|I_{\mathbf{k},\hat{e}}|^2, \quad (1)$$

where E denotes the photon energy and $I_{\mathbf{k},\hat{e}}$ the bound-continuum matrix element⁸

$$I_{\mathbf{k},\hat{e}} = k^{1/2}\langle\psi_f|\mathbf{r}\cdot\hat{\epsilon}|\psi_i\rangle. \quad (2)$$

For convenience, we discuss the one-electron case and consider ionization out of an initial orbital ψ_i into a continuum orbital $\psi_f(\hat{\mathbf{k}})$. In this equation, \mathbf{k} is the photoelectron momentum and $\hat{\epsilon}$ is the unit polarization vector of the photon. The unit vector \hat{n} corresponds to the direction of polarization for linearly polarized light and to the direction of propagation for circularly polarized light. Assuming a partial-wave expansion for $\psi_f(\hat{\mathbf{k}})$, we can write $I_{\mathbf{k},\hat{e}}$ as

$$I_{\mathbf{k},\hat{e}} = I_{\mathbf{k},\hat{e}}^{\mu_0} = \sum_{lm\mu} I_{lm\mu} Y_{lm}^*(\Omega_{\hat{k}}) D_{\mu,\mu_0}^l(\Omega_{\hat{e}}), \quad (3)$$

where the polarization index μ_0 is zero for linearly polarized light and ± 1 for circularly polarized light. The rotation matrices $D_{mm'}^l$ are defined in the convention of Rose.⁹ The dynamical coefficients $I_{lm\mu}$ are defined as

$$I_{lm\mu} = k^{1/2}\langle\psi_i|r_{\mu}|\psi_f\rangle_{lm} \quad (4a)$$

with

$$r_{\mu} = \begin{cases} \mp(x \pm iy)/2^{1/2} & \text{for } \mu = \pm 1, \\ z & \text{for } \mu = 0. \end{cases} \quad (4b)$$

In principle, the summation over l in Eq. (3) extends to infinity. However, in practice, this summation can be cut off at some $l = l_{\max}$ as very high partial waves contribute insignificantly to $I_{\mathbf{k},\hat{e}}^{\mu_0}$.

The CDAD signal is defined as the difference in the differential cross sections of Eq. (1) for left and right circularly polarized light. This quantity is proportional to the difference

$$|I_{\mathbf{k},\hat{e}}^L|^2 - |I_{\mathbf{k},\hat{e}}^R|^2 = |I_{\mathbf{k},\hat{e}}^{+1}|^2 - |I_{\mathbf{k},\hat{e}}^{-1}|^2. \quad (5)$$

Upon squaring of Eq. (3) and combining of spherical harmonics and rotation matrices, this difference can be

written as

$$|I_{\mathbf{k}, \hat{\mathbf{a}}}|_{\hat{L}-R}^2 = \frac{1}{\sqrt{3}} \langle 11, -11 | 10 \rangle \sum_{L=0}^{2l_{\max}} \sum_{M=-L}^L (2L+1)^{-1/2} \\ \times \sum_{\substack{l m \mu \\ l' m' \mu'}} (-1)^{m+\mu} [(2l+1)(2l'+1)]^{1/2} [I_{lm\mu} I_{l'm'\mu'}^* - I_{l, -m, -\mu} I_{l', -m', -\mu'}] \\ \times \langle l'00 | L0 \rangle \langle l', -mm' | LM \rangle \langle 11, -\mu\mu' | 1, -M \rangle Y_{LM}(\theta_k, \phi_k) Y_{1, -M}(\theta_p, \phi_p). \quad (6)$$

In the above equation, $M = m' - m = \mu - \mu'$ and, (θ_k, ϕ_k) and (θ_p, ϕ_p) denote respectively the spherical polar angles in the molecular frame for the electron and photon propagation directions. The molecular frame is defined with the z axis coinciding with the internuclear axis. Note that when we combine the rotation matrices $D_{\mu\mu_0}^1 D_{\mu\mu_0}^{1*}$ into $D_{\mu\mu_0}^2$, only $L' = 1$ terms survive in Eq. (6) because of the symmetry of the Clebsch-Gordan coefficients.

For linear molecules, $I_{lm\mu} = I_{l, -m, -\mu}$ and hence the $M = 0$ term vanishes in Eq. (6) and the $M = \pm 1$ and -1 terms become equal. $|I_{\mathbf{k}, \hat{\mathbf{a}}}|_{\hat{L}-R}^2$ then simplifies to

$$|I_{\mathbf{k}, \hat{\mathbf{a}}}|_{\hat{L}-R}^2 = \frac{4}{\sqrt{3}} \langle 11, -11 | 10 \rangle \sum_{L=0}^{2l_{\max}} (2L+1)^{-1/2} \sum_{\substack{l m \mu \\ l' m' \mu'}} (-1)^{m+\mu} [(2l+1)(2l'+1)]^{1/2} \langle l'00 | L0 \rangle \\ \times \langle l', -mm' | L, -1 \rangle \langle 11, -\mu\mu' | 11 \rangle \text{Im}[I_{lm\mu} I_{l'm'\mu'}^*] \text{Im}[Y_{L, -1}(\theta_k, \phi_k) Y_{11}(\theta_p, \phi_p)]. \quad (7)$$

This equation, combined with Eqs. (1) and (5), describes the CDAD from oriented linear molecules.

Several general features of CDAD follow from Eq. (7). These include the following:

(i) CDAD is due only to interference terms between degenerate photoelectron continua differing by ± 1 in their m values ($m' - m = \pm 1$). For example, in photoionization from a σ orbital, CDAD will be due solely to the interference between the $k\sigma$ and $k\pi$ continua. This follows from the Clebsch-Gordan coefficient $\langle l', -mm' | L, -1 \rangle$ and the interchangeability of m and m' .

(ii) CDAD vanishes if $\hat{\mathbf{k}}, \hat{\mathbf{n}}$ and the molecular axis are coplanar. This result arises because $\text{Im}[Y_{L, -1}(\theta_k, \phi_k) Y_{11}(\theta_p, \phi_p)]$ is proportional to $\sin(\phi_p - \phi_k)$ and, if $\phi_p - \phi_k = n\pi$ ($n = 0, \pm 1$), $\sin(\phi_p - \phi_k) = 0$. A physical interpretation of this second feature, the main criterion for observing CD, can be seen as follows. Let \hat{R} and \hat{L} denote respectively the interaction operator $\mathbf{r} \cdot \boldsymbol{\epsilon}$ for right and left circularly polarized light propagating in a given direction. These operators are related to each other by a reflection in a plane containing the propagation direction. If \hat{P} denotes this reflection operator, we have

$$\hat{R} = \hat{P}\hat{L}\hat{P}^{-1} = \hat{P}\hat{L}\hat{P}. \quad (8)$$

Then

$$|I_{\mathbf{k}, \hat{\mathbf{a}}}|_{\hat{L}}^2 = k |\langle \psi_i | \hat{L} | \psi_{f_{\mathbf{k}}}^{(-)} \rangle|^2 \quad (9a)$$

while

$$|I_{\mathbf{k}, \hat{\mathbf{a}}}|_{\hat{R}}^2 = k |\langle \psi_i | \hat{R} | \psi_{f_{\mathbf{k}}}^{(-)} \rangle|^2 \\ = k |\langle \psi_i | \hat{P}\hat{L}\hat{P} | \psi_{f_{\mathbf{k}}}^{(-)} \rangle|^2. \quad (9b)$$

Since the reflection plane can always be chosen to contain the molecular axis, $|\psi_i\rangle$ will always have definite parity with respect to \hat{P} . If \mathbf{k} lies in this plane, then $|\psi_{f_{\mathbf{k}}}^{(-)}\rangle$ will also have a definite parity under \hat{P} . In this case, $|I_{\mathbf{k}, \hat{\mathbf{a}}}|_{\hat{L}}^2 = |I_{\mathbf{k}, \hat{\mathbf{a}}}|_{\hat{R}}^2$ and CDAD vanishes. For linear molecules adsorbed normal to a surface, this conclusion implies that CDAD will not exist in the plane of incidence.

(iii) For linear molecules with an inversion center (homonuclear diatomics, for example), CDAD does not exist in the reflection plane perpendicular to the molecular axis. This result follows from the fact that for molecules with an inversion center, l, l' are either even (g states) or odd (u states). In this case, the Clebsch-Gordan coefficient $\langle l'00 | L0 \rangle$ insures that L is even. Because $\theta_k = \pi/2$ for the reflection plane perpendicular to the molecular axis, CDAD vanishes in this plane as $Y_{L, -1}(\pi/2, \phi_k) = 0$ for L even.

Molecules adsorbed on surfaces are good candidates for demonstrating CDAD. For example, CO is known to be adsorbed perpendicular to the Ni(100) surface with the carbon end pointing towards the surface.¹⁰ In Fig. 1(a), we present the results of our calculation of CDAD resulting from photoionization of the 4σ orbital for an isolated CO molecule oriented normal to a surface. Such a system can be a useful model for photoemission from actual adsorbed molecules.¹¹ We examine the case in which the photon approaches the surface at 45° with the normal [$(\theta_p, \phi_p) = (135^\circ, 0^\circ)$] and the electrons are collected in a plane perpendicular to the plane of incidence ($\phi_k = 90^\circ$). The continuum wave functions were obtained by the Schwinger varia-

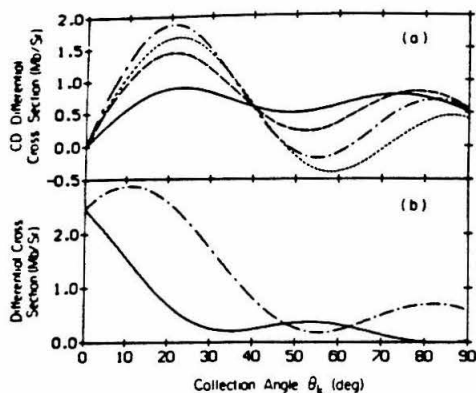


FIG. 1. (a) CD differential cross section vs the collection angle θ_k . Different curves correspond to photon energies $E = 30.7$ eV (solid line), 33.3 eV (long-dashed line), 36.2 eV (dot-dashed line), and 40.8 eV (short-dashed line). Photon propagation direction is $(\theta_p, \phi_p) = (135^\circ, 0^\circ)$ and electron collection is in the plane $\phi_k = 90^\circ$. (b) Differential cross sections for left (dot-dashed line) and right (solid line) circularly polarized light at $E = 36.2$ eV. Configuration of angles is as in (a).

tional method.^{8,12} The results are plotted as a function of θ_k for various photon energies E . The energy range chosen scans the well-known shape resonance in the $4\sigma - k\sigma$ channel.¹³ In Fig. 1(b) we have also plotted, for comparison, the differential cross sections for right and left circularly polarized light at $E = 36.2$ eV.

The most striking aspect of Fig. 1 is that CDAD is of the same order of magnitude as the differential cross section itself. Notice the "magic angle" at $\theta_k \approx 40^\circ$ at which all the distributions have the same magnitude. The behavior of CDAD at this angle can be understood as follows. The resonance feature in the 4σ ionization is known to be in the $l=3$ wave of the $k\sigma$ continuum.¹³ Thus, only I_{300} is rapidly varying with energy around the shape resonance and the CDAD's assume the character

$$Y_{30}(\theta_k, \phi_k) \sum_l I_{l'1, -1} Y_{l'1}^*(\theta_k, \phi_k).$$

The magic angle at $\theta_k \approx 40^\circ$ is due to the zero of $Y_{30}(\theta_k, \phi_k)$ at $\theta_k = 39.2^\circ$. Similarly, at $\theta_k = \pi/2$, the convergence of CDAD's is again due to the vanishing of $Y_{30}(\theta_k, \phi_k)$. CDAD itself is nonvanishing at these angles because of the contributions of $l \neq 3$ partial waves in the $k\sigma$ channel. Figure 1(a) clearly displays

how CDAD highlights the particular partial wave and the partial channel in which the resonances is located. In conclusion, we have shown that CDAD exists for oriented linear molecules within the electric dipole approximation and is of the same magnitude as the differential cross section. We have identified configurations of molecular orientation and photon-propagation and electron-detection directions in which CDAD will be seen. More importantly, we have shown that CDAD arises as a result only of interferences between degenerate continuum channels with $\Delta m = \pm 1$. For this reason, we believe CDAD studies can be useful in extracting information which can be more difficult to obtain from linear polarization studies. It should also be possible to use CDAD to study the characteristics of adsorbed molecules.

We thank Diane L. Lynch for supplying us with the CO 4σ dynamical coefficients. One of us (R.L.D.) acknowledges support from a National Science Foundation Predoctoral Research Fellowship. This material is based upon work supported by the National Science Foundation under Grant No. CHE-8218166. The research reported in this paper made use of the Dreyfus-National Science Foundation Theoretical Chemistry Computer which was funded through grants from the Camille & Henry Dreyfus Foundation, the National Science Foundation (Grant No. CHE-7820235), and the Sloan Fund of the California Institute of Technology.

¹See for example, L. Velluz, M. Legrand, and M. Grosjean, *Optical Circular Dichroism* (Academic, New York, 1965).

²B. Ritchie, *Phys. Rev. A* **13**, 1411 (1976).

³B. Ritchie, *Phys. Rev. A* **14**, 359 (1976).

⁴B. Ritchie, *Phys. Rev. A* **12**, 567 (1975).

⁵N. A. Cherepkov, *J. Phys. B* **16**, 1543 (1983).

⁶R. Parzynski, *Acta. Phys. Pol. A* **57**, 49 (1980).

⁷N. A. Cherepkov, *Chem. Phys. Lett.* **87**, 344 (1982).

⁸R. R. Lucchese, G. Raseev, and V. McKoy, *Phys. Rev. A* **25**, 2572 (1982).

⁹M. E. Rose, *Elementary Theory of Angular Momentum* (Wiley, New York, 1957).

¹⁰C. L. Allyn, T. Gustafsson, and E. W. Plummer, *Solid State Commun.* **28**, 85 (1978).

¹¹J. W. Davenport, *Phys. Rev. Lett.* **36**, 945 (1976).

¹²E. P. Leal, L. Mu-Tao, D. L. Lynch, and V. McKoy, to be published.

¹³See for example, T. Gustafsson, *Surf. Sci.* **94**, 593 (1980).

**Chapter 2: Circular Dichroism in Photoelectron Angular
Distributions from Adsorbed Atoms**

[The text of this chapter appeared in: R. L. Dubs, S. N. Dixit and V. McKoy, Phys. Rev. **B32**, 8389 (1985).]

Circular dichroism in photoelectron angular distributions from adsorbed atoms

Richard L. Dubs, S. N. Dixit, and V. McKoy

Arthur Amos Noyes Laboratory of Chemical Physics, California Institute of Technology,
Pasadena, California 91125

(Received 23 May 1985)

The theory of circular dichroism in the photoelectron angular distributions (CDAD) of oriented linear molecules is applied to the photoionization of adsorbed atoms. CDAD is shown to offer much greater detail about the atom than is available from standard angle-resolved photoionization studies. For oriented atomic orbitals, CDAD is shown to arise solely from interference between the $l \rightarrow l+1$ and $l \rightarrow l-1$ photoionization channels. In addition, for both adsorbed atoms and oriented molecules, CDAD is shown to arise entirely from the non-plane-wave nature of the final state. A simple calculation of CDAD from an oxygen-atom p orbital is given.

INTRODUCTION

Circular dichroism is a phenomenon in which the response of a system to left and right circularly polarized light is different. In a recent report,¹ we showed that circular dichroism in the photoelectron angular distributions (CDAD) from oriented linear molecules exists in the electric dipole approximation. In the present work, we point out that CDAD can be used to study atoms adsorbed on surfaces. While previous workers have discussed CDAD from molecules,² only one other worker has considered CDAD from atoms in the single-photon case. Parzyński³ showed that CDAD exists for strongly polarized alkali atoms in the presence of a magnetic field only when spin-orbit coupling is important. Here we show that CDAD exists from adsorbed atoms in the absence of any spin-orbit interaction. In addition, we show that CDAD from both adsorbed atoms and oriented linear molecules arises solely from the non-plane-wave nature of the final state.

When an atom is adsorbed on a surface, the orbitals other than s orbitals are no longer necessarily degenerate.⁴⁻⁶ For the case of an atom adsorbed at a fourfold site on the surface, the energy of the p_z orbital (perpendicular to the surface) will, in general, be different from that of the p_x, p_y pair. This p_z orbital is then an example of an atomic orbital of fixed spatial orientation. Grimley,⁵ Herbst,⁶ and Goldberg, Fadley, and Kono⁷ have considered angle-resolved photoelectron spectroscopy (ARPES) from oriented atomic p orbitals. In the present work, we will examine CDAD in the same spirit. The magnitude of the effect is illustrated by a simple calculation for an oriented oxygen p orbital.

THEORY

The formalism for CDAD has been developed in Ref. 1. For convenience, we consider the one-electron case. The final form for the difference in the differential cross section for left and right circularly polarized light $D_{L,R}$ is

$$D_{L,R} = \frac{16\pi^2 E}{c\sqrt{3}} (11-11|10) \sum_{L=0}^{2l_{\max}} (2L+1)^{-1/2} \sum_{\substack{l, m, \mu \\ l', m', \mu'}} (-1)^{m+\mu} [(2l+1)(2l'+1)]^{1/2} \\ \times \langle l' 0 0 | L 0 \rangle \langle l' - m' | L - 1 \rangle \langle 11 - \mu \mu' | 11 \rangle \\ \times \text{Im}(J_{lm\mu} J_{l'm'\mu}') \text{Im}[Y_{L-1}(\theta_k, \phi_k) Y_{11}(\theta_p, \phi_p)] \quad (1)$$

where E is the photon energy, c is the speed of light, and $J_{lm\mu}$ is the dynamical coefficient defined in Ref. 1 containing the radial matrix element. The angles (θ_p, ϕ_p) , (θ_k, ϕ_k) are the photon-propagation and electron-collection directions, respectively, measured relative to the atomic z axis. For an atom adsorbed on a surface we define this axis to be perpendicular to the surface plane.

Four important features of CDAD from oriented atomic orbitals follow from Eq. (1). The first three have been discussed in Ref. 1 and will therefore just be stated:

(i) CDAD is due only to interference terms between degenerate photoelectron continua differing by ± 1 in their m values ($\Delta m = m' - m = \pm 1$).

(ii) CDAD vanishes if \hat{k} , \hat{p} , and the axis of the atomic orbital are coplanar.

(iii) CDAD does not exist in the reflection plane perpendicular to the axis of the atomic orbital.

The fourth feature is unique to CDAD from adsorbed atoms.

(iv) CDAD from oriented atomic orbitals arises solely from interference between the $l'' \rightarrow l''+1$ and $l'' \rightarrow l''-1$ photoionization channels. This result arises from a combination of factors. First, a transition from an initial state l'' can only result in a final state $l'' \pm 1$ by the dipole selection rule. As shown in Eq. (1), CDAD is a result of interference terms $\text{Im}(J_{lm\mu} J_{l'm'\mu}')$, where l and l' represent orbital angular moments of the final states. Because the imaginary part of the product of the two dynamical coefficients is proportional to $\sin(\delta_l - \delta_{l'})$ where $\delta_l, \delta_{l'}$ are the partial-wave phase shifts of the continuum wave functions, CDAD

will vanish for $l=l'$. As a result, only interference terms for which $l \neq l'$ will contribute to CDAD; for an initial l'' , CDAD will arise solely from the interference of the $l'' \rightarrow l''+1$ and $l'' \rightarrow l''-1$ photoionization channels. This rule does not apply to oriented linear molecules, since in that case the phase shifts depend on both l and m and the initial states are not described by a well-defined l'' . Note that ARPES studies with linearly polarized light supply information about the cosine of the phase-shift difference. In this respect, CDAD nicely complements ARPES studies.

Finally, we comment on the feature that CDAD will not exist for plane-wave final states. A plane-wave final state has no "memory" of the symmetry of the initial state or the polarization of the incoming photon. That CDAD vanishes for this reason can be derived simply as follows: The double differential cross section D is

$$D \propto |\langle f | \mathbf{A} \cdot \mathbf{p} | i \rangle|^2, \quad (2)$$

where $\mathbf{A} = \hat{\mathbf{e}} A_0 e^{i\mathbf{k} \cdot \mathbf{r}} \approx A_0 \hat{\mathbf{e}}$ in the electric dipole approximation and $\mathbf{p} = -i\hbar \nabla$. $\hat{\mathbf{e}}$ is the unit polarization vector of the photon. The initial state is unimportant for now and may be that of an adsorbed atom or an oriented linear molecule. If the final state is a plane wave,³ then $|f\rangle = e^{i\mathbf{k}' \cdot \mathbf{r}}$ (ignoring normalization) and operating with ∇ on $|f\rangle$,

$$|\langle f | \mathbf{A} \cdot \mathbf{p} | i \rangle|^2 = |\hat{\mathbf{e}} \cdot \mathbf{k}|^2 |\langle e^{i\mathbf{k}' \cdot \mathbf{r}} | i \rangle|^2. \quad (3)$$

From this expression one can see immediately that for plane-wave final state CDAD does not exist in the electric dipole approximation, since $|\hat{\mathbf{e}} \cdot \mathbf{k}|^2$ is identical for left and right circularly polarized light. For non-plane-wave final states, however, Eq. (2) cannot be factored into the simple form of Eq. (3), and the differential cross section for left and right circularly polarized light will not necessarily be equal. Thus, CDAD is a direct consequence of the non-plane-wave nature of the final state.

CDAD FROM p ORBITALS

Consider the adsorption of an atom to a surface at a four-fold site. In this case, the p_x orbital of the adatom is no longer degenerate in energy with the p_x, p_y pair.⁴⁻⁶ Photoionization from this p_x orbital occurs through the following pathways:

- $p_x \rightarrow ks(00)$
- $\rightarrow kd(20)$
- $\rightarrow kd(21)$
- $\rightarrow kd(2-1)$,

where the numbers in the parentheses are the (lm) values for the continuum states. The expression for ARPES (Ref. 1) then consists of the following combinations of dynamical coefficients [recalling that $I_{lm\mu} = I_{l-m-\mu}$ and symbolically representing the combination $I_{lm\mu} I_{l'm'\mu}^*$ as $(lm) \times (l'm')$]:

- $(00) \times (00) \quad (00) \times (20)$
- $(20) \times (20) \quad (00) \times (21)$
- $(21) \times (21) \quad (20) \times (21)$.

Thus, although the degeneracy between the p_x orbital and the p_x, p_y pair has been broken by the interaction with the

surface, ARPES still contains contributions from many terms.

Now consider the terms which contribute to CDAD. From the features of CDAD discussed earlier, only one of the above terms contributes,

$$(00) \times (21).$$

CDAD from an adatom p_x orbital contains information solely about interference between the $p_x \rightarrow ks(00)$ and $p_x \rightarrow kd(21)$ [or $kd(2-1)$ channels]. This information is masked in ARPES.

The angular dependence of CDAD from adatom p orbitals may be derived simply. Due to the Clebsch-Gordon coefficient $\langle l'00 | LO \rangle$, CDAD exists only for $L=2$. The angular dependence is then $\sin(2\theta_k) \sin\theta_p \sin(\phi_p - \phi_k)$. For the collection plane at right angles to the incident plane ($\phi_p - \phi_k = 90^\circ$) CDAD will be maximized and will depend on the collection angle θ_k as $\sin(2\theta_k)$. (Both the incident and collection plane are assumed to include the z axis defined previously.)

In Fig. 1, we show the ARPES and CDAD spectra at 21.2 eV for photoionization from an oriented p orbital (along the z axis) of an oxygen atom. The radial matrix elements and phase shifts for the continuum functions were obtained from Ref. 7. The collection plane is at right angles to the incident plane. Note that the CDAD spectrum has the expected $\sin(2\theta_k)$ dependence. The magnitude of the spectrum is roughly half that of the ARPES spectra. This result follows from the fact that, in general, the $p \rightarrow kd$ transition is more intense than the $p \rightarrow ks$ transition,^{7,8} and while the magnitude of the ARPES spectra depends roughly on $|\langle p | \mu | kd \rangle|^2$, the CDAD spectrum depends on the interference term $|\langle p | \mu | kd \rangle| |\langle p | \mu | ks \rangle|$.

What about CDAD from the p_x, p_y pair? CDAD from this pair will be the same magnitude as CDAD from the p_x orbital but opposite in sign. This result follows from the fact that, when taken together, the three unperturbed p orbitals form a spherical initial state. CDAD from the three

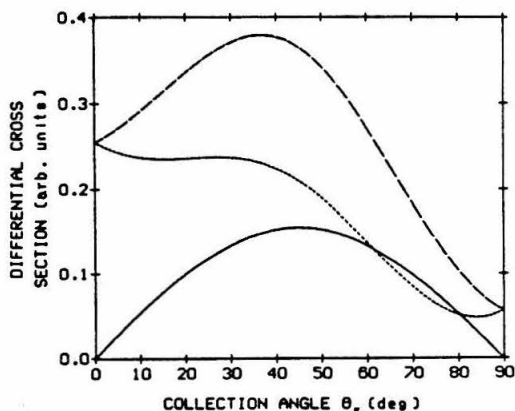


FIG. 1. Differential cross section vs the collection angle θ_k for left and right circularly polarized light and CDAD. Left (—), right (---), CDAD (— · —). Photon-propagation direction is $(\theta_p, \phi_p) = (135^\circ, 0^\circ)$ and electron collection is in the plane $\phi_k = 90^\circ$. Photon energy is 21.2 eV.

orbitals together must thus vanish.

Admittedly, exploring CDAD from adsorbed atoms by using unperturbed, oriented atomic orbitals is a crude first step. Nevertheless, that CDAD does exist from these atomic orbitals is an interesting and useful fact. Bonding of the adatom to the surface can be considered along the lines of Gadzuk's treatment⁹ for studying ARPES from adsorbed atoms. In this way, CDAD can be used to probe the orbitals of the surface atoms involved in bonding. In addition, we have only examined CDAD from *p* orbitals; the present treatment can easily be extended to *d* orbitals, etc.

In conclusion, we have shown that CDAD arises from atoms adsorbed on surfaces and that CDAD offers more detailed information than is provided by standard ARPES studies. CDAD from oriented atomic orbitals arises solely

from interference between the $l \rightarrow l+1$ and $l \rightarrow l-1$ photoionization channels. For both adsorbed atoms and oriented linear molecules CDAD has been shown to arise solely from the non-plane-wave nature of the final state. Finally, because standard ARPES studies provide information about the cosine of the phase-shift differences, while CDAD provides information about the sine of these differences, CDAD studies should nicely complement ARPES studies.

ACKNOWLEDGMENT

One of us (R.L.D.) gratefully acknowledges support from the National Science Foundation. This work was supported by National Science Foundation Grant No. CHE-8218166.

¹R. L. Dubs, S. N. Dixit, and V. McKoy, *Phys. Rev. Lett.* **54**, 1249 (1985).

²B. Ritchie, *Phys. Rev. A* **13**, 1411 (1976); **14**, 359 (1976); **12**, 567 (1975); N. A. Cherepkov, *J. Phys. B* **16**, 1543 (1983); *Chem. Phys. Lett.* **87**, 344 (1982); see also S. Wallace, D. Dill, and J. L. Dehmer, *Phys. Rev. B* **17**, 2004 (1978).

³P. Parzyński, *Acta Phys. Pol. A* **57**, 49 (1980).

⁴P. V. S. Rao and J. T. Waber, *Surf. Sci.* **28**, 299 (1971).

⁵T. B. Grimley, *Discuss. Faraday Soc.* **58**, 7 (1974).

⁶J. F. Herbst, *Phys. Rev. B* **15**, 3720 (1976).

⁷S. M. Goldberg, C. S. Fadley, and S. Kono, *J. Electron. Spectrosc. Relat. Phenom.* **21**, 285 (1981).

⁸J. W. Cooper, *Phys. Rev.* **128**, 681 (1962).

⁹J. W. Gadzuk, *Phys. Rev. B* **10**, 5030 (1974).

**Chapter 3: Circular Dichroism in Photoelectron Angular
Distributions as a Probe of Atomic and
Molecular Alignment**

[The text of this chapter appeared in: R. L. Dubs, S. N. Dixit and V. McKoy, J. Chem. Phys. **85**, 656 (1986).]

Circular dichroism in photoelectron angular distributions as a probe of atomic and molecular alignment

Richard L. Dubs, S. N. Dixit, and V. McKoy

Arthur Amos Noyes Laboratory of Chemical Physics,^{a)} California Institute of Technology, Pasadena, California 91125

(Received 24 December 1985; accepted 4 April 1986)

In this paper we show that circular dichroism in photoelectron angular distributions (CDAD) can be used to probe atomic and molecular alignment in the gas phase. Careful choice of photon (left or right circularly polarized) propagation and photoelectron collection directions breaks the cylindrical symmetry of the target, giving rise to dichroic effects. CDAD exists in the electric dipole approximation. We illustrate the sensitivity of CDAD to alignment by considering photoionization of the $A^2\Sigma^+$ state of NO. Most of the cases of alignment we consider are created by multiphoton absorption while the others, more general, might be created in fragmentation, desorption, etc. The alignment created by n -photon absorption quickly reaches a classical limit which is reflected in the CDAD spectrum. Finally, we show that CDAD is also a sensitive probe of gas phase atomic state alignment by considering photoionization of the $7P_{3/2}$ state of cesium created by single photon absorption from the ground state.

INTRODUCTION

In recent years, studies of orientational effects in chemical processes have attracted much attention due to the detailed dynamical information these studies can provide. Examples of such studies include atom-diatom collisions,¹ unimolecular processes,² electron stimulated desorption of adsorbed molecules,³ and molecular scattering from surfaces.⁴ Preparation of reactants with well characterized alignment and subsequent detection of product alignment/orientation are integral parts of such investigations. The methods for creating aligned species include electronic⁵ or atomic⁶ impact, application of external electric and magnetic fields,⁷ photofragmentation,^{8,9} and photoabsorption.¹⁰⁻¹² The detection of product alignment, on the other hand, has commonly been accomplished by measuring the fluorescence polarization^{9(a)} resulting from either direct spontaneous emission or laser induced fluorescence.

In this paper we propose a new method for probing the alignment in atomic and molecular systems; namely, measuring the circular dichroism in photoelectron angular distributions (CDAD). CDAD spectra are obtained by taking the difference between angle-resolved photoelectron spectra (ARPES) for left and right circularly polarized light. Historically, circular dichroism (CD) has been associated with chiral molecules which lack a plane of symmetry and an inversion center.¹³⁻¹⁶ However, recently we have shown that CD can exist in photoelectron angular distributions from photoionization of oriented linear molecules¹⁷ and adsorbed atoms.¹⁸ Though previous studies of CDAD^{14,15,19,20} assumed strong spin-orbit coupling or high multipole interactions, our analyses^{17,18} showed that a proper choice of electron collection and the photon propagation direction can break the cylindrical symmetry of the target and give rise to dichroic effects in the electric-dipole approximation. We have also pointed out that CDAD studies often provide in-

formation complementary to that obtained from the ARPES studies. In this paper, we demonstrate that CDAD can also be used as a probe of the alignment of a gas phase target state. Since CDAD cannot exist in an isotropic target for symmetry reasons, the very existence of CDAD, therefore, implies alignment of the target. In addition, the shape of the CDAD spectrum provides details about this alignment.

The state of an atom or a molecule with total angular momentum J is said to be aligned if the population of the M_J magnetic sublevels is nonuniform. Alignment is differentiated from orientation in that the former requires the populations of M_J and $-M_J$ states to be equal. Absorption of a linearly polarized photon from an isotropic initial state creates an aligned state whereas absorption of a circularly polarized photon gives rise to an oriented state. In this paper, we shall use the term "alignment" loosely to include orientation, the actual anisotropy being described by the populations of the M_J levels. CDAD exists from aligned as well as oriented states and, as we show, is very sensitive to the details of the alignment.

In this paper, we shall discuss CDAD arising from photoionization of the $A^2\Sigma^+$ state of NO. We shall consider alignment created in this $A^2\Sigma^+$ state by multiphoton absorption and will also choose some general alignments to illustrate the variation of CDAD with alignment. Finally, we examine CDAD in the photoionization of the $7P_{3/2}$ state of Cs created by a single photon excitation from the ground $6S_{1/2}$ state. It should be emphasized that while Parzynski's analysis²⁰ of CDAD from atoms required strong spin-orbit coupling, this coupling is not necessary for the existence of CDAD. We include this coupling in our calculations, however, since it is present in the cesium atom.

Finally, a pump-probe type experiment can be designed as follows to observe CDAD in gas-phase atomic and molecular systems: *Step 1:* (creation of alignment); n -linearly polarized photons resonantly excite the isotropic initial state of atoms or molecules. The polarization vector of these pho-

^{a)} Contribution No. 7339.

tions defines the laboratory frame z axis. *Step 2:* (measurement of the alignment); the excited state is photoionized by a second laser with either left or right circular polarization and co-propagating with the first laser beam. Photoelectron angular distributions are then measured in the plane perpendicular to the photon propagation direction by rotating the direction of linear polarization. By delaying the probe beam relative to the pump, CDAD can also be used to monitor the evolution of alignment due to collisions.^{9(b)}

THEORY

In this section we present the theory related to using CDAD as a probe of alignment. The analysis can be separated into a part dealing with the calculation of the anisotropy (alignment) in the atomic or molecular state and a part discussing CDAD from this aligned state. For the sake of simplicity we shall only consider alignment resulting from photoabsorption. Alignment created by other methods mentioned in the previous section can be calculated in an appropriate manner. Likewise, we will assume that the aligned state is ionized by a single left or right circularly polarized photon. Generalization to multiphoton ionization out of the aligned state can be carried out with a few additional steps.

$$\rho_{JM_J} \propto \sum_{M_k} \left| \sum_{k=1, n-1}^{J, M_k} \frac{\langle JM_J | D_0 | J_{n-1} M_{J_{n-1}} \rangle \langle J_{n-1} M_{J_{n-1}} | D_0 | J_{n-2} M_{J_{n-2}} \rangle \cdots \langle J_1 M_{J_1} | D_0 | J_0 M_{J_0} \rangle}{(E_0 - E_1 + \hbar\omega)(E_0 - E_2 + 2\hbar\omega) \cdots [E_0 - E_{n-1} + (n-1)\hbar\omega]} \right|^2,$$

where $\hbar\omega$ is the photon energy and E_k 's denote the energy of the $|J_k M_{J_k}\rangle$ state. Both Eqs. (2) and (3) are valid under weak field excitation conditions. For clarity, we have suppressed all other indices needed for the designation of various states. Note that ρ_{JM_J} , given by Eqs. (2) and (3), satisfy $\rho_{JM_J} = \rho_{J-M_J}$, i.e., the state J is aligned and not oriented. For one-photon absorption, relative values of ρ_{JM_J} depend only on the Clebsch-Gordan coefficients while for an n -photon ($n > 1$) absorption, even the relative values of ρ_{JM_J} depend on the particular atomic or molecular system. Only in special cases where $J = J_0 \pm n$ can the relative populations be represented purely by Clebsch-Gordan coefficients.

Probing the alignment using CDAD

In this subsection we shall discuss CDAD in photoionization out of an aligned state. If $(d^2\sigma/d\Omega_k d\Omega_k)(JM_J)$ denotes the differential photoionization cross section (DCS) for the state $|JM_J\rangle$ then the total (m -averaged) DCS out of the excited state is,¹¹

$$\frac{d^2\sigma}{d\Omega_k d\Omega_k} = \sum_{M_J} \rho_{JM_J} \frac{d^2\sigma}{d\Omega_k d\Omega_k}(JM_J), \quad (4)$$

where ρ_{JM_J} are populations in the states $|JM_J\rangle$ that characterize the alignment. The CDAD spectra are obtained by taking the difference in the DCS's from Eq. (4) for left and right circularly polarized light. The m -resolved DCS $(d^2\sigma/d\Omega_k d\Omega_k)(JM_J)$ is proportional to the square of the photoelectron matrix element $I_{k,\lambda}^{JM_J}$ written as²¹

Alignment of the excited state by multiphoton absorption

Consider an excited state alignment created by absorption of a single photon, linearly polarized along the z axis of the laboratory frame. In this case, the electric dipole moment operator can be written as

$$D_0 = \left(\frac{4\pi}{3}\right)^{1/2} \sum_s r_s Y_{10}(\hat{r}_s), \quad (1)$$

where r_s is the magnitude of the position vector of the s^{th} electron and \hat{r}_s is the position of this electron in the laboratory frame. For a transition from an isotropic initial state with total angular momentum J_0 (all M_{J_0} states are equally populated) to an intermediate state with angular momentum J , the alignment in the intermediate state, described by the population of various M_J sublevels ρ_{JM_J} , can be written as¹⁰

$$\rho_{JM_J} \propto \sum_{M_k} |\langle JM_J | D_0 | J_0 M_{J_0} \rangle|^2, \quad (2a)$$

$$\propto \langle J_0 1 M_{J_0} 0 | JM_J \rangle^2. \quad (2b)$$

In Eq. (2b), $\langle J_0 1 M_{J_0} 0 | JM_J \rangle$ denotes a Clebsch-Gordan coefficient. For a n -photon absorption from a $|J_0 M_{J_0}\rangle$ state to $|JM_J\rangle$, ρ_{JM_J} is similarly written as¹¹

$$I_{k,\lambda}^{JM_J} = \langle \psi_{JM_J}^{(-)} | D_{\mu_0} | \psi_{JM_J}^{(+)} \rangle. \quad (5)$$

In the above equation, μ_0 denotes the polarization index (0 for linear and ± 1 for circular polarization) in the ionizing photon frame, and $|\psi_{JM_J}^{(+)}\rangle$ and $|\psi_{JM_J}^{(-)}\rangle$ the initial and final states, respectively. In the following, we will describe the calculation of this bound-free matrix element for photoionization of the $A^2\Sigma^+$ state of NO and of the $7P_{3/2}$ state of Cs.

Molecules

For the $A^2\Sigma^+$ state of NO, the wave function $|\psi_{JM_J}\rangle$ can be described in Hund's case (b) as²²

$$\psi_{JM_J} = |\gamma \Lambda \Sigma S J M_J\rangle = \sqrt{\frac{2N+1}{8\pi^2}} \sum_{M_S M_J} \langle NS M M_S | JM_J \rangle \times \psi_{\gamma\Lambda}^{(s)}(\{r_i\}; R) D_{\Lambda M}^N(\hat{R}') \chi_{\nu}(R) |S M_S\rangle. \quad (6)$$

Here primed coordinates refer to the molecular frame while unprimed coordinates refer to the laboratory frame. $\psi_{\gamma\Lambda}^{(s)}$ is the electronic wave function that depends on the internuclear separation, R , $\chi_{\nu}(R)$ is the wave function for the vibrational state ν , and $|S M_S\rangle$ is the spin wave function. $D_{\Lambda M}^N(\hat{R}')$ denotes the symmetric top rotational wave function with total (rotational plus electronic) angular momentum N , the projection of this angular momentum along the z axis of the molecular frame being Λ ($\Lambda = 0$ for Σ states, ± 1 for Π states, etc.), and the projection along the z axis of the

laboratory frame being M . The notation of Rose²³ is used throughout. \hat{R}' refers to the coordinates of the laboratory z axis in the molecular frame. The factor $\sqrt{(2N_+ + 1)/8\pi^2}$ ensures normalization of the total wave function. γ contains all other subscripts necessary for an unambiguous designation of the state.

The continuum function $\psi_{f_k}^{(-)}$ is a product of wave functions for the photoelectron $|\phi\rangle$ and the resulting molecular ion $|\gamma_+ \Lambda_+ N_+ S_+ J_+ M_{J_+}\rangle$:

$$\psi_{f_k}^{(-)} = |\phi\rangle |\gamma_+ \Lambda_+ N_+ S_+ J_+ M_{J_+}\rangle. \quad (7)$$

We calculate $\psi_{f_k}^{(-)}$ using the iterative Schwinger variational technique.²¹ The electronic wave function for the continuum electron can be expanded in partial waves¹¹:

$$|\phi\rangle = \left| \frac{1}{2} m_\sigma \right\rangle \sum_{lm\lambda} i^l e^{-im_\sigma Y_{lm}^*(\hat{k})} D_{lm}^l(\hat{R}') \psi_{k\lambda}(\{r_i\}; R). \quad (8)$$

m_σ is the projection of the electron spin on the laboratory z axis. k denotes the photoelectron momentum and \hat{k} its direction in the laboratory frame. $lm\lambda$ denote, respectively, the angular momentum of the electron and its projections along the laboratory and molecular z axes. The ionic wave function can be written as

$$\begin{aligned} & |\lambda_+ \Lambda_+ N_+ S_+ J_+ M_{J_+}\rangle \\ &= \sqrt{\frac{2N_+ + 1}{8\pi^2}} \sum_{M_+ M_{S_+}} \langle N_+ S_+ M_+ M_{S_+} | J_+ M_{J_+} \rangle \\ & \times \psi_{\gamma_+ \Lambda_+}^{(\sigma)}(\{r_i\}; R) \chi_{v_+} |S_+ M_{S_+}\rangle D_{\Lambda_+ M_+}^{N_+}(\hat{R}'), \end{aligned} \quad (9)$$

where v_+ , J_+ , M_{J_+} , and Λ_+ denote, respectively, the ionic vibrational quantum number, the total angular momentum quantum number, and the projection of J_+ on the laboratory and molecular z axes. S_+ is the total spin of the ion and M_{S_+} its projection on the laboratory z axis.

In the single particle picture, D_{μ_+} of Eq. (5) can be written in the frame of the ionizing photon as

$$D_{\mu_+} = (4\pi/3)^{1/2} r Y_{1\mu_+}(\hat{p}). \quad (10)$$

As the coordinate frames of the exciting and ionizing photons need not coincide, we must transform D_{μ_+} into the frame of the exciting photon. D_{μ_+} can then be written as

$$D_{\mu_+} = \left(\frac{4\pi}{3}\right)^{1/2} r \sum_{\mu'} D_{\mu\mu'}^1(\hat{R}^*) \sum_{\mu''} D_{\mu''\mu}^1(\hat{R}') Y_{1\mu''}(\hat{p}'). \quad (11)$$

Here, \hat{R}^* specifies the coordinates of the z axis of the ionizing photon frame in the laboratory frame. \hat{p}' is the coordinate of the position vector in the molecular frame.

Substituting Eqs. (6), (7), (8), (9), and (11) into Eq. (5) and integrating over molecular orientations, Eq. (5) becomes

$$\begin{aligned} I_{k,\lambda}^{JM,\mu_+} &= \sqrt{\frac{4\pi}{3}} [(2N_+ + 1)(2N + 1)]^{1/2} \sum_{\substack{\mu_+ \\ lm\lambda \\ M_+ M_{S_+} \\ M_+ M_{S_+}}} \overline{r_{k'}^{\mu_+}} \langle S_+ 1/2 M_{S_+} m_\sigma | S M_S \rangle \\ & \times D_{\mu_+ \mu_+}^1(\hat{R}^*) \langle N_+ S_+ M_+ M_{S_+} | J_+ M_{J_+} \rangle \langle N S M M_S | J M_J \rangle \\ & \times (-i)^l e^{im_\sigma Y_{lm}^*(\hat{k})} (-1)^{\mu - \mu' + \Lambda_+ - M_+} \sum_{N'} \frac{1}{2N_+ + 1} \langle 1 - \lambda \mu' | N_+ \mu' - \lambda \rangle \langle 1 - m \mu | N_+ \mu - m \rangle \\ & \times \langle N N_+ M - M_+ | N_+ m - \mu \rangle \langle N N_+ \Lambda - \Lambda_+ | N_+ \lambda - \mu' \rangle, \end{aligned} \quad (12)$$

where

$$\overline{r_{k'}^{\mu_+}} = \int \chi_{v_+}(R) r_{k'}^{\mu_+} \chi_{v_+}(R) dR \quad (13)$$

and

$$r_{k'}^{\mu_+} = \langle \psi_{k\lambda}(\{r_i\}; R) \psi_{\gamma_+ \Lambda_+}^{(\sigma)}(\{r_i\}; R) | r Y_{1\mu_+}(\hat{p}') | \psi_{\gamma_+ \Lambda_+}^{(\sigma)}(\{r_i\}; R) \rangle \quad (14)$$

denotes the photoionization electronic transition moment.

Using Eq. (12), Eq. (4) can be written as

$$\frac{d^2\sigma}{d\Omega_k d\Omega_{\lambda}} = (-1)^{\mu_+} \sum_{M_+} \rho_{JM_+} \sum_{L'L'M'} \langle 11 - \mu_+ \mu_0 | L' 0 \rangle \beta_{L'L'M'}^{M_+} Y_{L-M'}(\theta_k, \phi_k) Y_{L'M'}(\theta_p, \phi_p), \quad (15)$$

where

$$\begin{aligned} \beta_{L'L'M'}^{M_+} &= [(2L + 1)(L' + 1)]^{-1/2} \sum_{m_+} \sum_{l'm_+'} I_{lm_+}^{\mu_+} I_{l'm_+'}^{\mu_+} (-1)^{m_+' - \mu_+} \\ & \times [(2l + 1)(2l' + 1)]^{1/2} \langle ll' 00 | L 0 \rangle \langle ll' - m m' | L M' \rangle \langle 11 - \mu \mu' | L' M' \rangle \end{aligned} \quad (16)$$

and

$$I_{lm\mu}^{\alpha} = [(2N_{+} + 1)(2N + 1)]^{1/2} \sqrt{\frac{4\pi}{3}} (-i)^l (-1)^{\Lambda - M_{+} - M_{-}} \sum_{\substack{\mu, \lambda \\ M_{+}, M_{-} \\ M_{S}}} (-1)^{\mu - \mu'} e^{i\mu\alpha} \overline{r_{\beta}^{(\mu')}} \langle S_{+} 1/2 M_{S_{+}} m_{\sigma} | S M_{S} \rangle \\ \times \langle NS M M_{S} | J M_{J} \rangle \langle N_{+} S_{+} M_{+} M_{S_{+}} | J_{+} M_{J_{+}} \rangle \sum_{M'} \frac{1}{(2N_{+} + 1)} \langle l 1 - \lambda \mu' | N_{+} \mu' - \lambda \rangle \\ \times \langle l 1 - m \mu | N_{+} \mu - m \rangle \langle N N_{+} \Lambda - \Lambda_{+} | N_{+} \lambda - \mu' \rangle \langle N N_{+} M - M_{+} | N_{+} m - \mu \rangle. \quad (17)$$

In the above equations, α refers to the variables $m_{\sigma}, N_{+}, J_{+}, M_{J_{+}}$ and (θ_k, ϕ_k) and (θ_p, ϕ_p) denote, respectively, the collection angle of the photoelectron and the propagation direction of the circularly polarized ionizing photon in the laboratory frame.

Equation (15) makes calculation of ARPES spectra simple. The $\beta_{LL'M'}$ are calculated once for a given photon energy, after which Eq. (15) is used to quickly calculate spectra for any alignment, light polarization, or experimental configuration of photon propagation direction or electron collection direction.

The CDAD signal is defined as the difference in the differential cross section of Eq. (14) for left and right circularly polarized light.¹⁷

$$\frac{d\sigma^{L-R}}{d\Omega_k d\Omega_h} = \frac{d\sigma^{+1}}{d\Omega_k d\Omega_h} - \frac{d\sigma^{-1}}{d\Omega_k d\Omega_h}. \quad (18)$$

In Eq. (15), only $(-1)^{m_{\sigma}} \langle 11 - \mu_0 \mu_0 | L' 0 \rangle$ depends on the polarization of the photon. Thus, due to the symmetry property

$$\langle 11 \mu_0 - \mu_0 | L' 0 \rangle = (-1)^{L'} \langle 11 - \mu_0 \mu_0 | L' 0 \rangle, \quad (19)$$

only terms in which $L' = 1$ will contribute to CDAD. In addition, due to the symmetry properties of $I_{lm\mu, M'}^{\alpha}$, only terms for which $M' = \pm 1$ will contribute to CDAD and the corresponding $\beta_{L1 \pm 1}$ will be pure imaginary numbers.¹⁷

Atoms

For atoms, the bound-continuum matrix element is still defined by Eq. (14) where²⁴

$$|\psi_{f\hat{k}}^{-1}\rangle = 4\pi \left[\frac{\pi}{2k} \right]^{1/2} \sum_{l'=0}^{\infty} \sum_{m'=-l'}^{l'} i^{l'} e^{-i\delta_{l'}} Y_{l'm'}^*(\hat{k}) \\ \times \sum_{J'm_j'} R_{El'J'}(r) \langle l' 1/2 m' m_{\sigma} | J' m_j' \rangle |l' 1/2 m_j'\rangle, \quad (20)$$

$$|\psi_i^{JM}\rangle = R_{nL}(r) |l' 1/2 m_j\rangle, \quad (21)$$

and

$$|l' 1/2 m_j\rangle = \sum_m \sum_{m_{\sigma}} \langle l' 1/2 m m_{\sigma} | J m_j \rangle Y_{lm}(\hat{p}) |l' m_{\sigma}\rangle. \quad (22)$$

Both the radial wave functions, $R_{El'J'}(r)$ and the phase shifts $\delta_{l'}$ are calculated as in Ref. 24. \hat{p} and \hat{k} are expressed in the laboratory frame. The dipole moment operator $D_{\mu\sigma}$, expressed in Eq. (10), is rewritten as

$$D_{\mu\sigma} = \left(\frac{4\pi}{3} \right)^{1/2} r \sum_{\mu} D_{\mu\sigma}^1(R^*) Y_{1\mu}(\hat{p}). \quad (23)$$

Substituting Eqs. (20)–(23) into Eq. (5), Eqs. (15)

and (16) are again obtained, with the sums over K_{+}, J_{+} , and M_{+} omitted and $\alpha = m_{\sigma}$ in Eq. (16). Now $I_{lm\mu}^{\alpha}$ is defined as

$$I_{lm\mu}^{\alpha} = (-i)^l e^{i\delta_{l'}} \overline{r_{\beta}^{(\mu')}} (-1)^{J+l+1/2} \\ \times \sqrt{\frac{3}{4\pi}} [(2J+1)(2l+1)]^{1/2} \\ \times \sum_{J'm_j'} \langle l' 1/2 m' m_{\sigma} | J' m_j' \rangle \begin{Bmatrix} l' & J' & 1 \\ J & l & 1 \end{Bmatrix} \\ \times \langle J 1 m_j u' | J' m_j' \rangle \langle l 1 0 0 | l' 0 \rangle, \quad (24)$$

where

$$\overline{r_{\beta}^{(\mu')}} = \langle R_{El'J'}(r) | r | R_{nL}(r) \rangle. \quad (25)$$

RESULTS AND DISCUSSION

Molecules

In this section we present the results for CDAD in photoionization of the $A^2\Sigma^+$ state of NO. The ionizing photon wavelength is chosen to be about 225 nm. The bound-free matrix elements were taken from the calculations presented in Ref. 22. In Fig. 1, we present ARPES spectra for left and right polarized light and the resulting CDAD spectra. Figure 1(a) corresponds to single photon $J_0 = 1/2 \rightarrow J = 3/2$ excitation to the A state while Fig. 1(b) corresponds to $J_0 = 3/2 \rightarrow J = 5/2$ excitation. The relative populations ρ_{JM} are given in Table I (cases A and B). Both CDAD spectra have a $\sin 2\theta_k$ dependence. This is a reflection of a one-photon absorption alignment. Mathematically, the $\sin 2\theta_k$ dependence arises because only $\beta_{21 \pm 1}$ contribute to CDAD in this case. At $\theta_k = 45^\circ$ CDAD spectra are about 15% of ARPES spectra. The relative strengths of CDAD and ARPES spectra depend on specific values of molecular parameters and could be different for other systems.

In Figs. 2(a)–2(c) we present CDAD and ARPES spectra for individual M_J (1/2, 3/2, and 5/2) states of the $A^2\Sigma^+$ ($J = 5/2$) level. The relative populations are again given in Table I (cases C, D, and E). Case C corresponds to two-photon excitation from a $J_0 = 1/2$ state. Although the alignments described by cases D and E cannot be produced by multiphoton absorption of linearly polarized light, they might result from photofragmentation reactions, gas–solid scattering, desorption, etc. In addition, a state initially prepared in a $M_J = \pm 1/2$ state may evolve, e.g., by collision, into a state with a distribution of M_J values.^{9(b)} In this case, the net CDAD spectrum will be a weighted sum of the spectra for individual M_J values. Note that from an isotropic

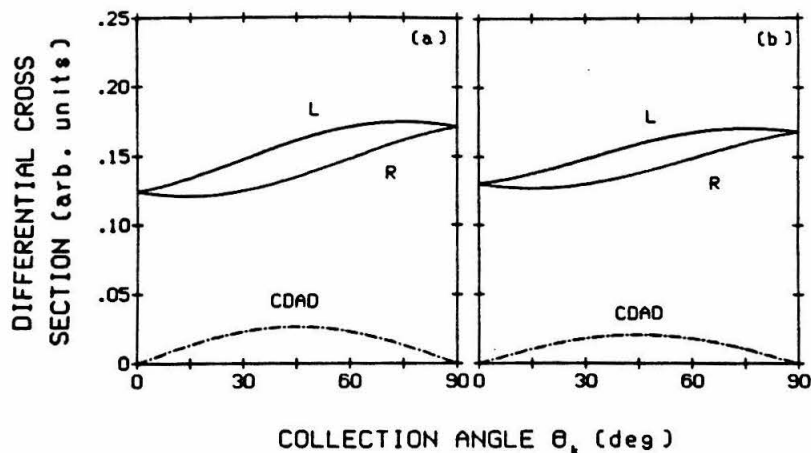


FIG. 1. Differential cross section vs the collection angle θ_k for left (L) and right (R) circularly polarized light and CDAD from the $A^2\Sigma^+$ state of NO. (a) $J_0 = 1/2 \rightarrow J = 3/2$ (Table I, case A); (b) $J_0 = 3/2 \rightarrow J = 5/2$ (Table I, case B). Both alignments created by one-photon absorption.

state (all M_J 's equally populated), CDAD cannot exist for symmetry reasons. The sum of the CDAD spectra in Figs. 2(a), 2(b), and 2(c) thus gives a spectrum of zero magnitude at all angles.

It is clear from these results that CDAD spectra are quite sensitive to the relative populations of the M_J states. Comparison of one- and two-photon CDAD [Figs. 1(b) and 2(a)] indicates that CDAD probes the anisotropy of the aligned excited state. While the single-photon excitation CDAD are proportional to $Y_{2\pm 1}(\theta_k, \phi_k)$, the two-photon excitation CDAD can be expressed as a linear combination of $Y_{2\pm 1}(\theta_k, \phi_k)$ and $Y_{4\pm 1}(\theta_k, \phi_k)$, the relative weights of which depend on the particulars of the process. In fact, one can show (although the algebra is quite tedious) that CDAD spectra in photoionization from an n -photon excited state will contain terms $Y_{2\pm 1}, Y_{4\pm 1}, \dots$ up to $Y_{2n, \pm 1}(\theta_k, \phi_k)$. The ARPES spectra, on the other hand, contain terms up to $Y_{2(n+1), m}(\theta_k, \phi_k)$. This difference is a consequence of the fact that CDAD spectra, each being a difference between two ARPES spectra, have lost the infor-

mation about the final photoionization step and are therefore only sensitive to the alignment in the n -photon excited state. Mathematically, this result is a direct consequence of the fact that, for the ionizing photon, L' can only take the value of 1 for CDAD¹⁷ while it can have its maximum value of 2 for ARPES.

What happens to the CDAD spectra as more and more pump photons are absorbed? In Fig. 3, the ARPES and CDAD spectra are shown for photoionization from the A state with the alignment created by the $J_0 = 1/2 \rightarrow J = 11/2$ five-photon absorption from the X state (case F in Table I). Note that the magnitude of the CDAD spectrum has increased slightly to 25% of the ARPES spectra, but otherwise appears very similar to that for the alignment created by two-photon absorption [Fig. 2(a)]. The CDAD spectrum for photoionization out of an aligned state prepared by the $J_0 = 1/2 \rightarrow J = 21/2$ ten-photon absorption is found to be virtually identical to that in Fig. 3. Thus, the alignment of the molecule appears to quickly reach a limit after which absorption of additional photons has little effect.

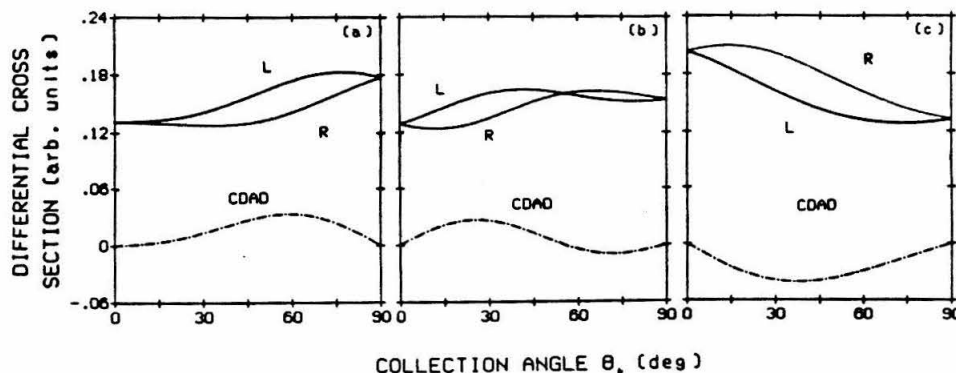


FIG. 2. Differential cross section vs the collection angle θ_k for left (L) and right (R) circularly polarized light and CDAD from the $A^2\Sigma^+$ state of NO. For all cases $J = 5/2$. (a) $M_J = \pm 1/2$ (Table I case C); (b) $M_J = \pm 3/2$ (Table I, case D); (c) $M_J = \pm 5/2$ (Table I, case E). Alignment for (a) created by two-photon absorption $J_0 = 1/2 \rightarrow J = 5/2$.

TABLE I. Relative populations $2\rho_{JM}$, of M_J states.

Case	J	-11/2	-9/2	-7/2	-5/2	-3/2	-1/2	1/2	3/2	5/2	7/2	9/2	11/2	Comment
A	3/2					0	1	1	0					One-photon 1/2→3/2
B	5/2				0	2/5	3/5	3/5	2/5	0				One-photon 3/2→5/2
C	5/2				0	0	1	1	0	0				Two-photon 1/2→5/2
D	5/2				0	1	0	0	1	0				See the text
E	5/2				1	0	0	0	0	1				See the text
F	11/2	0	0	0	0	0	1	1	0	0	0	0	0	Five-photon 1/2→11/2

THE CLASSICAL PICTURE OF THE ALIGNMENT

To understand the above limiting behavior, let us consider a rigid rotor in a $|J_0, M_0\rangle$ state. If all the M_0 states are equally populated, the spatial distribution of the rotor axis is simply

$$P(\theta, \phi) = \sum_{M_0} P_{J_0, M_0}(\theta, \phi) = |Y_{00}|^2 = \text{const.} \quad (26)$$

In the absence of the spin-orbit coupling, absorption of n -linearly polarized photons will lead to a spatial distribution $|Y_{n0}|^2$. Absorption of n -photons in molecules with spin-orbit coupling will give rise to spatial distributions involving $|Y_{n,m}|^2, m \neq 0$ as well. For example, a two-photon transition from $|1/2, 1/2\rangle \rightarrow |5/2, 1/2\rangle$ in NO will lead to a spatial distribution

$$P_{5/2, 1/2}(\theta, \phi) = \langle 2, 1/2, 0, 1/2 | 5/2, 1/2 \rangle^2 |Y_{20}|^2 + \langle 2, 1/2, 1, -1/2 | 5/2, 1/2 \rangle^2 |Y_{21}|^2. \quad (27)$$

Similarly a five-photon $1/2 \rightarrow 11/2$ transition implies

$$P_{11/2, 1/2}(\theta, \phi) = \langle 5, 1/2, 0, 1/2 | 11/2, 1/2 \rangle^2 |Y_{50}|^2 + \langle 5, 1/2, 1, -1/2 | 11/2, 1/2 \rangle^2 |Y_{51}|^2. \quad (28)$$

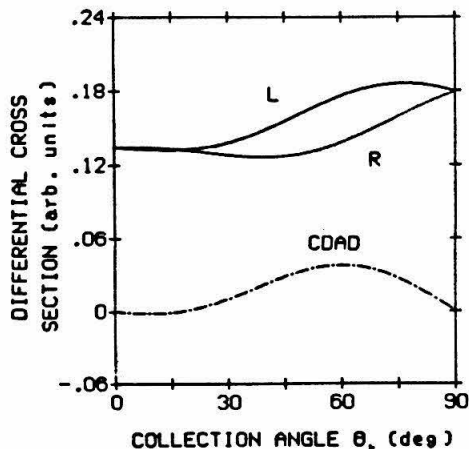


FIG. 3. Differential cross section vs the collection angle θ_c for left (L) and right (R) circularly polarized light and CDAD from the $A^2\Sigma^+$ state of NO. Alignment created by five-photon absorption $J_0 = 1/2 \rightarrow J = 11/2$ (Table I, case F).

Using the method described in Ref. 25, we have performed photoionization calculations from oriented NO molecules (ignoring spin) whose orientations in space are weighted by $|Y_{JM}|^2$. The results for $|Y_{20}(\theta, \phi)|^2$ and $|Y_{50}(\theta, \phi)|^2$ are shown in Figs. 4(a) and 4(b), respectively. Comparing these with fully quantum mechanical calculations [Figs. 2(a) and 3], we see that the classical calculation agrees well with the quantum mechanical one for five-photon absorption ($|Y_{50}|^2$) while for two-photon absorption the agreement is poor. This discrepancy is not due to a diminishing distribution of $|Y_{J1}|^2$ with increasing J but rather due to the fact that the distributions $|Y_{J0}|^2$ and $|Y_{J1}|^2$ become more and more similar for high J . In other words, $|Y_{50}|^2$ and $|Y_{51}|^2$ have similar spatial distributions whereas $|Y_{20}|^2$ and $|Y_{21}|^2$ have quite different ones. Thus as J increases, $|Y_{J0}|^2$ accurately describes the spatial orientation of the excited $A^2\Sigma^+$ state. This statement is also a reflection of the decreasing importance of the $1/2$ unit spin at high J .

We are now in a position to understand our earlier observation that alignment of a molecule appears to quickly reach a limit after which absorption of additional photons has little effect. To examine the θ dependence of the alignment of a molecule after it has absorbed J photons we look at

$$|Y_{J0}(\theta, \phi)|^2 \sin \theta, \quad (29)$$

where the $\sin \theta$ accounts for the increase in solid angle with increasing θ . As J increases, the $|Y_{J0}(\theta, \phi)|^2$ oscillates more and more rapidly (with J nodes from $\theta = 0$ to $\theta = \pi$). If we replace this rapidly oscillating part by its average value,²⁶ we find

$$|Y_{J0}(\theta, \phi)|^2 = \frac{1}{2\pi^2 \sin \theta} \text{ for } J \text{ large and } \theta \gg \frac{1}{J}. \quad (30)$$

Near the z axis $|Y_{J0}(\theta, \phi)|^2$ has a large finite value; however, this contribution is cancelled by the $\sin \theta$ in Eq. (29). Note that the right-hand side of Eq. (30) is independent of J . For this reason, after a few photons are absorbed, the alignment quickly reaches a limit. As we have shown, the CDAD spectra clearly reflect this fact.

Atoms

In Fig. 5, ARPES and CDAD spectra are shown for photoionization from the $7P_{3/2}$ state of Cs. The alignment of the state is created by one-photon absorption from the $6S_{1/2}$ state (Table I, case A). The energy of the ionizing photon is assumed to be equal to the energy difference between the $6S_{1/2}$ and $7P_{3/2}$ states. The required atomic parameters were calculated using the quantum-defect theory. We again note

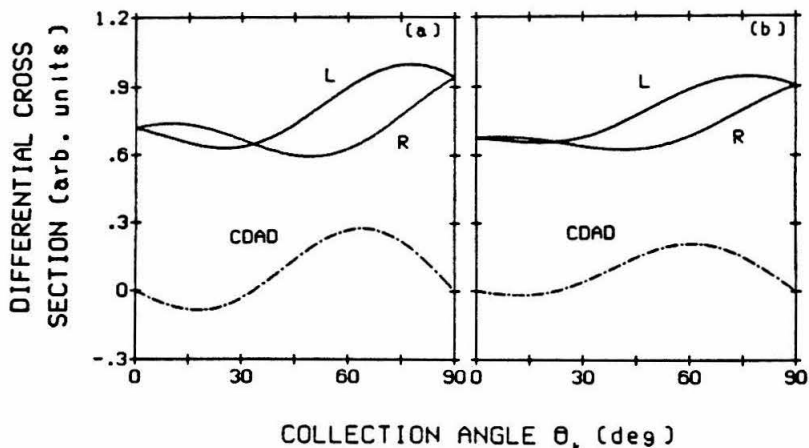


FIG. 4. Differential cross section vs the collection angle θ_k for left (L) and right (R) circularly polarized light and CDAD from the $A^2\Sigma^+$ state of NO. Classical alignment ignoring spin: (a) $(J,M) = (2,0)$; (b) $(J,M) = (5,0)$.

the $\sin 2\theta_k$ dependence of the CDAD spectrum, a signature of the one-photon alignment.

The magnitude of the CDAD spectrum is only about 25% that of the ARPES spectra. However, in Ref. 18 we showed that the magnitude of the CDAD spectrum for photoionization from an oriented oxygen p orbital was about 50% that of the ARPES spectra. The reason for this difference in relative magnitude is threefold:

(1) As discussed in Ref. 18, CDAD from atoms arises solely from interference between the $l \rightarrow l + 1$ and $l \rightarrow l - 1$ photoionization channels. Thus, while the magnitude of the ARPES spectra depend roughly on $|\langle p|r|kd \rangle|^2$, the CDAD spectra depend on $|\langle p|r|ks \rangle| \cdot |\langle p|r|kd \rangle|$. By itself, this fact actually makes the relative magnitude of the O atom CDAD spectrum about 75% that of Cs.

(2) CDAD from atoms depends on $\sin(\delta_{l+1} - \delta_{l-1})$ where $\delta_{l+1}, \delta_{l-1}$ are the phase shifts for the $l + 1$ and $l - 1$ photoionization channels, respectively.⁵ This fact favors the

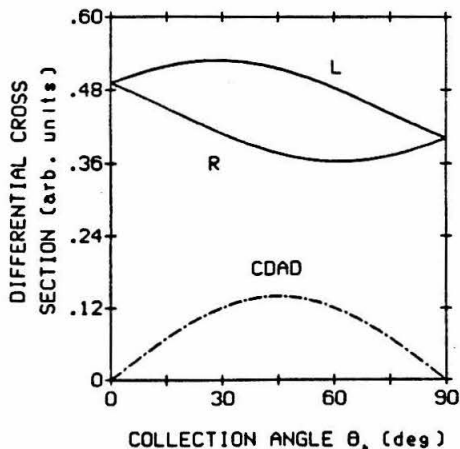


FIG. 5. Differential cross section vs collection angle θ_k for left (L) and right (R) circularly polarized light and CDAD from the $7P_{3/2}$ state of Cs. Alignment created by one-photon absorption $6S_{1/2} \rightarrow 7P_{3/2}$.

magnitude of the O atom CDAD spectrum over that for Cs by a factor of ~ 2 .

(3) The Cs calculation incorporates spin-orbit coupling. The $P_{3/2}$ state is actually a linear combination of $(J,M) = (1,0)$ and $(1,1)$. Photoionization from a $(1,0)$ state has a $\sin 2\theta_k$ dependence, while photoionization from a $(1,1)$ state has the same dependence, but opposite in sign and half the magnitude.⁸ This result is a consequence of the fact that CDAD from an isotropic distribution of states, i.e., equal population of $(1,0)$, $(1,1)$, and $(1-1)$, must vanish¹⁸ and that CDAD spectra for photoionization from the $(1,1)$ and $(1-1)$ states are identical. The net result favors the magnitude of the O atom CDAD spectrum over that for Cs by 4/3.

The three abovementioned factors give rise to the overall factor of 2 between the relative magnitudes of the CDAD spectrum for O atom and Cs when compared to their corresponding ARPES spectra.

As a final note, we point out that the 15%–25% magnitude of all the CDAD spectra shown should not be discouraging. For alignment created by photoabsorption or photofragmentation in which the polarization of the light defines the laboratory frame of the experiment, only the polarization vector must be rotated to vary θ_k —the electron detector need not be moved. In addition, CDAD must vanish for symmetry reasons at $\theta_k = 0$ and $\theta_k = 90^\circ$,¹⁸ and, therefore, the ARPES spectra at these angles for left and right circularly polarized light must be equal. This should make normalization of the left and right ARPES spectra convenient.

CONCLUSIONS

We have demonstrated that CDAD can be used to probe alignment of atomic and molecular states in the gas phase. CDAD exists in the electric dipole approximation without the necessity of spin-orbit coupling. Although we used multiphoton absorption to create alignment, CDAD should be useful in probing alignment created by other means as well. Our results indicate that CDAD is about 15%–25% of ARPES for photoionization of the $A^2\Sigma^+$ state of NO and for photoionization of the $7P_{3/2}$ state of cesium. We believe that the estimated 15%–25% magnitude of CDAD makes

these measurements feasible. Because the ARPES spectra for right and left circularly polarized light can be normalized at $\theta_k = 0^\circ$ and $\theta_k = 90^\circ$ (where CDAD must vanish by symmetry),^{17,18} some of the uncertainties in the experimental data could be eliminated.

ACKNOWLEDGMENTS

This material is based upon research supported by the National Science Foundation Under Grant No. CHE-8218166. The research reported in this paper made use of the Dreyfus-NSF Theoretical Chemistry Computer which was funded through grants from the Camille and Henry Dreyfus Foundation, the National Science Foundation (Grant No. CHE-7820235), and the Sloan Fund of the California Institute of Technology. One of us (R.L.D.) gratefully acknowledges support through a National Science Foundation Graduate Fellowship.

¹See, for example, E. Marinero, C. T. Rettner, and R. N. Zare, *J. Chem. Phys.* **80**, 4142 (1984).

²See, for example, R. Vasudev, R. N. Zare, and R. N. Dixon, *J. Chem. Phys.* **80**, 4863 (1984); I. Nadler, J. Pfab, H. Reisler, and C. Wittig, *ibid.* **81**, 653 (1984); S. Buelow, G. Radhakrishnan, J. Catanzarite, and C. Wittig, *ibid.* **83**, 444 (1985).

³See, for example, A. R. Burns, *Phys. Rev. Lett.* **55**, 525 (1985).

⁴See, for example, G. M. McClelland, G. D. Kubiak, H. G. Rennagel, and R. N. Zare, *Phys. Rev. Lett.* **46**, 831 (1981); F. Frenkel, J. Häger, H. Krieger, H. Walther, C. T. Campbell, G. Ertl, H. Kuipers, and J. Segner, *ibid.* **46**, 152 (1981).

⁵W. Jitschin, S. Osimitsch, H. Reihl, H. Kleinpoppen, and H. O. Lutz, *J.*

Phys. B **17**, 1899 (1984).

⁶P. Franken, K. Sands, and J. Hobart, *Phys. Rev. Lett.* **1**, 118 (1958); R. Novick and H. E. Peters, *ibid.* **1**, 54 (1958).

⁷D. H. Parker, K. K. Chakravorty, and R. B. Bernstein, *J. Phys. Chem.* **85**, 466 (1981).

⁸E. D. Poliakoff, J. L. Dehmer, D. Dill, A. C. Parr, K. H. Jackson, and R. N. Zare, *Phys. Rev. Lett.* **46**, 907 (1981).

⁹(a) C. H. Greene and R. N. Zare, *Annu. Rev. Phys. Chem.* **33**, 119 (1982); *J. Chem. Phys.* **78**, 6741 (1983); (b) R. E. Drullinger and R. N. Zare, *ibid.* **59**, 4225 (1973).

¹⁰R. N. Zare, *Ber. Bunsenges. Phys. Chem.* **86**, 422 (1982).

¹¹S. N. Dixit and V. McKoy, *J. Chem. Phys.* **82**, 3546 (1985).

¹²M. G. White, W. A. Chupka, M. Seaver, A. Woodward, and S. D. Colson, *J. Chem. Phys.* **80**, 678 (1984); W. J. Kessler and E. D. Poliakoff, *ibid.* **84**, 3647 (1986).

¹³See, for example, L. Velluz, M. Legrand, and M. Grosjean, *Optical Circular Dichroism* (Academic, New York, 1965).

¹⁴B. Ritchie, *Phys. Rev. A* **13**, 1411 (1976); **14**, 359 (1976); **14**, 1396 (1976).

¹⁵N. A. Cherepkov, *J. Phys. B* **16**, 1543 (1983).

¹⁶E. A. Power and T. Thirunamachandran, *J. Chem. Phys.* **60**, 3695 (1974); E. A. Power, *ibid.* **63**, 1348 (1975).

¹⁷R. L. Dubs, S. N. Dixit, and V. McKoy, *Phys. Rev. Lett.* **54**, 1249 (1985).

¹⁸R. L. Dubs, S. N. Dixit, and V. McKoy, *Phys. Rev. B* **32**, 8389 (1985).

¹⁹B. Ritchie, *Phys. Rev. A* **12**, 567 (1975).

²⁰R. Parzynski, *Act. Phys. Pol. A* **57**, 49 (1980).

²¹R. R. Lucchese, G. Raseev, and V. McKoy, *Phys. Rev. A* **25**, 2572 (1982).

²²S. N. Dixit, D. L. Lynch, V. McKoy, and W. M. Huo, *Phys. Rev. A* **32**, 1267 (1985).

²³M. E. Rose, *Elementary Theory of Angular Momentum* (Wiley, New York, 1957).

²⁴S. N. Dixit and P. Lambropoulos, *Phys. Rev. A* **27**, 861 (1983).

²⁵J. C. Tully, R. S. Berry, and B. J. Dalton, *Phys. Rev.* **176**, 95 (1968).

²⁶P. J. Brussaard and H. A. Tolhoek, *Physica* **23**, 955 (1957); R. N. Zare (unpublished).

**Chapter 4: Extraction of Alignment Parameters from Circular
Dichroic Photoelectron Angular Distribution (CDAD)
Measurements**

[The text of this chapter appeared in: R. L. Dubs, S. N. Dixit, and
V. McKoy, J. Chem. Phys. **85**, 6267 (1986).]

Extraction of alignment parameters from circular dichroic photoelectron angular distribution (CDAD) measurements

Richard L. Dubs, S. N. Dixit, and V. McKoy
 Arthur Amos Noyes Laboratory of Chemical Physics,^{*)} California Institute of Technology, Pasadena,
 California 91125

(Received 23 June 1986; accepted 28 August 1986)

In a previous paper, we showed that circular dichroism in photoelectron angular distributions (CDAD) can be used to probe alignment in gas phase atoms and linear molecules. Often this alignment is parametrized through the *moments* of alignment $A^{(2)}$, $A^{(4)}$, etc., which are commonly extracted from fluorescence polarization measurements. In this paper we show how these can be simply extracted from CDAD spectra. This technique can be used in principle to extract the moments to *any* order.

INTRODUCTION

Circular dichroism in photoelectron angular distributions (CDAD) involves photoionization with left and right circularly polarized light.¹⁻³ The CDAD spectrum is defined as the difference in the photoelectron angular distributions obtained for these two cases.¹⁻³ Recently we showed that CDAD can be used to probe alignment in gas phase atoms and linear molecules.¹ Alignment can arise in a variety of experimental situations, including photoabsorption,⁴ atom-diatom collisions,⁵ unimolecular processes,⁶ electron stimulated desorption of adsorbed molecules,⁷ and molecular scattering from surfaces.⁸ Often this alignment is parametrized through the *moments* of alignment $A^{(2)}$, $A^{(4)}$, etc., which are commonly extracted from fluorescence polarization experiments.⁹⁻¹² In this paper we show how these moments can be simply extracted from CDAD spectra. As in saturated laser optical pumping experiments,¹³ this technique can be used in principle to extract the moments to *any* order. This feature differs from that of a standard laser-induced fluorescence (LIF) experiment¹² in which $L_{MAX} = 2N + 2$, where N is the number of exciting photons. The reason for this difference is that in the angle-resolved photoionization process the electron can carry away an arbitrary amount of angular momentum from the system whereas in LIF the fluorescence photon can only carry away one unit.

In the experiment we consider here, linearly polarized light is used to pump the molecular sample to an aligned excited state (though we emphasize that CDAD can be used in principle to probe alignment created by any of the above methods). The light is polarized along the z axis of the laboratory frame and propagates along the x axis. After the alignment is created, circularly polarized light (left or right), copropagating with the original pump light, is used to photoionize the sample. The electrons are collected in the plane at *right angles* to the propagation direction of the light (Fig. 1). In our laboratory frame, the angles (θ_p, ϕ_p) for the propagation vector of the circularly polarized light are hence $(90^\circ, 0^\circ)$ and the electron collection angles (θ_k, ϕ_k) are $(\theta_k, 90^\circ)$.

THE ALIGNMENT

Consider a molecule in a $J = 5/2$ state. The state has six magnetic substates, $M_J = +5/2, +3/2, +1/2, -1/2, -3/2, -5/2$. If all the substates are equally populated, the state is considered *isotropic*. However, if the substates with different $|M_J|$ values have different populations, the state is considered *aligned*.¹¹ For example,

$J = 5/2$						
Relative population	0	2	3	3	2	0
M_J	5/2	3/2	1/2	-1/2	-3/2	-5/2

represents an aligned state. As shown in Ref. 1, molecules which are aligned exhibit CDAD.

The CDAD spectrum for a molecule in a given M_J state can be written^{1,14} as

$$I_{M_J}(\theta_k) = Y_{11}(\theta_p, \phi_p) \sum_{L'} \beta_{L'}^{M_J} Y_{L'-1}(\theta_k, \phi_k), \quad (1)$$

where $I(\theta)$ is the CDAD intensity and $Y_{LM}(\theta, \phi)$ is a spherical harmonic. The calculation of the $\beta_{L'}^{M_J}$'s which contain all the dynamical information about the molecule of interest has been described in Ref. 1. (Here $\beta_{L'}^{M_J} = 2\sqrt{2}\beta_{L'11}^{M_J}$ of Ref. 1.) The details are not of interest here. The important point is that each M_J substate has a *different* CDAD spectrum (Fig. 2 of Ref. 1). The CDAD spectrum for an arbitrary alignment will be a sum of the spectra for given M_J 's weighted by the relative population of each substate:

$$I(\theta_k) = \sum_{M_J} N_{M_J} I_{M_J}(\theta_k), \quad (2)$$

where N_{M_J} represents the relative populations of the substates.¹⁵ These N_{M_J} 's are the values of interest for they contain all the alignment information. At this point, to extract the N_{M_J} 's, one would have to calculate the CDAD spectrum for each M_J and determine by fit which linear combination of spectra reproduces the experimental spectrum. We will now discuss a much cleaner method to determine the alignment.

As an alternative to the N_{M_J} description of alignment, we can express the alignment in a "spherical" basis¹¹:

$$N_{M_J} = \sum_L A^{(L)} T_L^{M_J}. \quad (3)$$

^{*)} Contribution No. 7422.

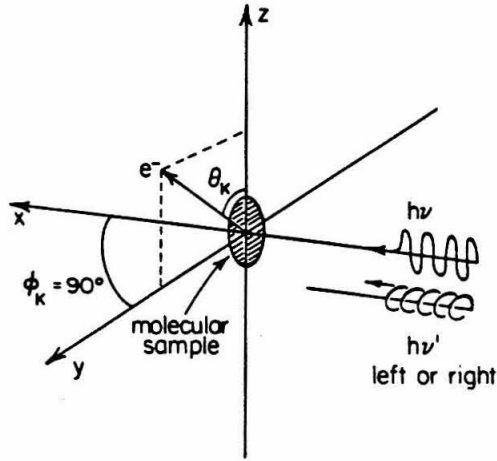


FIG. 1. Experimental configuration for measurement of CDAD spectra.

- 1) Creation of Alignment
- 2) Probe of Alignment

Here the $A^{(L)}$ are the state multipole moments of the alignment ($A^{(0)}$ is the monopole moment, $A^{(1)}$ is the dipole moment, etc.). The $T_L^{M_j}$ are spherical tensor operators defined as¹¹

$$T_L^{M_j} = (-1)^{J-M_j} \langle JJM_j - M_j | L 0 \rangle, \quad (4)$$

where $\langle JJM_j - M_j | L 0 \rangle$ is a Clebsch-Gordan coefficient. For example, for $J = 5/2$,

$$\begin{aligned} T_0 &= \left(\frac{1}{\sqrt{6}}\right) \times 1 & 1 & 1 & 1 & 1 & 1, \\ T_1 &= \left(\frac{1}{\sqrt{70}}\right) \times 5 & 3 & 1 & -1 & -3 & -5, \\ T_2 &= \left(\frac{1}{\sqrt{84}}\right) \times 5 & -1 & -4 & -4 & -1 & 5, \\ T_3 &= \left(\frac{1}{\sqrt{180}}\right) \times 5 & -7 & -4 & 4 & 7 & -5, \\ T_4 &= \left(\frac{1}{\sqrt{28}}\right) \times 1 & -3 & 2 & 2 & -3 & 1, \\ T_5 &= \left(\frac{1}{\sqrt{252}}\right) \times 1 & -5 & 10 & -10 & 5 & -1, \\ M_j &= & 5/2 & 3/2 & 1/2 & -1/2 & -3/2 & -5/2 \end{aligned}$$

For any distribution of N_{M_j} , an equivalent linear combination of $T_L^{M_j}$ can be found to describe the distribution. Because the $T_L^{M_j}$ are known, a knowledge of all $A^{(L)}$ is equivalent to a knowledge of all N_{M_j} .

The advantage of using the $T_L^{M_j}$ can be seen as follows. Substitution of Eqs. (1) and (3) into Eq. (2):

$$\begin{aligned} I(\theta_k) &= Y_{11}(\theta_p, \phi_p) \sum_L A^{(L)} \sum_{M_j} T_L^{M_j} \\ &\times \sum_{L'} \beta_{L'}^{M_j} Y_{L'-1}(\theta_k, \phi_k). \end{aligned} \quad (5)$$

On performing the sum over M_j in the above equation, one

obtains $L = L'$. Then

$$I(\theta_k) = Y_{11}(\theta_p, \phi_p) \sum_L A^{(L)} \bar{\beta}_L Y_{L-1}(\theta_k, \phi_k) \quad (6)$$

with

$$\bar{\beta}_L = \sum_{M_j} T_L^{M_j} \beta_L^{M_j}. \quad (7)$$

Equation (7) requires that only even L will contribute to CDAD. This result arises because $\beta_L^{M_j} = 0$ for L odd. Thus, CDAD only provides $A^{(2)}, A^{(4)}, A^{(6)}$, etc. CDAD from $A^{(0)}$, which represents equal population of all M_j levels, vanishes because this distribution lacks any alignment.¹

In an actual experiment, the photon direction (θ_p, ϕ_p) and the electron collection plane (ϕ_k) are both fixed. We will now specialize, Eq. (6) to the experimental configuration described earlier, i.e., $(\theta_p, \phi_p) = (90^\circ, 0^\circ)$ and $\phi_k = 90^\circ$. Then

$$I(\theta_k) = \sum_L A^{(L)} \bar{\beta}_L P_L^1(\cos \theta_k), \quad (8)$$

where

$$\bar{\beta}_L = \frac{i}{4\pi} \left[\frac{3(2L+1)}{2L(L+1)} \right]^{1/2} \bar{\beta}_L. \quad (9)$$

In Eq. (8), $P_L^1(\cos \theta)$ is an associated Legendre polynomial. The imaginary factor "i" in Eq. (9) is a necessary result since, as pointed out in Ref. 1, the $\beta_L^{M_j}$ are pure imaginary and $I(\theta_k)$ must be real. Equation (8) is the key result of this paper. It shows that the quadrupole moment of the alignment $A^{(2)}$ will make a $P_2^1(\cos \theta_k)$ contribution to the shape of the CDAD spectra, the hexadecapole moment a $P_4^1(\cos \theta_k)$ contribution, and so on. The relative weights of these contributions depend on the molecular details of the problem. From the orthogonality of the P_L^1 , the moments of

the alignment can be written as

$$A^{(L)} \bar{\beta}_L = \frac{(2L+1)}{2(L+1)(L)} \int_0^\pi I(\theta_k) \times P_L^1(\cos \theta_k) \sin \theta_k d\theta_k \quad (10)$$

$$= \frac{(2L+1)}{(L+1)(L)} \int_0^{\pi/2} I(\theta_k) \times P_L^1(\cos \theta_k) \sin \theta_k d\theta_k, \quad (11)$$

where Eq. (11) follows from Eq. (10) because L is even as described earlier.

Using Eq. (11), the alignment parameters $A^{(L)}$ (L even) can be easily obtained once the $\bar{\beta}_L$ are known.¹⁶ These $\bar{\beta}^L$ can be calculated in a straightforward way by *ab initio* methods.¹⁻³ Alternatively, if the molecules can be prepared in a state of *known* alignment (i.e., known $A^{(L)}$), the $\bar{\beta}_L$ can be experimentally determined. These values can then be used to probe unknown alignments. Note that Eq. (11) puts no upper limit on the value of L .

ACKNOWLEDGMENTS

This material is based upon research supported by the National Science Foundation under Grant No. CHE-8521391. The research reported in this paper made use of the Dreyfus-NSF Theoretical Chemistry Computer which was funded through grants from the Camille and Henry Dreyfus Foundation, the National Science Foundation (Grant No. CHE-7820235), and the Sloan Fund of the California Institute of Technology. One of us (R.L.D.) gratefully acknowledges support through a National Science Foundation Graduate Fellowship.

¹R. L. Dubs, S. N. Dixit, and V. McKoy, *J. Chem. Phys.* **85**, 656 (1986).

²R. L. Dubs, S. N. Dixit, and V. McKoy, *Phys. Rev. Lett.* **54**, 1249 (1985).

³R. L. Dubs, S. N. Dixit, and V. McKoy, *Phys. Rev. B* **32**, 8389 (1985).

⁴R. N. Zare, *Ber. Bunsenges. Phys. Chem.* **86**, 422 (1982); S. N. Dixit and V. McKoy, *J. Chem. Phys.* **82**, 3546 (1985); M. G. White, W. A. Chupka, M. Seaver, A. Woodward, and S. D. Colson, *ibid.* **80**, 678 (1984); W. J. Kessler and E. D. Poliakov, *ibid.* **84**, 3647 (1986).

⁵See, for example, E. Marinero, C. T. Rettner, and R. N. Zare, *J. Chem. Phys.* **80**, 4142 (1984).

⁶See, for example, R. Vasudev, R. N. Zare, and R. N. Dixon, *J. Chem. Phys.* **80**, 4863 (1984); I. Hadler, J. Pfab, H. Reisler, and C. Wittig, *ibid.* **81**, 653 (1984); S. Beulow, G. Radhakrishnan, J. Catanzarite, and C. Wittig, *ibid.* **83**, 444 (1985).

⁷See, for example, A. R. Burns, *Phys. Rev. Lett.* **55**, 525 (1985).

⁸See, for example, G. M. McClelland, G. D. Kubiak, H. G. Rennagel, and R. N. Zare, *Phys. Rev. Lett.* **46**, 831 (1981); F. Frenkel, J. Häger, H. Krieger, H. Walther, C. T. Campbell, G. Ertl, H. Kuipers, and J. Segner, *ibid.* **46**, 152 (1981).

⁹(a) U. Fano and J. H. Macek, *Rev. Mod. Phys.* **45**, 553 (1973); (b) D. A. Case, G. M. McClelland, and D. R. Herschbach, *Mol. Phys.* **35**, 541 (1978).

¹⁰G. E. Hall, N. Sivakumar, and P. L. Houston, *J. Chem. Phys.* **84**, 2120 (1986).

¹¹C. H. Greene and R. N. Zare, *Annu. Rev. Phys. Chem.* **33**, 119 (1982).

¹²C. H. Greene and R. N. Zare, *J. Chem. Phys.* **78**, 6741 (1983).

¹³U. Hefter, G. Ziegler, A. Mattheus, A. Fischer, and K. Bergmann, *J. Chem. Phys.* **85**, 286 (1986).

¹⁴Generally, one must take the real part of the right-hand side of Eq. (1). However, in this letter we only consider cases for which $\sin(\phi_k - \phi_p) = \pm 1$, i.e., right angle collection—the configuration for which CDAD is a maximum. For this case, Eq. (1) is correct as it stands.

¹⁵These N_{MJ} are normalized such that $\sum_{MJ} N_{MJ} = 1$ for any value of J .

¹⁶U. Hefter *et al.* (Ref. 13) have found, using saturated laser optical pumping, that for highly aligned molecules, direct solution of an equation similar to Eq. (8) (as a set of linear equations for different values of θ_k) is numerically more stable than integration [Eq. (11)]. They find integration preferred, however, if only a few moments are necessary to characterize the alignment.

**Chapter 5: Circular Dichroism in Photoelectron Angular
 Distributions from Two-Color (1+1) REMPI of NO**

[The text of this chapter appeared in: J. R. Appling, M. G. White, R.
L. Dubs, S. N. Dixit and V. McKoy, J. Chem. Phys. **87**, 6927 (1987).]

Circular dichroism in photoelectron angular distributions from two-color (1+1) REMPI of NO

J. R. Appling^{a)} and M. G. White

Department of Chemistry, Brookhaven National Laboratory, Upton, New York 11973

R. L. Dubs

Arthur Amos Noyes Laboratory of Chemical Physics,^{b)} California Institute of Technology, Pasadena, California 91125

S. N. Dixit

Lawrence Livermore National Laboratory, L401, P.O. Box 808, Livermore, California 94550

V. McKoy

Arthur Amos Noyes Laboratory of Chemical Physics,^{b)} California Institute of Technology, Pasadena, California 91125

(Received 13 August 1987; accepted 10 September 1987)

A detailed experimental and theoretical study of dichroic effects in photoelectron angular distributions is reported for (1 + 1), two-color REMPI of NO via the $A^2\Sigma^+$, $v = 0$ state. Optically aligned A state rotational levels are probed through ionization by circularly polarized light. Resultant photoelectron angular distributions exhibit significant left-right asymmetry, the phase and magnitude of which are shown to be related to the curvature of the excited state M_J distribution. Theoretical calculations involving a full *ab initio* treatment of the ionization dynamics result in circularly dichroic angular distribution (CDAD) parameters in good agreement with those derived experimentally. Additional effects including hyperfine depolarization and coherence are also discussed in relation to the observed CDAD data.

I. INTRODUCTION

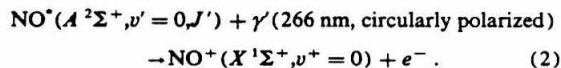
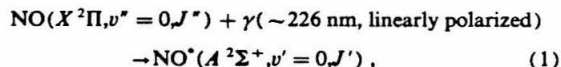
An ($n + m$) resonantly enhanced multiphoton ionization (REMPI) process can be perceived as an m -photon ionization out of an aligned/oriented excited state created by the n -photon optical excitation. Atomic and molecular states can also be aligned by a variety of other methods including external fields,^{1,2} particle excitation,³ surface scattering,⁴ photodissociation,⁵ etc. In conventional methods for probing the state alignment, the anisotropy of either the fluorescence emitted by the state itself or the laser induced fluorescence (LIF) out the state is observed.⁶ More recently, a (1 + 1) REMPI technique based on angle integrated cross sections has also been developed to probe ground state alignment.⁷

Recently, the photoelectron angular distributions resulting from ionization out of an aligned state have been shown to exhibit a dichroic behavior; i.e., electron angular distributions from aligned target states are different for photoionization with left or right circularly polarized light. This circular dichroism in angular distributions (CDAD) exists for nonchiral molecules, persists at the electric dipole approximation level, and is a direct signature of the state alignment. Predictions were made for the magnitude of the CDAD signal for adsorbed atoms and molecules,^{8,9} and also for gas-phase atoms and molecules whose state alignment is created by the absorption of linearly polarized photons.¹⁰ The first experimental demonstration of CDAD was recently reported.¹³

These theoretical and experimental CDAD studies have

illustrated the magnitude of the effect and raise the possibility of employing CDAD as a technique for extracting the alignment of the initial state of the system.¹² There are two features that strengthen this possibility. First is the factorization of the photoionization matrix elements out of the CDAD expressions and second is the ease of backtransforming the alignment of the resonant state to that of the initial state in an (n linear + 1 circular)-type CDAD experiment.

As a prelude to this application, we have carried out an experimental and theoretical CDAD study of excitation-induced alignment of NO in (1 + 1) REMPI via the $A^2\Sigma^+$, $v = 0$ state. The two-color photoionization process utilized in this work can be expressed as a pump-probe sequence as follows:



The pump radiation in process (1) is tuned to induce known rotational transitions and produce aligned populations of A state $|J'M_J\rangle$ substates (M_J is the space-fixed projection of total angular momentum J'). This alignment is detected through subsequent ionization of A state molecules with fixed-frequency, circularly polarized probe laser radiation. Photoelectron angular distributions are a measure of the photoelectron intensity variation as a function of the angle between the linear polarization vector of the pump beam and the electron detection axis. Circular dichroism in photoelectron angular distributions (CDAD) is determined as the difference between photoionizations carried out using left-

^{a)} Present address: Department of Chemistry, University of Kentucky, Lexington, KY 40506-0055.

^{b)} Contribution No. 7642.

and right-handed circularly polarized probe radiation.

II. EXPERIMENTAL

As shown schematically in Fig. 1, circular dichroism measurements require a pump-probe arrangement of two laser beams with independently controllable polarizations. The tunable laser radiation used for the excitation (pump) step was obtained by nonlinear mixing (Quanta Ray WEX) of the frequency doubled output from a dye laser (Quanta Ray PDL) with residual IR photons from the pulsed (20 Hz) Nd:YAG pump laser (Quanta Ray DCR). Output powers of up-mixed dye laser radiation at 226 nm are typically in the range 0.5–1.5 mJ/pulse using a mixture of R590 and R610 laser dyes (Exciton) in a ratio of approximately 10:1. The ionization (probe) laser beam is generated simultaneously by the same laser system. A 5% beam splitter inserted into the dye laser directs a portion of the 532 nm Nd:YAG output through telescopic optics to a frequency doubling crystal cell (in rad) which produces a beam at 266 nm with powers in the range 1–2 mJ/pulse.

Both laser beam outputs are linearly polarized greater than 95%; however, each beam passes through a Glan polarizing prism to ensure 100% polarization purity before the polarization vectors are modified further. The polarization vector of the tunable dye laser radiation is rotated with a Soleil-Babinet (Karl Lambrecht) compensator tuned to 1/2 wave retardation at the wavelength of interest. The probe laser beam is passed through a 1/4 wave plate (CVI) which converts linearly polarized 266 nm radiation to circularly polarized radiation when the axis of the 1/4 wave plate is at an angle of 45° with respect to the incoming polarization vector. The axis of the 1/4 wave plate can occupy two inequivalent positions corresponding to production of opposite-handed circular polarization designated "left" and "right." The pump beam is admitted to the photoelectron spectrometer chamber unfocused and the counterpropagating probe

beam is focused through a 250 nm focal length lens mounted on a translation stage to allow adjustable beam overlap for maximum two-color (1 + 1) REMPI signal.

A complete description and illustration of the photoelectron spectrometer system can be found in Ref. 14. In the present investigation, two different sample introduction methods were utilized to admit nitric oxide target molecules to the interaction region of the spectrometer system. To reduce the congestion of the A state ($v = 0$) rotational spectrum, angular distribution measurements were performed on rotationally "cold" NO produced by high pressure expansions (40 psi) of a 4% mixture of NO (Matheson, 99.6% purity) in argon. The chamber pressure was typically 0.6– 1.5×10^{-5} Torr for pulsed molecular beam valve (Newport Corp. BV 1000) operation in the PES apparatus. The NO/Ar gas pulses enter the interaction region at right angles to both the propagation direction of the laser and the detector axis of the spectrometer flight tube. Measurements for transitions of high J'' or of $^2\Pi_{3/2}$ ground state (P_{12} branch) molecules were performed with neat, room temperature NO gas samples admitted through an effusive nozzle (70 μm diameter) attached below the interaction region and facing the 1.5 mm aperture entrance to the PES flight tube.

Circular dichroism measurements of photoelectron angular distributions are the result of the difference between an experiment performed with the probe laser converted to left-handed polarization and a subsequent scan taken with right-handed circular polarization. Photoelectrons ejected at right angles to the counterpropagating pump/probe laser beams were collected ($\sim 1 \times 10^{-3}$ sr) as a function of the angle (θ) between the linear polarization vector of the pump beam and the detector axis of the TOF spectrometer. A photodiode triggered by the dye laser pulse provides a time zero for the photoelectron time of flight. The TOF photoelectron spectrum presented in Fig. 2 shows the relative amounts of two-color (1 + 1) and one-color (1 + 1) ionization when the dye laser polarization is parallel to the detector axis. The

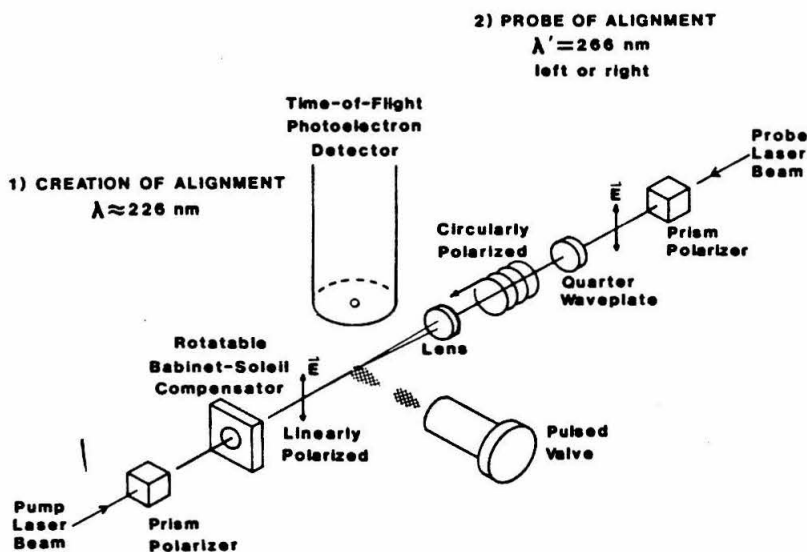


FIG. 1. Schematic of the experimental setup. Individual components described in the text.

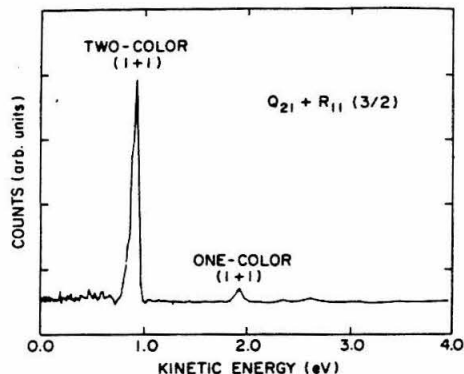


FIG. 2. Photoelectron spectrum resulting from (1 + 1), one- and two-color REMPI of NO via the $Q_{21} + R_{11}(3/2)$ rotational branch of the $A, v' = 0 \leftarrow X, v'' = 0$ transition. Both laser beams were linearly polarized with their polarization directions at $\theta = 0^\circ$. The difference in kinetic energies between the photoelectron peaks correspond to the energy difference between the 266 (two-color) and 226.3 nm (one-color) ionizing photons.

Rydberg character of the A state is manifested by the existence of a single photoelectron peak corresponding to production of $v^+ = 0$ states of the NO^+ ion. Thus, the angular dependence is determined by monitoring the REMPI photoelectrons in the two-color $v^+ = 0$ channel for a specific rotational transition as a function of pump laser polarization angle determined by the Soleil-Babinet compensator. Data was accumulated for 50 laser shots for each angle incremented by 10° during 12 scans of 360° . Collection of the digitized output of the multichannel plate photoelectron detector and control of Soleil-Babinet stage rotations were accomplished through the use of CAMAC modules (Kinetic Systems 3912 Crate Controller, LeCroy 8828 Transient Recorder, Kinetic Systems 3112 12-bit DAC) interfaced to a PDP 11/73 minicomputer.

Angular scans were taken under similar conditions for both left- and right-handed probe polarizations. The first and last 180° segments of the 360° scans were averaged, three-point smoothed and normalized to the cross section at 90° before the difference was taken between left- and right-handed data. The resultant CDAD curves were fit analytically to associated Legendre polynomials to extract coefficients indicative of the excited state alignment.

III. THEORY

A. Alignment

In the present experiment, the ground state molecules are distributed isotropically, i.e., all the M_J sublevels for a given J'' level have the same population. However, after one photon absorption of linearly polarized light, the substates of different values of $|M_J|$ acquire different populations, resulting in an "aligned" excited state.⁶ The details of this alignment depend on the excitation branch (P , Q , or R) and are reflected qualitatively by the sign of the state multipole moment A_2 (Fig. 3). Note that a $J' = 1/2$ state cannot support any alignment ($A_2 = 0$) since the $M_J = 1/2$ and

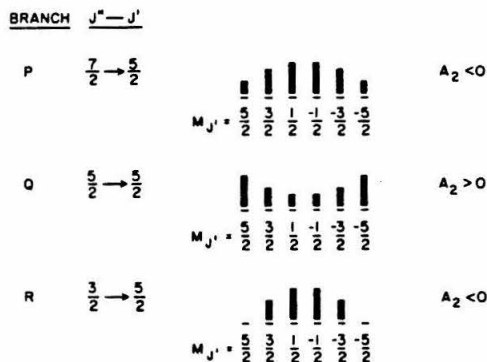


FIG. 3. Relative M_J population distributions for an upper $J' = 5/2$ level populated via one-photon P , Q , and R transitions. A_2 is the quadrupole moment of the alignment as described in the text.

$M_J = -1/2$ sublevels will always have the same population. For one photon excitation from an isotropic initial state with linearly polarized light, the relative populations $N(M_{J'})$ of the excited state are given by¹⁵

$$N(M_{J'}) \propto \begin{pmatrix} J' & 1 & J'' \\ M_{J'} & 0 & -M_{J'} \end{pmatrix}^2, \quad (3)$$

where J'' represents the total angular momentum of the initial state and J' that of the excited state. The conversion from the $N(M_{J'})$ description of alignment to that of A_L is straightforward.⁶

B. CDAD

The CDAD intensity, defined as $I_{\text{CDAD}}(\theta) = I_{\text{LEFT}}(\theta) - I_{\text{RIGHT}}(\theta)$, is given by¹¹

$$I_{\text{CDAD}}(\theta) = \sum a_L P_L^1(\cos \theta), \quad (4a)$$

where

$$a_L = A_L \bar{\beta}_L. \quad (4b)$$

A_L are the state multipole moments of the alignment for the resonant state, $P_L^1(\cos \theta)$ are associated Legendre polynomials, and θ is the angle between the pump photon polarization vector and the electron collection direction. All information concerning the photoionization dynamics are incorporated in $\bar{\beta}_L$. The fact that the moment index L of the alignment (A_L) is the same as that for the photoelectron ($\bar{\beta}_L$) is unique to CDAD and is not true for typical photoelectron angular distributions. It is this fact that makes CDAD so useful for studying alignment.

In general, the alignment of a state is characterized by even moments A_0, A_2, A_4 , etc. However, for one photon excitation from an unaligned ground state, only A_0 and A_2 are nonzero. Since A_0 does not contribute to the alignment (A_0 relates only to the total population of the state⁶) the CDAD intensity reduces to

$$I_{\text{CDAD}}(\theta) = A_2 \bar{\beta}_2 P_2^1(\cos \theta) \quad (5a)$$

$$= \frac{1}{2} A_2 \bar{\beta}_2 \sin 2\theta. \quad (5b)$$

The J dependence of $\bar{\beta}_L$ can be factored out as

$$\bar{\beta}_L(J') = X_L(J') \cdot \bar{\beta}_L, \quad (6)$$

where $\bar{\beta}_L$ is explicitly independent of J' ; it depends on J' only through the variation of the cross section with the photoelectron kinetic energy. Because rotational spacings are small, we can ignore this latter dependence and treat $\bar{\beta}_L$ as a constant. $X_2(J')$ has a simple expression in J' , the value of which quickly approaches a high J' limit of $-\sqrt{(J'/2)}$.¹⁶ The important point here is that all $\bar{\beta}_L$ (for any value of J') have the same sign, so that any change in the sign of $A_2\bar{\beta}_2$ is due to a change in the sign of the moment A_2 (ignoring coherence effects).

C. Normalization of the CDAD spectra

The experimental and theoretical values of $A_2\bar{\beta}_2$ presented in this work are all normalized by dividing the raw value by the intensity of the left or right spectrum at 90° [$I_{L,R}(90^\circ)$]. In this way the relative magnitude of the CDAD signal to the left or right photoionization signal can be obtained. However, the photoionization dynamics and alignment are intimately entangled in the value of $I_{L,R}(90^\circ)$. (The alignment dependence can be seen in Fig. 2 of Ref. 10.) Nevertheless, a semiquantitative statement can be made about the trends in the $A_2\bar{\beta}_2$ values reported in this fashion. The value of $I_{L,R}(90^\circ)$ can be written

$$I_{L,R}(90^\circ) = c_0 A_0 + c_2 A_2, \quad (7)$$

where c_0 and c_2 depend on the photoionization dynamics and on J' . Generally, the leading term $c_0 A_0$ dominates the expression and so we can write

$$I_{L,R}(90^\circ) \sim c_0 A_0 \quad (8)$$

from which it follows that

$$\frac{A_2\bar{\beta}_2}{I_{L,R}(90^\circ)} \propto \left[\frac{(2J' - 1)(2J' + 3)}{J'(J' + 1)} \right]^{1/2} \cdot \frac{A_2}{A_0}, \quad (9)$$

where the explicit J' dependent part of the above expression is that for the ratio $(\bar{\beta}_2/c_0)$.¹⁶ Indeed, if one plots the theoretical values of the left-hand side of Eq. (9) vs those of the right-hand side for all the clean branches given in this paper, a graph very close to a straight line is obtained (Fig. 4). Note that this approximation cannot be applied to the mixed branches. For one photon excitation with linearly polarized light from an unaligned initial state the following relations hold:

P branch:

$$\frac{A_2}{A_0} = - \left[\frac{(2J'' - 3)(J'' - 1)}{5(2J'' + 1)J''} \right]^{1/2}; \quad (10)$$

R branch:

$$\frac{A_2}{A_0} = - \left[\frac{(2J'' + 5)(J'' + 2)}{5(2J'' + 1)(J'' + 1)} \right]^{1/2}. \quad (11)$$

The right-hand side of Eq. (9) is directly proportional to the alignment parameter $A_0^{(2)}$ commonly used in LIF studies.^{5,6}

D. Coherence

Mixed branches such as $Q_{21} + R_{11}$ offer two indistinguishable pathways (within the resolution of this experiment) to ionization. In addition to direct contributions to

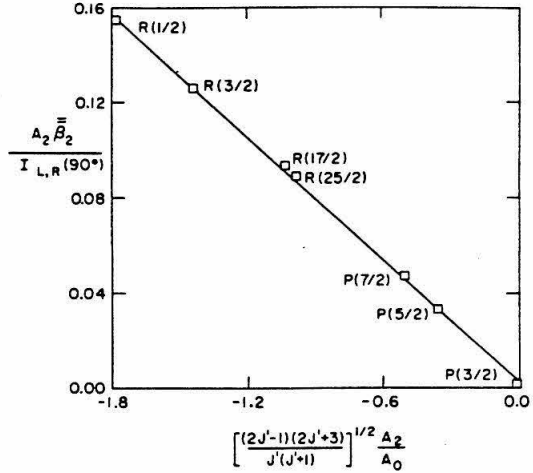


FIG. 4. Graphical representation of the direct relationship between the CDAD intensity normalized at $\theta = 90^\circ$ and the relative moments of the excited state alignment for one photon excitation with linearly polarized light [see Eq. (9) in the text].

the photoelectron signal by each branch individually, a coherent contribution arising from interference between the pathways can also contribute to the signal. The transition probability then involves a *coherent* sum over these two paths

Transition probability

$$= |R_{\text{path}} + Q_{\text{path}}|^2 \quad (12a)$$

$$= |R_{\text{path}}|^2 + |Q_{\text{path}}|^2 + 2 \text{Re}(R_{\text{path}} Q_{\text{path}}^*), \quad (12b)$$

where the last term in Eq. (12b) represents the interference of the R and Q excitation paths. Whether or not this coherence contributes depends on the energy splitting ΔE between the unresolved intermediate states. The coherence lifetime ($\tau_{\text{coh}} = \hbar/\Delta E$) associated with this splitting must be longer than the apparent "lifetime" of the state (in this case the excited state is ionized within the laser pulse duration ~ 10 ns). If τ_{coh} is shorter than this time, the coherence dies away before the intermediate state is probed.

E. Calculations

The details for obtaining the value of $A_2\bar{\beta}_2$ are given in Refs. 10 and 11. The calculations "with hyperfine" include long-time limit, average hyperfine depolarization as described in Ref. 6. For mixed branches, the spectra for the individual branches are weighted by the relative line strengths given in Ref. 17. The coherence effects are treated in the two extreme limits; one in which complete coherence persists and the other wherein the coherence is time averaged out.

IV. RESULTS AND DISCUSSION

The CDAD results obtained in this investigation of two-color (1 + 1) photoionization of NO are shown in Figs. 5-7

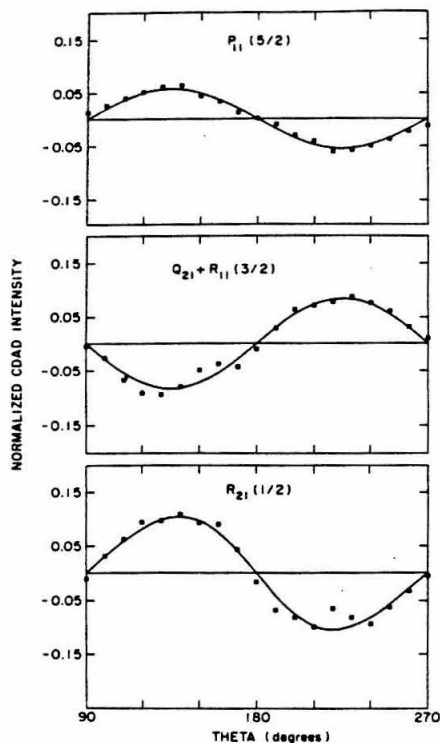


FIG. 5. Experimental CDAD for three rotational transitions which lead to $J' = 3/2$ [$Q_{21}(3/2)$ contribution dominates the $R_{11}(3/2), J' = 5/2$ component]. ■ Experimental data; - - - least-squares fit to Eq. (5).

and summarized in Table I. The alignment parameters $A_2\bar{\beta}_2$ listed Table I for each transition are extracted as coefficients of an analytical least-squares fit of the angular distribution data to the associated Legendre polynomials series of Eq. (4a). The coefficients are normalized to the intensity of the left or right spectrum at 90° . Coefficient errors listed are statistical errors determined by the analytical fit and do not

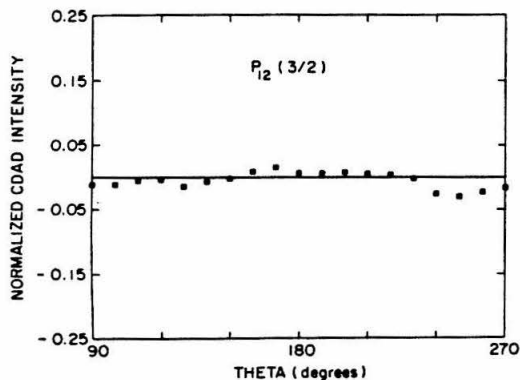


FIG. 6. Experimental CDAD for the $P_{12}(3/2)$ rotational transition leading to the isotropic $J' = 1/2$ level. ■ Experimental data; - - - least-squares fit to Eq. (5).

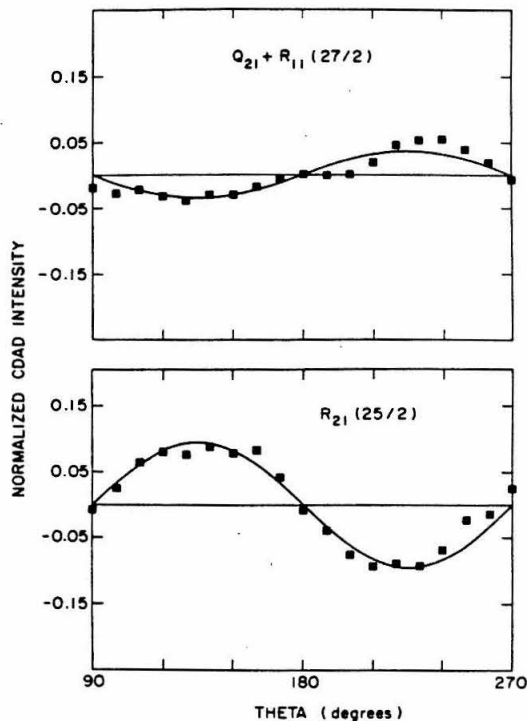


FIG. 7. Experimental CDAD for two rotational transitions leading to high J' . ■ Experimental data; - - - least-squares fit to Eq. (5).

represent confidence level or reproducibility.

Theoretical values for $A_2\bar{\beta}_2$ are also listed in Table I. The "theory with hyperfine" values have been calculated for low J only since hyperfine effects are negligible at higher J .⁶ These latter values represent the average depolarization one would expect in the long-time limit. However, in these experiments the excited molecules are ionized after 5–10 ns. Because the hyperfine precession occurs on the same time scale,¹⁸ a rigorous investigation of the extent of depolarization would require a more sophisticated dynamical treatment. The theory with hyperfine values then should be interpreted as long time limit values which would be completely attained if the time delay between pump and probe laser pulses was increased.

The phases of the experimental and theoretical $A_2\bar{\beta}_2$ are clearly branch dependent as seen in Table I. Because $A_2\bar{\beta}_2$ values for the mixed branches are opposite in sign from the clean P and R branches, the experimental data indicate that the mixed branches are dominated by the Q component, a fact which is supported by calculation [the anomalous $Q_{21} + R_{11}(1/2)$ result will be addressed later]. The opposite phase for the Q branch is most clearly seen in Fig. 5, in which all three spectra arise from the same $J' = 3/2$ intermediate state. This opposite phase for the Q branch is a direct result of the opposite alignment shown in Fig. 3.

In terms of the magnitudes of the $A_2\bar{\beta}_2$ values, the experimental data fall into two groups relative to the theoretical values. The first group is comprised of the low J' values,

TABLE I. Summary of results for experimental and theoretical CDAD parameters for (1 + 1), two-color REMPI of NO through various rotational transitions.

Branch	J''	Experiment ^a $A_2\bar{\beta}_2$	Theory $A_2\bar{\beta}_2$	Theory with hyperfine ^b $A_2\bar{\beta}_2$
P_{11}	3/2	+ 0.004(0.005)	0	0
P_{11}	5/2	+ 0.038(0.005)	+ 0.033	+ 0.010
P_{11}	7/2	+ 0.036(0.006)	+ 0.047	+ 0.029
P_{12}	3/2	- 0.001(0.003)	0	0
P_{12}	5/2	+ 0.035(0.002)	+ 0.033	+ 0.010
P_{12}	7/2	+ 0.028(0.004)	+ 0.047	+ 0.029
$Q_{11} + P_{21}$	31/2	- 0.060(0.004)	- 0.136	
$Q_{11} + P_{21}$	33/2	- 0.069(0.003)	- 0.137	
$Q_{21} + R_{11}$	1/2	- 0.050(0.008)	+ 0.054 ^c	+ 0.016
$Q_{21} + R_{11}$	3/2	- 0.056(0.008)	- 0.034 ^d	+ 0.006
$Q_{21} + R_{11}$	27/2	- 0.024(0.002)	- 0.032	
R_{21}	1/2	+ 0.070(0.003)	+ 0.155	+ 0.048
R_{21}	3/2	+ 0.069(0.004)	+ 0.126	+ 0.078
R_{21}	17/2	+ 0.058(0.003)	+ 0.093	
R_{21}	25/2	+ 0.063(0.003)	+ 0.089	

^aNormalized to the differential cross section at $\theta = 90^\circ$. Tabulated coefficients represent averages determined from all experiments performed on each line. Errors given in parentheses only represent the statistical accuracy of the parameters extracted from the fitting procedure.

^bOnly calculated for low J'' .

^c- 0.182 with coherence.

^d- 0.139 with coherence.

which lie in general between the theoretical values with and without hyperfine depolarization. For the $P_{11}(3/2)$ and $P_{12}(3/2)$ branches, which both access a $J' = 1/2$ intermediate state, $A_2\bar{\beta}_2$ is found to be zero within experimental error since this intermediate state cannot support any alignment. The experimental CDAD spectrum for the $P_{12}(3/2)$ branch is shown in Fig. 6. It is apparent from Table I and Fig. 5 that the $A_2\bar{\beta}_2$ values for the P branches are smaller than those for R branches. It should also be noted that in the weak field regime, the clean $P_{11}(J'')$ and $P_{12}(J'')$ branches yield identical CDAD which reflects the independence of the A_2/A_0 on the fine structure component of the ground state. These results are predicted by Eqs. (10) and (11).

The second group of data is comprised of high J'' results in which the experimental $A_2\bar{\beta}_2$ values are systematically lower than the theoretical values. The origin of this quantitative discrepancy is not clear at this time. Nevertheless, both the experimental and theoretical results indicate that the $Q_{21} + R_{11}(27/2)$ $A_2\bar{\beta}_2$ value is much lower than the other values at high J'' . The reason for this result is straightforward. The $R_{21}(17/2)$ and $R_{21}(25/2)$ branches are "clean" excitations while the $Q_{11} + P_{21}(31/2)$ and $Q_{11} + P_{21}(33/2)$ excitations have a Q component with a line strength roughly five times that of the P component.¹⁷ The Q and R components of the $Q_{21} + R_{11}(27/2)$ transition, on the other hand, have roughly the same line strengths.¹⁷ Because Q and R branches have opposite CDAD phases, the CDAD spectrum for this mixed branch is almost completely annihilated, with a small amount of R character surviving. CDAD spectra for the $Q_{21} + R_{11}(27/2)$ and $R_{21}(25/2)$ lines are shown in Fig. 7.

The most surprising $A_2\bar{\beta}_2$ value obtained is that for the

$Q_{21} + R_{11}(1/2)$ transition. The experimental phase is opposite that of theory. For this mixed line, the Q component accesses $J' = 1/2$ in the intermediate state while the R component accesses $J' = 3/2$. The Q component cannot contribute directly to CDAD since it leads to a $J' = 1/2$ upper state which cannot support any alignment. For this reason, one would predict the $Q_{21} + R_{11}(1/2)$ line to have an $A_2\bar{\beta}_2$ value with the same phase as the clean R branches. However, experimentally the opposite phase is found. Various experimental conditions were changed in an attempt to eliminate possible artifacts which could give rise to this reverse phase effect, e.g., laser pulse duration (10 to 2 ns), laser beam intensities, focal volumes, and external fields. Under all conditions the CDAD remained unchanged. A linear dependence of the integrated two-color (1 + 1) photoelectron signal on pump laser power also verified that the measurements were not made in a saturated power regime.

We attribute the anomalous CDAD phase to coherent excitation of the intermediate state. The coherent lifetime τ_{coh} associated with the $J' = 1/2, 3/2$ energy splitting is approximately ~ 45 ns. Clearly, coherence can survive the time delay between excitation and ionization. Therefore, while the Q component of the $Q_{21} + R_{11}(1/2)$ branch cannot contribute *directly* to the CDAD spectrum, it can contribute by interfering with the R component. The interference contribution in Eq. (12) is calculated to have the opposite phase and a larger magnitude than the direct R contribution as indicated in Table I.

As J' increases the splitting between the energy levels increases and τ_{coh} decreases. For $N = 1, J' = 3/2, 5/2$, τ_{coh} is found to be ~ 27 ns. In this case, coherence can contribute to the $Q_{21} + R_{11}(3/2)$ transition, although the Q contribu-

tion is already dominant without coherence. At high J' , however, the coherent lifetime becomes too short for coherence to affect the CDAD spectra; e.g., at $J' = 29/2, 31/2$, $\tau_{\text{coh}} \approx 4$ ns. Note that with complete coherence included, the experimental $A_2\beta_2$ values for the $Q_{21} + R_{11}(1/2)$ and $(3/2)$ transitions fall between the theoretical values with and without hyperfine depolarization. (The with hyperfine results are long time limit results in which the coherence is assumed to have died away.)

The presence of coherence seems to be the only plausible explanation for the $Q_{21} + R_{11}(1/2)$ result. Coherence might be studied further by examining the magnitude and phase of the CDAD spectrum for this mixed branch as a function of the delay time between pump and probe pulses. Such experiments will be the focus of future investigations.

V. CONCLUSIONS

The role of the CDAD method in determination of excited state alignment has been firmly established by this and the previous study for REMPI-PES of nitric oxide.¹³ CDAD has the same characteristic as fluorescence anisotropy measurements in LIF in that it provides a direct positive identification of excited state alignment just by the existence of a dichroic signal. CDAD studies are of more general applicability than LIF since the target levels are not required to be connected to fluorescing states for detection. The ability of photoelectron angular distributions to probe higher moments of the excited state alignment ($L > 4$) is an additional feature of CDAD measurements.^{11,16} At present, however, the CDAD technique is more experimentally demanding than fluorescence methods due to the smaller inherent collection solid angle of the electron analyzer and the necessity for two laser beams with independently controlled polarizations.

The $A_2\beta_2$ values obtained from CDAD measurements contain information about excited state alignment in both their phase and magnitude; the former relates to the *shape* of the excited state M_J distribution and the latter relates to the *degree* of the alignment. The possibility of probing coherent excitation with CDAD is suggested by some of results presented here.

The present studies provide a foundation for extensions of the CDAD technique to the study of ground state alignment induced by chemical processes. In particular, the usefulness of $(1+1)$ CDAD as a probe of photofragment alignment was addressed in a recent paper.¹² That work showed that if the $A_2\beta_2$ values for two different branches

arising from the same J' were compared, the initial state alignment can be obtained independent of the photoionization dynamics. Experimental studies of ground state alignment induced by photofragmentation of molecular precursors containing weakly bound NO (e.g., CH_3ONO) are currently in progress.

ACKNOWLEDGMENTS

The research at the Brookhaven National Laboratory was supported under Contract No. DE-AC02-76CH00016 with the U. S. Department of Energy and by its Division of Chemical Sciences, Office of Basic Energy Sciences. Work at the California Institute of Technology was supported by grants from the National Science Foundation (CHE-8521391), Air Force Office of Scientific Research (Contract No. 87-0039), and the Office of Health and Environmental Research of the U. S. Department of Energy (DE-FG03-87ER60513). R.L.D. and V.M. also acknowledge the use of the resources of the San Diego Super Computer Center, which is supported by the National Science Foundation. Research at Lawrence Livermore National Laboratory was performed under Contract No. W-7405-ENG-48 with the U. S. Department of Energy.

¹J. Reuss, *Adv. Chem. Phys.* **30**, 389 (1975).

²P. R. Brooks, *Science* **193**, 11 (1976).

³R. Bersohn and S. H. Lin, *Adv. Chem. Phys.* **16**, 67 (1969).

⁴M. C. Lin and G. Ertl, *Annu. Rev. Phys. Chem.* **37**, 587 (1986), and references therein.

⁵Recent representative papers include R. Vasudev, R. N. Zare, and R. N. Dixon, *J. Chem. Phys.* **80**, 4863 (1984); G. E. Hall, N. Sivakumar, and P. L. Houston, *ibid.* **84**, 2120 (1986); M. Dubs, U. Bruhlmann, and J. R. Huber, *ibid.* **84**, 3106 (1986); F. Lahmani, C. Lardeux, and D. Solgadi, *Chem. Phys. Lett.* **129**, 24 (1986).

⁶C. H. Greene and R. N. Zare, *Annu. Rev. Phys. Chem.* **33**, 119 (1982); *J. Chem. Phys.* **78**, 6741 (1983).

⁷D. C. Jacobs and R. N. Zare, *J. Chem. Phys.* **85**, 5457 (1986); D. C. Jacobs, R. J. Madix, and R. N. Zare, *ibid.* **85**, 5469 (1986).

⁸R. L. Dubs, S. N. Dixit, and V. McKoy, *Phys. Rev. Lett.* **54**, 1249 (1985).

⁹R. L. Dubs, S. N. Dixit, and V. McKoy, *Phys. Rev. B* **32**, 8389 (1985).

¹⁰R. L. Dubs, S. N. Dixit, and V. McKoy, *J. Chem. Phys.* **85**, 656 (1986).

¹¹R. L. Dubs, S. N. Dixit, and V. McKoy, *J. Chem. Phys.* **85**, 6267 (1986).

¹²R. L. Dubs, S. N. Dixit, and V. McKoy, *J. Chem. Phys.* **86**, 5886 (1987).

¹³J. R. Appling, M. G. White, T. M. Orlando, and S. L. Anderson, *J. Chem. Phys.* **85**, 6803 (1986).

¹⁴J. R. Appling, M. G. White, W. J. Kessler, R. Fernandez, and E. D. Poliakoff, *J. Chem. Phys.* (to be published).

¹⁵S. N. Dixit, D. L. Lynch, V. McKoy, and W. M. Huo, *Phys. Rev. A* **32**, 1267 (1985).

¹⁶R. L. Dubs, S. N. Dixit, and V. McKoy, *J. Chem. Phys.* (to be published).

¹⁷L. T. Earls, *Phys. Rev.* **48**, 423 (1935).

¹⁸T. Bergeman and R. N. Zare, *J. Chem. Phys.* **61**, 4500 (1974).

**Chapter 6: (1+1) CDAD: A New Technique for Studying Photofragment
Alignment**

[The text of this chapter appeared in: R. L. Dubs, S. N. Dixit and V. McKoy, J. Chem. Phys. **86**, 5886 (1987).]

(1 + 1) CDAD: A new technique for studying photofragment alignment

Richard L. Dubs, S. N. Dixit,^{a)} and V. McKoy

Arthur Amos Noyes Laboratory of Chemical Physics,^{b)} California Institute of Technology, Pasadena, California 91125

(Received 5 January 1987; accepted 27 January 1987)

In recent years, the alignment of photofragments created by photodissociation of polyatomic molecules has been under intense investigation.¹⁻⁴ Alignment information provides insight into the dynamics of the photodissociation process. Until now, fluorescence techniques (most often laser-induced fluorescence or LIF) have been used almost exclusively to determine the photofragment alignment.¹⁻⁴ In this Comment we report a new method for probing photofragment alignment, namely, circular dichroism in the photoelectron angular distributions (CDAD).^{5,6} Most importantly, we demonstrate here that the photofragment alignment can be extracted from the CDAD spectra in a straightforward manner, *independent* of the photoionization dynamics. We believe this characteristic should enhance the practicality of this technique. CDAD has recently been observed experimentally.⁷ Here, we only give the highlights of this new method: the details will be given in a later publication.⁸

The (1 + 1) CDAD experiment involves excitation of the photofragment with linearly polarized light to an electronically excited state followed by photoionization with left or right circularly polarized light.^{5,6} To simplify the description of the experimental arrangement, we assume the dissociation laser and excitation laser to be the same. The CDAD experiment is then performed as follows: Through the molecular sample, the linearly polarized dissociation/excitation pump laser is co-/counterpropagated with the circularly polarized probe laser. The polarization vector of the pump laser is rotated by a polarizer. A photoelectron detector is *fixed* in the plane at right angles to the propagation directions of the lasers. Angular distributions are obtained as a function of θ , the angle between the pump polarization direction and the photoelectron collection direction.

The difference between the photoelectron angular distributions obtained using left and right circularly polarized light is called the CDAD spectrum.^{5,6} In a recent paper,⁶ we

have shown that the CDAD spectrum has the simple form

$$I(\theta) = \sum_L a_L P_L^1(\cos \theta), \quad (1)$$

where

$$a_L = A_L \bar{\beta}_L. \quad (2)$$

Here, A_L is the state multipole moment describing the *excited state* alignment and $\bar{\beta}_L$ is a J -dependent quantity (where J is the total angular momentum of the excited state) which contains dynamical information about the photoionization process.^{5,6} For a photofragmentation reaction in which the ground state alignment of the photofragment is described solely by A_0' and A_2' ⁹ (primes for the ground state), L in Eq. (1) can take two values, 2 and 4.

The ground state photofragment alignment is typically characterized by one parameter $A_0^{(2)9}$ which is related by a simple formula to the ratio A_2'/A_0' .³ To obtain $A_0^{(2)}$ with CDAD, one measures the $(1+1)$ CDAD spectra for two different branches, i and k , and determines the ratio $R = a_2^i/a_2^k$ [a_2 from Eq. (1)]. The ground state alignment is then given simply by

$$A_0^{(2)} = \frac{(M_0^i - M_0^k R)}{(M_2^i - M_2^k R)}. \quad (3)$$

The M 's have general analytical forms which are too lengthy to express or derive here.⁸ We specialize them here for the $(1+1)$ scheme in NO, $X^2\Pi \rightarrow A^2\Sigma^-$ ion (Table I). The E values in the table are the one-photon relative line intensities for the different branches which are given in analytical form for a $^2\Pi \rightarrow ^2\Sigma$ transition by Earls.¹⁰ to get the M values for a mixed branch ($P_{21} + Q_{11}$ for example) one simply adds the M values (with the correct values of E) for the individual branches. We emphasize that these expressions are *not* classical limits but rather a result of lengthy algebraic evaluation of $3J$, $6J$, and $9J$ symbols.

Why does Eq. (3) look so simple? The answer is that the β_L in Eq. (2) can be factored into a J -dependent part (with $3J$ and $6J$ symbols) and a dynamical part *independent* of J .⁸ The latter part cancels in the ratio R so that the dynamical information about the photoionization process is removed from Eq. (3). The M 's also contain the angular momentum algebra necessary to convert the excited state alignment created by one-photon absorption back into the ground state alignment (neglecting saturation effects). Simple expressions for the M 's as in Table I should be obtainable for other molecules and other transition schemes as well.

Which branches should be chosen to determine $A_0^{(2)}$? It will be shown elsewhere⁸ that P and R branches exhibit the greatest CDAD effect when $A_0^{(2)}$ is negative, while Q branches show the greatest effect when $A_0^{(2)}$ is positive. Since the value of $A_0^{(2)}$ is to be determined, a few branches should be checked to find two suitable for use in Eq. (3). Our calculations indicate that the maximum CDAD intensity in favor-

TABLE I. M expressions for $(1+1)$ CDAD through the $A^2\Sigma$ state of NO (Hund's case b). Here J is the total angular momentum of the photofragment *initial state*. E is described in the text.

Branch	M_0	M_2
P	$E \frac{(2J-3)}{J}$	$E \frac{25(J+1)(2J-3)}{7J(2J-1)}$
Q	$-E \frac{(2J-1)(2J+3)}{J(J+1)}$	$E \frac{5(11J^2+11J-15)}{7J(J+1)}$
R	$E \frac{(2J+5)}{(J+1)}$	$E \frac{25J(2J+5)}{7(J+1)(2J+3)}$

able branches will be about 20% of the intensity at 0° of the left (or right) spectrum. This is well within the current experimental capability.⁷ Measurements of photofragment alignment of NO by $(1+1)$ CDAD are currently underway.¹¹

For NO photofragments in the $^2\Pi$ ground state, uneven population of Λ doublet components (Π^+ and Π^-) in each of the manifolds ($^2\Pi_{1/2}$ and $^2\Pi_{3/2}$) is possible.^{1,3,4} This effect can be unraveled in a straightforward manner, requiring only the relative intensities of the left (or right) spectra at $\theta = 0^\circ$ for a few specific branches. The CDAD spectra themselves are not even required. Unwanted contributions to the photoelectron signal from pump laser ionization can likewise be accounted for by similar measurements at $\theta = 0^\circ$. Ionization by the pump laser can also be clearly suppressed by choosing an $(n+1)$ CDAD scheme. Details will be published elsewhere.⁸

This material is based upon research supported by the National Science Foundation under Grant No. CHE-8521391 and the Air Force Office of Scientific Research under Grant No. 87-0039. One of us (R.L.D.) gratefully acknowledges support through a National Science Foundation Graduate Fellowship.

¹ Present address: Lawrence Livermore National Laboratory, L-421, P.O. Box 808, Livermore, CA 94550.

² Contribution No. 7533.

³ R. Vasudev, R. N. Zare, and R. N. Dixon, *J. Chem. Phys.* **80**, 4863 (1984).

⁴ G. E. Hall, N. Sivakumar, and P. L. Houston, *J. Chem. Phys.* **84**, 2120 (1986).

⁵ M. Dubs, U. Bruhlmann, and J. R. Huber, *J. Chem. Phys.* **84**, 3106 (1986).

⁶ F. Lahmani, C. Lardeux, and D. Solgadi, *Chem. Phys. Lett.* **129**, 24 (1986).

⁷ R. L. Dubs, S. N. Dixit, and V. McKoy, *J. Chem. Phys.* **85**, 656 (1986).

⁸ R. L. Dubs, S. N. Dixit, and V. McKoy, *J. Chem. Phys.* **85**, 6267 (1986).

⁹ J. R. Appling, M. G. White, T. M. Orlando, and S. L. Anderson, *J. Chem. Phys.* **85**, 6803 (1986).

¹⁰ R. L. Dubs, S. N. Dixit, and V. McKoy, *J. Chem. Phys.* (to be published).

¹¹ C. H. Greene and R. N. Zare, *J. Chem. Phys.* **78**, 6741 (1986).

¹² L. T. Earls, *Phys. Rev.* **48**, 423 (1935).

¹³ M. G. White (private communication).

**Chapter 7: Atomic and Molecular Alignment from Photoelectron
Angular Distributions in (n+1) Resonantly Enhanced
Multiphoton Ionization**

[The text of this chapter appeared in: R. L. Dubs, V. McKoy and S. N. Dixit, J. Chem. Phys. **88**, 968 (1988).]

Atomic and molecular alignment from photoelectron angular distributions in $(n+1)$ resonantly enhanced multiphoton ionization

Richard L. Dubs and V. McKoy

Arthur Amos Noyes Laboratory of Chemical Physics,^{a)} California Institute of Technology, Pasadena, California 91125

S. N. Dixit

Lawrence Livermore National Laboratory, L401, Livermore, California 94550

(Received 4 September 1987; accepted 25 September 1987)

Two distinct $(n+1)$ REMPI techniques for obtaining the alignment of gas phase atoms and molecules from photoelectron angular distributions are presented. In both methods, the alignment is extracted from the angular distributions *independently* of the photoionization dynamics. The first method, which takes advantage of circular dichroism in the angular distributions (CDAD) has already been established experimentally as a useful probe of state alignment. The theory outlined in previous work is expanded here. The second method involves photoionization with light *linearly polarized along the photoelectron collection direction* and is presented here for the first time.

I. INTRODUCTION

The investigation of gas phase atomic and molecular alignment has been intense in recent years. Alignment of atoms and molecules occurs by a variety of processes including particle excitation,¹ surface scattering,² photoabsorption,³⁻⁵ photodissociation,⁶⁻¹⁵ interaction with external fields,¹⁶⁻¹⁸ etc. Conventionally, fluorescence techniques are used to probe this state alignment. When the state of interest does not fluoresce itself,^{6,7,14,19} laser induced fluorescence (LIF) methods are used. Both one-^{8,9,15,20-22} and two-photon^{10-13,23} LIF schemes are now common. Saturated laser optical pumping has been coupled to LIF to probe state alignment as well.²⁴ On the other hand, angle-resolved $(n+1)$ resonantly enhanced multiphoton ionization (REMPI) is not commonly used to probe state alignment. The bound-free nature of the ionization step, coupled with the anisotropy associated with photon absorption, causes the state alignment information to be intimately entangled with the photoionization dynamics. Even angle-integrated cross sections from $(n+1)$ REMPI contain alignment information mixed with the photoionization dynamics.²⁵

In this paper we present two distinct methods for probing initial state alignment using photoelectron angular distributions obtained from $(n+1)$ REMPI processes. Both these methods determine the initial state alignment *independently* of the photoionization dynamics. The first method takes advantage of circular dichroism in the angular distributions (CDAD).²⁶⁻³⁰ $(n+1)$ CDAD has already been established experimentally as a useful technique for the study of state alignment.^{31,32} Here we present many important features of CDAD which have been presented previously only in condensed form.^{29,30} The second method, introduced here for the first time, involves $(n+1)$ REMPI with the ionization laser linearly polarized along the photoelectron collection direction. For convenience, we will refer to this angle-resolved $(n+1)$ REMPI technique as PINDAD: *polarization into detector-angular distributions*.

II. THEORY

We treat both $(n+1)$ REMPI methods as two steps^{28,33}: (1) n -photon excitation to a resonant intermediate state, and (2) one-photon ionization of the intermediate state.

A. n -photon excitation to the intermediate state

In both CDAD and PINDAD experiments the first step is n -photon excitation of the initial state to a resonant intermediate state by light linearly polarized along the laboratory frame z axis. The intermediate state alignment will depend on the initial state alignment and the anisotropy of the n -photon absorption process.

Consider one-photon absorption from an initial state with total angular momentum J'' and relative substrate populations $N_{M_j''}$. The relative excited state populations, $N_{M_j'}$, following one-photon absorption of light linearly polarized along the laboratory frame z axis, are given by

$$N_{M_j'} = \sum_{M_j''} N_{M_j''} \begin{pmatrix} J' & 1 & J'' \\ M_j' & 0 & -M_j'' \end{pmatrix}^2 \langle J' \| D \| J'' \rangle^2, \quad (1)$$

where $\langle J' \| D \| J'' \rangle$ is a reduced matrix element whose value will be set equal to unity for now. The $N_{M_j'}$ are normalized such that²⁹

$$\sum_{M_j'} N_{M_j'} = 1. \quad (2)$$

As discussed in Ref. 29, an attractive alternative to the $N_{M_j'}$ description of alignment is the A_L description, where the A_L 's are the state multipole moments²¹:

$$N_{M_j'} = \sum_L A_L T_L^{M_j'}. \quad (3)$$

Here,

$$T_L^{M_j'} = (-1)^{J-M_j'} (2L+1)^{1/2} \begin{pmatrix} J & J & L \\ M_j & -M_j & 0 \end{pmatrix}. \quad (4)$$

^{a)} Contribution No. 7659.

TABLE I. Analytical expressions for C_{00} , C_{02} , and C_{22} for one-photon absorption.

Branch	C_{00}	C_{02}	C_{22}
P	$\frac{1}{3[(2J''+1)(2J''-1)]^{1/2}}$	$\frac{-1}{3(2J''+1)} \left[\frac{(2J''-3)(J''-1)}{5J''(2J''-1)} \right]^{1/2}$	$\frac{5[(J''-1)(J''+1)(2J''+3)(2J''-3)]^{1/2}}{21J''(2J''+1)(2J''-1)}$
Q	$\frac{1}{3(2J''+1)}$	$\frac{1}{3(2J''+1)} \left[\frac{(2J''-1)(2J''+3)}{5J''(J''+1)} \right]^{1/2}$	$\frac{(11J''^2+11J''-15)}{21J''(J''+1)(2J''+1)}$
R	$\frac{1}{3[(2J''+1)(2J''+3)]^{1/2}}$	$\frac{-1}{3(2J''+1)} \left[\frac{(2J''+5)(J''+2)}{5(J''+1)(2J''+3)} \right]^{1/2}$	$\frac{5[(J''+2)(J''+5)(2J''-1)]^{1/2}}{21(J''+1)(2J''+1)(2J''+3)}$

Substituting Eqs. (3) and (4) into Eq. (1) and rearranging we get

$$A_L = \sum_{L'} \tilde{A}_{L'} \cdot C_{L'L} \quad (5)$$

For a given set of initial state alignment parameters $\tilde{A}_{L'}$ (here the tilde indicates the initial state), Eq. (5) can be used to calculate the intermediate state alignment parameters A_L after n -photon absorption. For one-photon absorption, the $C_{L'L}$ are given by

$$C_{L'L} = (-1)^{L+1} [(2L''+1)(2L+1)]^{1/2} \times \sum_{L'} (2L+1) \begin{Bmatrix} 1 & 1 & L \\ J' & J'' & L'' \end{Bmatrix} \times \begin{pmatrix} 1 & 1 & L \\ 0 & 0 & 0 \end{pmatrix} \begin{pmatrix} L'' & L & L \\ 0 & 0 & 0 \end{pmatrix} \quad (6)$$

For the case of two-photon absorption the $C_{L'L}$ are given by¹⁰ (see Ref. 34 for an exception)

$$C_{L'L} = (-1)^L [(2L''+1)(2L+1)]^{1/2} \times \sum_{L'} (2L+1) \begin{Bmatrix} 2 & 2 & L \\ J' & J'' & L'' \end{Bmatrix} \times \begin{pmatrix} 2 & 2 & L \\ 0 & 0 & 0 \end{pmatrix} \begin{pmatrix} L'' & L & L \\ 0 & 0 & 0 \end{pmatrix} \quad (7)$$

We restrict our consideration to initial states which are "aligned" (substrates of the same $|M_{J'}|$ have the same population) and not "oriented" (no restriction on relative $M_{J'}$ population). In this case, both L'' and L are even.^{21,22} Simplified analytical expressions for C_{00} , C_{02} , and C_{22} for both

one- and two-photon absorption are given in Tables I and II.

The relationship between the state multipole moments \tilde{A}_0 and \tilde{A}_2 and the alignment parameters $A_0^{(2)}$ commonly extracted from LIF experiments is given by¹⁰

$$A_0^{(2)} = \left[\frac{(2J''+3)(2J''-1)}{5J''(J''+1)} \right]^{1/2} \cdot \frac{\tilde{A}_2}{\tilde{A}_0} \quad (8)$$

B. Photoionization of the resonant intermediate state

In Ref. 28, the differential cross section for photoionization of a resonant intermediate state was written in the form

$$\frac{\partial \sigma}{\partial \Omega_k \partial \Omega_p} = \sum_{\substack{L'L''M' \\ M_J}} N_{M_J} \beta_{L'L''M'}^{M_J \mu_0} Y_{L-M'}(\theta_k, \phi_k) Y_{L'M'}(\theta_p, \phi_p), \quad (9)$$

where

$$\beta_{L'L''M'}^{M_J \mu_0} = (-1)^{\mu_0} (2L'+1)^{1/2} \begin{pmatrix} 1 & 1 & L' \\ -\mu_0 & \mu_0 & 0 \end{pmatrix} \beta_{L'L''M'}^{M_J} \quad (10)$$

In Eq. (9), (θ_k, ϕ_k) denotes the collection angle of the photoelectron and (θ_p, ϕ_p) denotes the photon polarization direction for linearly polarized light or the photon propagation direction for circularly polarized light. All the angles are measured in the laboratory frame. N_{M_J} represents the relative populations of the M_J sublevels for the state being ionized and $\beta_{L'L''M'}^{M_J \mu_0}$ contains all the dynamical information

TABLE II. Analytical expressions for C_{00} , C_{02} , and C_{22} for two-photon absorption.

Branch	C_{00}	C_{02}	C_{22}
O	$\frac{1}{5[(2J''+1)(2J''-3)]^{1/2}}$	$\frac{-2}{7} \left[\frac{(J''-2)(2J''-5)}{5(J''-1)(2J''+1)(2J''-1)(2J''-3)} \right]^{1/2}$	$\frac{1}{7(2J''-1)} \left[\frac{(2J''+3)(J''-2)(2J''-5)(J''+1)}{J''(J''-1)(2J''-3)(2J''+1)} \right]^{1/2}$
P	$\frac{1}{5[(2J''+1)(2J''-1)]^{1/2}}$	$\frac{(J''+5)}{7(2J''+1)} \left[\frac{(2J''-3)}{5J''(J''-1)(2J''-1)} \right]^{1/2}$	$\frac{(J''^2-7)}{7J''(2J''-1)(2J''+1)} \left[\frac{(2J''+3)(2J''-3)}{(J''-1)(J''+1)} \right]^{1/2}$
Q	$\frac{1}{5(2J''+1)}$	$\frac{(2J''+5)(2J''-3)}{7(2J''+1)[5J''(J''+1)(2J''-1)(2J''+3)]^{1/2}}$	$\frac{3[J''(J''+1)(2J''+5)(2J''-3)+21]}{7J''(J''+1)(2J''-1)(2J''+1)(2J''+3)}$
R	$\frac{1}{5[(2J''+1)(2J''+3)]^{1/2}}$	$\frac{(J''-4)}{7(2J''+1)} \left[\frac{(2J''+5)}{5(J''+1)(J''+2)(2J''+3)} \right]^{1/2}$	$\frac{[(J''+1)^2-7]}{7(J''+1)(2J''+1)(2J''+3)} \left[\frac{(2J''+5)(2J''-1)}{J''(J''+2)} \right]^{1/2}$
S	$\frac{1}{5[(2J''+1)(2J''+5)]^{1/2}}$	$\frac{-2}{7} \left[\frac{(J''+3)(2J''+7)}{5(J''+2)(2J''+1)(2J''+3)(2J''+5)} \right]^{1/2}$	$\frac{1}{7(2J''+3)} \left[\frac{(2J''+7)(J''+2)(2J''-1)(J''+3)}{(J''+2)(J''+1)(2J''+1)(2J''+5)} \right]^{1/2}$

about the photoionization process. Also $\mu_0 = 0$ for linearly polarized light, $\mu_0 = +1$ or -1 for left or right circularly polarized light, respectively, and $Y_{LM}(\theta, \phi)$ is a spherical harmonic. Although Eqs. (9) and (10) are appropriate for photoionization of both atomic and molecular states,²⁸ only the molecular case will be considered here.

In Ref. 28, an expression for $\beta_{LL'M'}^{M_J \mu_0}$ is given which explicitly contains quantum numbers for the total (J_+) and rotational (N_+) angular momentum of the ion, as well as the projection of these quantities and the photoelectron and ion spin on the laboratory z axis. This expression is very cumbersome,

and for the experiments of interest here, these quantities remain unresolved.^{31,32} In this case, these quantum numbers can be summed over, and a much simpler expression for $\beta_{LL'M'}^{M_J \mu_0}$ obtained. The equivalence of the rotationally explicit form²⁸ and the simple form is well known³⁵⁻³⁸; the derivation is very tedious and will not be given here.³⁹ Recently, Hansen and Berry derived this simpler form for the specific case of $(l+1)$ REMPI from an unaligned initial state.³⁸

The simplified expression for $\beta_{LL'M'}^{M_J \mu_0}$ for photoionization of a state described in Hund's case (b)⁴⁰ is

$$\begin{aligned} \beta_{LL'M'}^{M_J \mu_0} = & \frac{4\pi}{3} K \sum_{\substack{L'' \mu'' \\ L' \lambda' \mu'}} \bar{r}_R^{(L' \mu')} \bar{r}_R^{(L'' \mu'')} e^{i(\eta_1 - \eta_2)} (-i)^l (i)^{l'} (-1)^P \\ & \times (2N' + 1)(2J' + 1)(2L' + 1)[(2l + 1)(2l' + 1)(2L + 1)(2L' + 1)]^{1/2} \\ & \times (-1)^{S' + 2J' - M_J + \lambda'} \begin{Bmatrix} J' & N' & S' \\ N' & J' & L' \end{Bmatrix} \begin{pmatrix} J' & J' & L' \\ M_J & -M_J & 0 \end{pmatrix} \begin{pmatrix} N' & N' & L' \\ \lambda' & -\lambda' & 0 \end{pmatrix} \\ & \times \begin{pmatrix} L & L' & L' \\ -M' & M' & 0 \end{pmatrix} \begin{pmatrix} L & L' & L' \\ \lambda' - \lambda & \mu - \mu' & 0 \end{pmatrix} \begin{pmatrix} l & l' & L \\ 0 & 0 & 0 \end{pmatrix} \begin{pmatrix} l & l' & L \\ \lambda & -\lambda & \lambda' - \lambda \end{pmatrix} \\ & \times \begin{pmatrix} 1 & 1 & L' \\ \mu_0 & -\mu_0 & 0 \end{pmatrix} \begin{pmatrix} 1 & 1 & L' \\ \mu' & -\mu & \mu - \mu' \end{pmatrix}, \end{aligned} \quad (11)$$

where

$$P = \mu_0 + L + L' + \lambda' + \mu. \quad (12)$$

In the single-particle picture, $\bar{r}_R^{(L' \mu')}$ is the dipole matrix element between the initial orbital and the photoelectron wave function in the molecular frame; its form is given in Ref. 41. K is a proportionality constant which depends on the photon energy.⁴² Excluding spin (i.e., $S' = 0$) Eq. (11) is identical to that obtained by averaging the expression for a perfectly oriented⁴³ molecule over a distribution of orientations $|Y_{J, M_J}|^2$.³⁵⁻³⁸

Converting the N_{M_J} description of alignment to the A_L description by substituting Eqs. (3), (4), and (10)-(12) into Eq. (9), summing over M_J , and observing the orthogonality of the $3j$ symbols⁴⁴:

$$\sum_{M_J} \begin{pmatrix} J' & J' & L \\ M_J & -M_J & 0 \end{pmatrix} \begin{pmatrix} J' & J' & L' \\ M_J & -M_J & 0 \end{pmatrix} = (2L + 1)^{-1} \delta_{L, L'} \quad (13)$$

we obtain

$$\frac{\partial \sigma}{\partial \Omega_k \partial \Omega_p} = \sum_{L, L', M'} A_L \beta_{LL'M'}^{L \mu_0} Y_{L-M'}(\theta_k, \phi_k) Y_{L'M'}(\theta_p, \phi_p) \quad (14)$$

with

$$\beta_{LL'M'}^{L \mu_0} = \sum_{M_J} T_L^{M_J} \beta_{LL'M'}^{M_J \mu_0} \quad (15a)$$

$$\begin{aligned} & = \frac{4\pi}{3} K \sum_{\substack{L'' \mu'' \\ L' \lambda' \mu'}} \bar{r}_R^{(L' \mu')} \bar{r}_R^{(L'' \mu'')} e^{i(\eta_1 - \eta_2)} (-i)^l (i)^{l'} (-1)^P \\ & \times (2N' + 1)(2J' + 1)[(2L + 1)(2l + 1)(2l' + 1)(2L + 1)(2L' + 1)]^{1/2} \\ & \times (-1)^{S' + J' + \lambda'} \begin{Bmatrix} J' & N' & S' \\ N' & J' & L' \end{Bmatrix} \begin{pmatrix} N' & N' & L \\ \lambda' & -\lambda' & 0 \end{pmatrix} \begin{pmatrix} 1 & 1 & L' \\ \mu' & -\mu & \mu - \mu' \end{pmatrix} \\ & \times \begin{pmatrix} L & L' & L' \\ -M' & M' & 0 \end{pmatrix} \begin{pmatrix} L & L' & L' \\ \lambda' - \lambda & \mu - \mu' & 0 \end{pmatrix} \begin{pmatrix} l & l' & L \\ 0 & 0 & 0 \end{pmatrix} \begin{pmatrix} l & l' & L \\ \lambda & -\lambda' & \lambda' - \lambda \end{pmatrix} \begin{pmatrix} 1 & 1 & L' \\ \mu_0 & -\mu_0 & 0 \end{pmatrix}. \end{aligned} \quad (15b)$$

Equation (14) is very general. The alignment information for the state being ionized is contained solely in the moments A_L . Nothing has been said about how the alignment is attained, whether it be by photoabsorption, photofragmentation, collisions, external fields, etc.

The most important result contained in Eq. (14) is that the index L of the alignment is *different* from that of the photoelectron, L . For photoelectron angular distributions in general, then, the alignment information is intimately intertwined with the photoionization dynamics. Even angle-integrated cross sections, in which an integration over (θ_k, ϕ_k) forces $L = 0$, are dependent on alignment.²⁵ Until recently, this complexity has discouraged the use of photoelectron angular distributions for extraction of alignment information. However, as we now demonstrate, two distinct experiments are possible which both yield the alignment information in a straightforward manner, independently of the photoionization dynamics.

III. EXPERIMENT 1: CDAD

The usefulness of CDAD as a probe of gas phase molecular alignment has now been established both theoretically and experimentally.²⁸⁻³² Nevertheless, many of the important properties of the CDAD spectra have been given previously in condensed form,^{29,30} without the detailed analysis presented here.

A. A simple picture for understanding CDAD

Traditionally, one thinks of circular dichroism or optical activity in terms of mirror images and symmetry planes or the lack thereof.⁴⁵ Circular dichroism is normally associated with chiral molecules and not with gas phase aligned atoms and linear molecules. For this reason we present a simple picture for understanding CDAD.

Consider Fig. 1(a) in which left and right circularly polarized light impinge on an oriented⁴³ diatomic molecule. The light propagates perpendicularly to the molecular axis and into the plane of the figure. Figure 1(a) represents the case of photoabsorption. Because the left and right cases are mirror images of each other (ignoring the hash-mark shading of the molecules), the two cases are physically identical, and no circular dichroism exists. However, if the photon has enough energy to ionize the molecule, and the electrons are collected in the plane at right angles to the light propagation direction (i.e., in the plane of the page), the left and right cases are no longer mirror images [Fig. 1(b)]—the photoelectron breaks the symmetry of the final state. For this reason, CDAD exists from oriented linear molecules.^{26,46} In fact as shown in Ref. 26, CDAD in this case is not a small effect, as it already exists in the electric dipole approximation.⁴⁶

If the linear molecules are not oriented,⁴³ but rather completely random in direction as in the gas phase, CDAD will not exist. However, after molecules absorb light, scatter off surfaces, etc., they can obtain an "alignment" in which all possible orientations of the molecular axis in space are not equally probable. CDAD can exist from these aligned molecules,²⁸ although the intensity of the CDAD signal will not

be as strong as that from a perfectly oriented⁴³ molecule. Indeed, these CDAD signals have been measured.^{31,32}

B. Experimental configuration for CDAD

The experimental configuration for the $(n + 1)$ CDAD experiment is given in Fig. 1 of Ref. 29. Light, linearly polarized along the laboratory frame z axis, induces n -photon absorption by the gas sample to yield a resonant intermediate state. Left or right circularly polarized light counterpropagating⁴⁷ with the first beam is then used to photoionize the sample. Photoelectrons are collected in the plane perpendicular to the propagation axis of the two beams. θ_k is defined as the angle between the direction of linear polarization and the electron collection direction.

C. CDAD theory

CDAD manifests itself in the difference between photoelectron signals obtained with left ($\mu_0 = +1$) and right ($\mu_0 = -1$) circularly polarized light.²⁶⁻³² As discussed in Ref. 28, due to the symmetry property⁴⁴

$$\begin{pmatrix} 1 & 1 & L' \\ \mu_0 & -\mu_0 & 0 \end{pmatrix} = (-1)^L \begin{pmatrix} 1 & 1 & L' \\ -\mu_0 & \mu_0 & 0 \end{pmatrix}, \quad (16)$$

only terms with $L' = 1$ switch sign upon changing from left to right polarization and thus only these terms contribute to CDAD. All the major features of CDAD follow from this fact. For a cylindrically symmetric system which displays alignment but not orientation, both L and L are even for symmetry reasons.^{22,33} Because $L' = 1$, it follows from the triangle relationship⁴⁴ implied by the 3- j symbols involving $L, L',$ and L in Eq. (15b) that $L = L$ for CDAD. This fact was used without proof in Ref. 29 along with the Kronecker delta in Eq. (13) to derive the simple expression for the CDAD intensity $I_{\text{CDAD}}(\theta_k)$:

$$I_{\text{CDAD}}(\theta_k) = \sum_L a_L P_L^1(\cos \theta_k), \quad (17a)$$

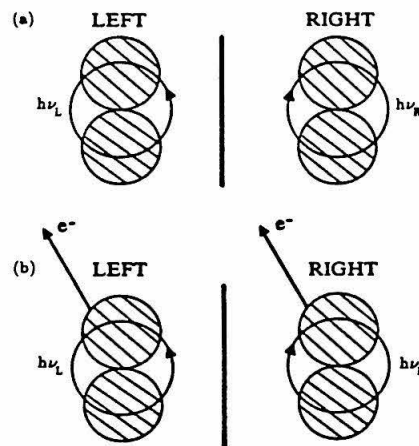


FIG. 1. A simple illustration of the physical basis for CDAD.

where

$$a_L = A_L \bar{\beta}_L \quad (17b)$$

and

$$\bar{\beta}_L = \frac{i}{\pi} \left[\frac{3(2L+1)}{2L(L+1)} \right]^{1/2} \beta_{L11}^L, \quad (18)$$

$P_L^1(\cos \theta)$ is an associated Legendre polynomial. Equations (17) and (18) are obtained from Eqs. (14) and (15) by fixing the experimental configuration at $(\theta_p, \phi_p) = (90^\circ, 0^\circ)$ and $\phi_k = 90^\circ$. The fact that the indices L for the alignment and the photoelectron are the same is what makes CDAD such a useful probe of alignment.

The J dependence of $\bar{\beta}_L$ can be factored out^{30,32}:

$$\bar{\beta}_L(J') = X_L(J') \bar{\beta}_L, \quad (19)$$

where $\bar{\beta}_L$ is explicitly independent of J' ; it depends on J' only through the variation of the cross section with the photoelectron kinetic energy. Because rotational spacings are small, we can ignore this latter dependence and treat $\bar{\beta}_L$ as a constant. The expression for $X_L(J')$ is

$$X_L(J') = (-1)^{J'+S'+\Lambda'} (2J'+1)(2N'+1) \times \begin{Bmatrix} J' & N' & S' \\ N' & J' & L \end{Bmatrix} \begin{pmatrix} N' & N' & L \\ \Lambda' & -\Lambda' & 0 \end{pmatrix}. \quad (20)$$

For photoionization of a $^2\Sigma$ state such as the $A^2\Sigma$ state of NO, $\Lambda' = 0$ and $S' = 1/2$. In this case, X_0 and X_2 become

$$X_0(J') = (2J'+1)^{1/2}, \quad (21)$$

$$X_2(J') = \frac{-1}{4} \left[\frac{(2J'+1)(2J'-1)(2J'+3)}{J'(J'+1)} \right]^{1/2}. \quad (22)$$

Note that Eqs. (21) and (22) are independent of N' .

$$\beta_L = \frac{(4\pi)^{1/2}}{3} K \sum_{\substack{\mu, \mu' \\ L, L'}} \bar{r}_L^{(\mu)} \bar{r}_L^{(\mu')*} e^{i(\eta_L - \eta_{L'})} (-i)^l (i)^{l'} \times (2N'+1)(2J'+1)[(2L+1)(2l+1)(2l'+1)(2L+1)(2L'+1)]^{1/2} \times (-1)^{S'+J'+\Lambda'+\lambda'+\mu} \begin{Bmatrix} J' & N' & S' \\ N' & J' & L \end{Bmatrix} \begin{pmatrix} N' & N' & L \\ \mu' & -\mu & \mu - \mu' \end{pmatrix} \times \begin{pmatrix} L & L' & L \\ \lambda' - \lambda & \mu - \mu' & 0 \end{pmatrix} \begin{pmatrix} l & l' & L \\ 0 & 0 & 0 \end{pmatrix} \begin{pmatrix} l & l' & L \\ \lambda & -\lambda' & \lambda' - \lambda \end{pmatrix} \begin{pmatrix} 1 & 1 & L' \\ 0 & 0 & 0 \end{pmatrix}. \quad (26)$$

$P_L(\cos \theta)$ is a Legendre polynomial [in contrast to $P_L^1(\cos \theta)$ in Eq. (17a)].⁴⁴ Once again, the indices for the alignment and the photoelectron are the same. Note that an $L = 0$ term contributes to the PINDAD signal while it does not to the CDAD signal.

Although the β_L for PINDAD are different from the $\bar{\beta}_L$ for CDAD, the J' dependence of the two is the same. Thus, the PINDAD β_L can be factored in an exactly analogous way to Eq. (19):

$$\beta_L(J') = X_L(J') \bar{\beta}_L, \quad (27)$$

where $X_L(J')$ is given in Eq. (20).

IV. EXPERIMENT 2: PINDAD

A. Experimental configuration for PINDAD

The experimental configuration for PINDAD is identical to that for CDAD except that the circularly polarized ionizing probe beam is replaced by a linearly polarized beam in which the polarization vector is *always directed along the photoelectron collection direction*.

B. PINDAD theory

The PINDAD configuration requires $(\theta_p, \phi_p) = (\theta_k, \phi_k)$ in Eq. (14). Using the relations⁴⁸

$$Y_{L0}(\theta_k, \phi_k) = (-1)^{L'-L} (2L+1)^{1/2} \sum_{M'} \begin{pmatrix} L & L' & L \\ -M' & M' & 0 \end{pmatrix} Y_{L-M'}(\theta_k, \phi_k) Y_{L'M'}(\theta_k, \phi_k) \quad (23)$$

and

$$Y_{L0}(\theta_k, \phi_k) = \left[\frac{(2L+1)}{4\pi} \right]^{1/2} P_L(\cos \theta_k), \quad (24)$$

it follows directly that

$$I_{\text{PINDAD}}(\theta_k) = \sum_L a_L^2 P_L(\cos \theta_k), \quad (25a)$$

where

$$a_L^2 = A_L \beta_L \quad (25b)$$

and

V. DETERMINATION OF PHOTOFRAGMENT ALIGNMENT

In Ref. 30, we stated that the alignment of an initial state could be determined by measurement of $(1+1)$ CDAD through two different excitation branches. Further we stated that this alignment could be determined *independently* of the photoionization dynamics. Consider an initial state which requires only \bar{A}_0 and \bar{A}_2 for a complete description of the alignment. Then using Eqs. (5), (17b), and (19),

$$a_2 = A_2 \bar{\beta}_2 = [\bar{A}_0 C_{02} + \bar{A}_2 C_{22}] \cdot X_2 \bar{\beta}_2. \quad (28)$$

In the ratio $R = a_2^2/a_0^2$ for two different excitation branches i

and k , the $\bar{\beta}_2$ values cancel, thus eliminating the photoionization dynamics from R . The ratio R is then simply a combination of 3- j , 6- j , and 9- j symbols which can be evaluated analytically. Using Eqs. (8) and (28) we can derive an expression for the initial state alignment³⁰:

$$A_0^{(2)} = \frac{(M_0^l - M_0^k R)}{(M_2^l - M_2^k R)} \quad (29)$$

Simplified expressions for the M values can be obtained from Eqs. (21) and (22) and Tables I and II. For one-photon absorption the M expressions are given in Table I of Ref. 30. For two-photon absorption, the M expressions are given here in Table III. The H values in Table III are the two-photon line intensities given by Halpern *et al.*⁴⁹ The line intensities appear when we explicitly consider the reduced matrix elements [as in Eq. (1)] which we previously set equal to unity. Note that because the M values only appear as ratios in Eq. (29), they can all be multiplied by a constant without changing value of $A_0^{(2)}$. For mixed branches, such as $Q_{11} + P_{21}$, the M values for the individual branches are simply added (ignoring coherence effects).³²

We now make a very important point: the ratio $R = a_2^l/a_2^k$ for CDAD will be equal to the ratio $R' = a_2^l/a_2^k$ for PINDAD. This result follows directly from the fact that the β 's for both methods can be factored in the same manner, as shown in Eqs. (19) and (27). The photoionization dynamics cancel in R' in the same way as in R . Thus, Eq. (29) and the same M values can be used to obtain the initial state alignment for CDAD or PINDAD.

VI. COMPARISON OF CDAD AND PINDAD

It remains to be explored experimentally whether CDAD or PINDAD provides a distinct advantage over the other for determining initial state alignment. The experimental configurations for the two methods are similar enough that the two techniques can be used together. Nevertheless, the following points are relevant:

(1) For a given initial state alignment, the % CDAD (relative to the intensity of the left or right spectrum) will be approximately the same as the % change in the intensity of PINDAD over the whole spectrum.⁵⁰

(2) Spectra are typically measured over 360° and then

averaged.^{31,32} The CDAD spectrum does not have to be obtained using left and right polarization, but rather just one of them. Two of the opposite 90° quadrants will then correspond to the "left" spectrum and the other two to the "right." On the other hand, all four quadrants of the PINDAD spectrum will be equivalent.

(3) The CDAD spectrum is determined as the difference between two measurements^{31,32}; as such, it contains twice the error of a single PINDAD measurement. On the other hand, certain systematic errors are eliminated in a difference spectrum.

(4) The intensity of the CDAD spectrum at $\theta_k = 0^\circ$ and $\theta_k = 90^\circ$ is zero.^{28,31,32} There is no corresponding fact for the PINDAD spectrum.

VII. SOME FURTHER COMMENTS ABOUT PINDAD

Three alternative ways for extracting initial state alignment with PINDAD exist. All take advantage of the fact that a_0^l is obtainable from Eq. (25a).

The first method requires that the ratio of a_0^l values, rather than the ratio of a_2^l values, for two different branches be determined. An expression for the initial state alignment can be derived in an analogous way to the derivation of Eq. (29). However, the a_0^l values will be less sensitive to the initial state alignment than the a_2^l values.⁵¹

The second method recognizes the fact that the coefficients extracted from a spectra using Eq. (25a) are usually normalized by a_0 ; that is, instead of obtaining a_0^l , a_2^l , and a_4^l , one obtains 1, b_2^l , and b_4^l where $b_2^l = a_2^l/a_0^l$ and $b_4^l = a_4^l/a_0^l$. The expression for b_2^l can be written

$$b_2^l = \frac{a_2^l}{a_0^l} = \frac{A_2 X_2 \bar{\beta}_2^l}{A_0 X_0 \bar{\beta}_0^l} \quad (30)$$

The ratio $\bar{\beta}_2^l/\bar{\beta}_0^l$ is a constant, but unknown. However, it can be obtained by performing an independent experiment on an unaligned initial state.⁵² A graph of b_2^l vs the theoretical value of $(A_2 X_2)/(A_0 X_0)$ for a number of J values (after being corrected for population differences due to the temperature of the sample) will yield the ratio $\bar{\beta}_2^l/\bar{\beta}_0^l$ from the slope. Once this ratio is known, it can be used to extract an unknown state alignment from the b_2^l value of a single PINDAD spectrum.

TABLE III. M expressions for $(2 + 1)$ CDAD through the $A^2\Sigma$ state of NO [Hund's case (b)]. H is described in the text.

Branch	M_0	M_2
O	$H \frac{2(2J^* - 5)}{(J^* - 1)}$	$H \frac{5(J^* + 1)(2J^* - 5)}{(J^* - 1)(2J^* - 1)}$
P	$-H \frac{(J^* + 5)(2J^* - 3)}{J^*(J^* - 1)}$	$H \frac{5(J^* - 7)(2J^* - 3)}{J^*(J^* - 1)(2J^* - 1)}$
Q	$-H \frac{(2J^* + 5)(2J^* - 3)}{J^*(J^* + 1)}$	$H \frac{15[J^*(J^* + 1)(2J^* + 5)(2J^* - 3) + 21]}{J^*(J^* + 1)(2J^* - 1)(2J^* + 3)}$
R	$-H \frac{(J^* - 4)(2J^* + 5)}{(J^* + 1)(J^* + 2)}$	$H \frac{5[(J^* + 1)^2 - 7](2J^* + 5)}{(J^* + 1)(J^* + 2)(2J^* + 3)}$
S	$H \frac{2(2J^* + 7)}{(J^* + 2)}$	$H \frac{5J^*(2J^* + 7)}{(J^* + 2)(2J^* + 3)}$

In the third method, the ratio of b_1^2 values for two different branches is obtained. This ratio is also independent of the photoionization dynamics although it depends on the initial state alignment in a quadratic manner. While the expressions for $A_0^{(2)}$ are simple to derive from Eq. (30), they are complicated in appearance in this case.

All three of the above methods depend on an accurate determination of the value of a_0' . This value represents a constant contribution to the angular distributions [$P_0(\cos\theta) = 1$] and is directly affected by any unwanted constant background in the spectra. For this reason the ratio of a_1' coefficients for two different excitation branches might yield more quantitative results.

VIII. CONCLUSIONS

Two independent angular-resolved ($n+1$) REMPI techniques for obtaining the alignment of gas phase atoms and molecules have been presented. Both techniques provide initial state alignment, independently of the photoionization dynamics. Whether or not one technique provides a distinct advantage over the other in providing quantitative results remains to be established experimentally. Because the two techniques differ only in the polarization of the ionizing laser, they are similar enough to be used together.

ACKNOWLEDGMENTS

Work at the California Institute of Technology was supported by grants from the National Science Foundation (CHE-8521391), Air Force Office of Scientific Research (Contract No. 87-0039), and the Office of Health and Environmental Research of the U. S. Department of Energy (DE-FG03-87ER60513). Research at Lawrence Livermore National Laboratory was performed under contract W-7405-ENG-48 with the U. S. Department of Energy. Two of us (R. L. D. and V. M.) acknowledge use of the resources of the San Diego Supercomputer Center which is supported by the National Science Foundation.

- ¹R. Bersohn and S. H. Lin, *Adv. Chem. Phys.* **16**, 67 (1969).
²(a) M. C. Lin and G. Ertl, *Annu. Rev. Phys. Chem.* **37**, 587 (1986), and references therein; (b) G. O. Sitz, A. C. Kummel, and R. N. Zare, *J. Vac. Sci. Technol. A* **5**, 513 (1987); *J. Chem. Phys.* **87**, 3247 (1987).
³R. E. Drullinger and R. N. Zare, *J. Chem. Phys.* **51**, 5532 (1969).
⁴R. N. Zare, *Ber. Bunsenges. Phys. Chem.* **86**, 422 (1982).
⁵W. J. Kessler and E. D. Poliakoff, *J. Chem. Phys.* **84**, 3647 (1986).
⁶M. T. MacPherson, J. P. Simons, and R. N. Zare, *Mol. Phys.* **38**, 2049 (1979).
⁷G. W. Loge and J. R. Wiesenfeld, *Chem. Phys. Lett.* **78**, 32 (1981); *J. Chem. Phys.* **75**, 2795 (1981).
⁸R. Vasudev, R. N. Zare, and R. N. Dixon, *J. Chem. Phys.* **80**, 4863 (1984).
⁹G. E. Hall, N. Sivakumar, and P. L. Houston, *J. Chem. Phys.* **84**, 2120 (1986).
¹⁰M. Dubs, U. Bruhlmann, and J. R. Huber, *J. Chem. Phys.* **84**, 3106 (1986).
¹¹F. Lahmani, C. Lardeux, and D. Solgadi, *Chem. Phys. Lett.* **129**, 24 (1986).
¹²U. Bruhlmann, M. Dubs, and J. R. Huber, *J. Chem. Phys.* **86**, 1249 (1987).
¹³M. R. S. McCoustra, J. A. Dyet, and J. Pfab, *Chem. Phys. Lett.* **136**, 231 (1987).
¹⁴J. A. Guest and F. Webster, *J. Chem. Phys.* **86**, 5479 (1987).
¹⁵M. A. O'Halloran, H. Joswig, and R. N. Zare, *J. Chem. Phys.* **87**, 303 (1987).
¹⁶J. Reuss, *Adv. Chem. Phys.* **30**, 389 (1975).
¹⁷P. R. Brooks, *Science* **193**, 11 (1976).
¹⁸D. H. Parker, K. K. Chakrovorty, and R. B. Bernstein, *Chem. Phys. Lett.* **86**, 113 (1982), and references therein.
¹⁹U. Fano and J. H. Macek, *Rev. Mod. Phys.* **45**, 553 (1973).
²⁰D. A. Case, G. M. McClelland, and D. R. Hershbach, *Mol. Phys.* **35**, 541 (1978).
²¹C. H. Greene and R. N. Zare, *Annu. Rev. Phys. Chem.* **33**, 119 (1982).
²²C. H. Greene and R. N. Zare, *J. Chem. Phys.* **78**, 6741 (1983).
²³A. C. Kummel, G. O. Sitz, and R. N. Zare, *J. Chem. Phys.* **85**, 6874 (1986).
²⁴U. Hefter, G. Ziegler, A. Matthews, A. Fischer, and K. Bergmann, *J. Chem. Phys.* **85**, 286 (1986).
²⁵See D. C. Jacobs and R. N. Zare, *J. Chem. Phys.* **85**, 5457 (1986); D. C. Jacobs, R. N. Madix, and R. N. Zare, *ibid.* **85**, 5469 (1986) for a method to extract alignment information from angle-integrated cross sections. See also Refs. 2(b) and 23.
²⁶R. L. Dubs, S. N. Dixit, and V. McKoy, *Phys. Rev. Lett.* **54**, 1249 (1985).
²⁷R. L. Dubs, S. N. Dixit, and V. McKoy, *Phys. Rev. B* **32**, 8389 (1985).
²⁸R. L. Dubs, S. N. Dixit, and V. McKoy, *J. Chem. Phys.* **85**, 656 (1986).
²⁹R. L. Dubs, S. N. Dixit, and V. McKoy, *J. Chem. Phys.* **85**, 6267 (1986).
³⁰R. L. Dubs, S. N. Dixit, and V. McKoy, *J. Chem. Phys.* **86**, 5886 (1987).
³¹J. R. Appling, M. G. White, T. M. Orlando, and S. L. Anderson, *J. Chem. Phys.* **85**, 6803 (1986).
³²J. R. Appling, M. G. White, R. L. Dubs, S. N. Dixit, and V. McKoy, *J. Chem. Phys.* (to be published).
³³S. N. Dixit and V. McKoy, *J. Chem. Phys.* **82**, 3546 (1985).
³⁴For the specific case of a two-photon Q transition ($J' = J''$) between two electronic states which both have Σ symmetry or both have Π symmetry, etc. Equation (7) must be generalized. See Ref. 10.
³⁵J. C. Tully, R. S. Berry, and B. J. Dalton, *Phys. Rev.* **176**, 95 (1968).
³⁶A. D. Buckingham, B. J. Orr, and J. M. Sichel, *Philos. Trans. R. Soc. London Sect. A* **268**, 147 (1970).
³⁷Y. Itikawa, *Chem. Phys.* **28**, 461 (1978).
³⁸J. C. Hansen and R. S. Berry, *J. Chem. Phys.* **80**, 4078 (1984).
³⁹S. N. Dixit, R. L. Dubs, and V. McKoy, *J. Chem. Phys.* (to be published).
⁴⁰We have in mind the specific case of photoionization of the $A^2\Sigma$ state of NO.
⁴¹S. N. Dixit, D. L. Lynch, V. McKoy, and W. M. Huo, *Phys. Rev. A* **32**, 1267 (1985).
⁴²R. R. Lucchese, G. Raseev, and V. McKoy, *Phys. Rev. A* **25**, 2572 (1982).
⁴³In this context, "oriented" means the molecular axis is fixed in space.
⁴⁴A. R. Edmonds, *Angular Momentum in Quantum Mechanics* (Princeton University, Princeton, 1974).
⁴⁵J. E. Brady and G. E. Humiston, *General Chemistry: Principles and Structure*, 2nd ed. (Wiley, New York, 1978).
⁴⁶N. A. Cherepkov, *Chem. Phys. Lett.* **87**, 344 (1982).
⁴⁷Although Fig. 1 of Ref. 29 shows the two beams copropagating, it is more convenient experimentally to counterpropagate the beams. See Refs. 31 and 32.
⁴⁸M. Weissbluth, *Atoms and Molecules* (Academic, New York, 1978).
⁴⁹J. B. Halpern, H. Zacharias, and R. Wallenstein, *J. Mol. Spectrosc.* **79**, 1 (1980).
⁵⁰R. L. Dubs (unpublished results).
⁵¹This result follows from the fact that $|C_{22}/C_{02}| > |C_{20}/C_{00}|$ in general.
⁵²This independent experiment can be performed on a gas phase sample of NO, but might not be possible for an unstable photofragment.

**Chapter 8: Studies of Angle-Resolved Photoelectron Spectra from
 Oriented NiCO: A Model for Adsorbed CO**

[The text of this chapter appeared in: R. L. Dubs, M. E. Smith and V.
McKoy, Phys. Rev. **B37**, 2812 (1988).

Studies of angle-resolved photoelectron spectra from oriented NiCO: A model for adsorbed CO

Richard L. Dubs, Maile E. Smith,* and V. McKoy

Arthur Amos Noyes Laboratory of Chemical Physics, California Institute of Technology, Pasadena, California 91125

(Received 10 August 1987)

We present a study of angle-resolved photoelectron spectra from oriented, linear NiCO. We address the question: How well do simple cluster models such as oriented NiCO simulate adsorbate molecules with respect to photoemission? The photoemission cross sections are obtained using Hartree-Fock electronic continuum orbitals. For the bonding 5σ orbital, we find oriented NiCO to be a better model than oriented CO. The large magnitude of the 5σ photoionization cross sections relative to the 4σ cross section cannot, however, be explained by our calculations without consideration of backscattering of the photoelectrons ejected "downward" into the detector.

I. INTRODUCTION

Angle-resolved photoelectron spectroscopy (ARPES) has evolved into a powerful probe of adsorbate-substrate interactions. This technique provides detailed information concerning both site geometry and electronic bonding character. For example, ARPES can help determine the orientation of adsorbed molecules and the orbital symmetries associated with photoelectron spectra.¹⁻³

The prototype adsorbate-substrate system for ARPES studies has been CO on Ni.⁴⁻¹² Early continuum multiple-scattering calculations by Davenport⁴ were helpful in establishing that, in most cases, CO bonds perpendicular to the Ni surface with the carbon end down. In these studies it was originally assumed that the only role of the surface was to orient the molecule, and ARPES from an oriented CO molecule was taken as a model for photoemission from adsorbed CO. For ARPES from orbitals not directly involved in bonding to the surface, e.g., 1π and 4σ , this approximation is a good one, and good qualitative agreement between theory and experiment is found for such cases.^{5,8} However, as expected, oriented CO is a poor model for ARPES from orbitals directly involved in bonding to the metal surface, e.g., the 5σ orbital. A molecular fragment such as NiCO can be expected to be a more realistic model for photoemission from such orbitals. Recent studies have shown that local cluster models, e.g., NiCO, NiN₂, Ni₂CO, etc., can be good models for the chemisorption of N₂ and CO on Ni with regard to several spectroscopic properties.^{13,14} Indeed, Davenport has studied the angle-resolved photoemission from the oriented, linear triatomic NiCO, again using the multiple-scattering method.⁵

The principle objective of the present studies is to answer the question, "How well do simple cluster models such as oriented NiCO simulate adsorbate molecules with respect to photoemission?" In an effort to assess NiCO as a model for CO adsorbed on Ni, we have carried out *ab initio* calculations of the ARPES spectra for NiCO as a function of energy. In these calculations, we

use a Hartree-Fock wave function for the initial state of NiCO and frozen-core Hartree-Fock continuum orbitals in the final state. This method has been very successful in predicting and explaining a wide variety of phenomena relating to gas-phase molecular photoionization dynamics.¹⁵ Our results indicate that oriented NiCO is a better model than oriented CO for the bonding 5σ orbital, while CO itself is adequate for the nonbonding, 4σ and 1π , orbitals. However, the magnitude of the measured 5σ photoemission cross section relative to that of the 4σ along the surface normal cannot be accounted for in our calculations without inclusion of backscattering of "downward" ejected photoelectrons into the detector.

II. METHOD

The cross section for photoionization of an initial bound state Ψ_i into a final state $\Psi_{f,k}$ by linearly polarized light is proportional to the square of the dipole matrix element (in the length approximation)

$$I_{k,\hat{n}} = k^{1/2} \langle \Psi_i | \mathbf{r} \cdot \hat{n} | \Psi_{f,k}^{-1} \rangle, \quad (1)$$

where \hat{n} is the direction of polarization of the light and \mathbf{k} is the momentum of the photoelectron. The doubly differential cross section in the molecular frame is then given by

$$\frac{d^2\sigma}{d\Omega_k d\Omega_{\hat{n}}} = \frac{4\pi^2 E}{c} |I_{k,\hat{n}}|^2. \quad (2)$$

In these studies we use the Hartree-Fock wave function for Ψ_i in Eq. (1). For $\Psi_{f,k}^{-1}$ we invoke the frozen-core Hartree-Fock approximation in which the wave function is represented by an antisymmetrized product of $N-1$ bound orbitals, constrained to be identical to those of Ψ_i , and the photoelectron orbital. The determination of these photoelectron or continuum Hartree-Fock orbitals is a key step in the study of molecular photoionization.

In this approximation the photoelectron orbital satisfies the one-electron Schrödinger equation

$$\left[-\frac{1}{2}\nabla^2 + V_{N-1}(\mathbf{r}, R) - k^2/2 \right] \Phi_k(\mathbf{r}, R) = 0, \quad (3)$$

where V_{N-1} is the molecular ion potential at internuclear distance R , $k^2/2$ is the photoelectron kinetic energy, and $\Phi_{\mathbf{k}}$ satisfies the appropriate boundary condition. To obtain $\Phi_{\mathbf{k}}$ it is convenient to work with the integral form of Eq. (3), i.e.,

$$\Phi_{\mathbf{k}} = \Phi_{\mathbf{k}}^c + G_c^{(-)} V \Phi_{\mathbf{k}}, \quad (4)$$

where $\Phi_{\mathbf{k}}^c$ is the Coulomb scattering wave function, V is the molecular ion potential V_{N-1} with the Coulomb potential removed, i.e.,

$$V = V_{N-1} + \frac{1}{r}, \quad (5)$$

and $G_c^{(-)}$ is the Coulomb Green's function with incoming-wave boundary conditions, i.e.,

$$\left[-\frac{1}{2} \nabla^2 - \frac{1}{r} - \frac{k^2}{2} \right] G_c(\mathbf{r}, \mathbf{r}') = -\delta(\mathbf{r} - \mathbf{r}'). \quad (6)$$

Expansion of $\Phi_{\mathbf{k}}$ in a partial wave series about \mathbf{k} ,

$$\Phi_{\mathbf{k}}(\mathbf{r}) = \left[\frac{2}{\pi} \right]^{1/2} \sum_{l=0}^l \sum_{m=-l}^l i^l \Psi_{klm}(\mathbf{r}) Y_{lm}^*(\hat{\mathbf{k}}), \quad (7)$$

and substitution of this expansion in Eq. (4) shows that each Ψ_{klm} satisfies its own integral or Lippmann-Schwinger equation

$$\Psi_{klm}(\mathbf{r}) = S_{klm} + G_c^{(-)} V \Psi_{klm}, \quad (8)$$

where S_{klm} is a partial wave Coulomb function. In Eq. (7) an infinite sum over l has been truncated at $l=l_p$.

To solve Eq. (8) we use two different methods both of which rely on separable approximations to a potential U of the form:

$$U(\mathbf{r}, \mathbf{r}') = U^*(\mathbf{r}, \mathbf{r}') = \sum_{i,j} \langle \mathbf{r} | U | \alpha_i \rangle (U^{-1})_{ij} \langle \alpha_j | U | \mathbf{r}' \rangle, \quad (9)$$

where the matrix $(U^{-1})_{ij}$ is the inverse of the matrix with elements $\langle \alpha_i | U | \alpha_j \rangle$. In one method, referred to as method A, the entire potential V of Eq. (4) is approximated by the separable expansion of Eq. (9). With this approximation the solutions of Eq. (8) are given by

$$\Psi_{klm}^{(0)} = S_{klm}(\mathbf{r}) + \sum_{i,j} \langle \mathbf{r} | G_c^{(-)} V | \alpha_i \rangle (D^{-1})_{ij} \times \langle \alpha_j | V | S_{klm} \rangle, \quad (10)$$

where the matrix $(D^{-1})_{ij}$ is the inverse of the matrix with elements

$$D_{ij} = \langle \alpha_i | V - V G_c^{(-)} V | \alpha_j \rangle. \quad (11)$$

In the second method, referred to as method B, the potential V of Eq. (4) is broken into its direct and exchange

components, V_{dir} and V_{ex} , respectively, the integral equation associated with V_{dir} is numerically integrated, and only the exchange potential is approximated by the separable expansion of Eq. (9). The full solution of Eq. (4) can then be readily obtained.¹⁶ Since only the truly short-range exchange potential is approximated by Eq. (9), method B is particularly effective for obtaining solutions of Eq. (8) for the long-range potentials associated with strongly polar ions.

The basis functions $\alpha_i(\mathbf{r})$ in Eq. (9) can be chosen to be entirely discrete functions such as Cartesian Gaussian, spherical Gaussian, or Slater functions. In these studies we used a Cartesian Gaussian basis set centered on the nuclei. Such basis functions have been used successfully in electronic-structure calculations and are known to be effective in representing the multicenter nature of the scattering wave function in the near-molecular region. It is important to note that with only these discrete basis functions in the expansion of Eq. (9), the approximate scattering solutions $\Psi_{klm}^{(0)}$ of Eq. (10) do satisfy scattering boundary conditions. With adequate basis sets the continuum solutions $\Psi_{klm}^{(0)}$ can already provide quantitatively reliable and, at the Hartree-Fock level, variationally stable photoionization cross sections. In addition, we have developed iterative techniques for obtaining converged solutions of Eq. (8) and the associated cross sections.¹⁶ Details of these iterative techniques and of the related numerical procedures which we have developed for solving these equations are discussed elsewhere.^{16,17}

To obtain the ARPES spectra we expand the dipole matrix element of Eq. (2) in spherical harmonics

$$I_{\mathbf{k}, \hat{\mathbf{a}}} = \left[\frac{4\pi}{3} \right]^{1/2} \sum_{l,m,\mu} I_{lm\mu} Y_{lm}^*(\hat{\mathbf{k}}) Y_{l\mu}^*(\hat{\mathbf{a}}), \quad (12)$$

where the dynamical coefficients $I_{lm\mu}$ are defined as

$$I_{lm\mu} = k^{1/2} \langle \Phi_i | r_{\mu} | \Psi_{klm}^{(-)} \rangle \quad (13)$$

for photoionization out of an orbital Φ_i and

$$r_{\mu} = \begin{cases} \mp(x \pm iy)/\sqrt{2} & \text{for } \mu = \pm 1 \\ z & \text{for } \mu = 0. \end{cases} \quad (14)$$

In practice the summation over l in Eq. (12) is truncated at some $l=l_{\text{max}}$. To obtain the differential cross sections of Eq. (2) we write $|I_{\mathbf{k}, \hat{\mathbf{a}}}|^2$ as

$$|I_{\mathbf{k}, \hat{\mathbf{a}}}|^2 = \sum_{L'=0}^{2l_{\text{max}}} \sum_{L=0}^2 \sum_{M=-L}^L \beta_{L'L M} Y_{L'-M}(\theta_k, \phi_k) \times Y_{LM}(\theta_n, \phi_n), \quad (15)$$

where

$$\beta_{L'L M} = [(2L+1)(2L'+1)]^{-1/2} \langle 1100 | L0 \rangle \sum_{l,m,\mu} \sum_{l',m',\mu'} (-1)^{m+\mu} [(2l+1)(2l'+1)]^{1/2} I_{lm\mu} I_{l'm'\mu'}^* \times \langle l'l'00 | L'0 \rangle \langle l'l'-mm' | L'-M \rangle \langle 11-\mu\mu' | LM \rangle. \quad (16)$$

Here (θ_k, ϕ_k) and (θ_n, ϕ_n) denote the polar angles for electron collection and photon polarization, respectively, in the molecular frame and $\langle l_1 l_2 m_1 m_2 | l_3 m_3 \rangle$ denotes a Clebsch-Gordan coefficient. The internuclear axis lies along the z axis of the molecular frame. In these studies we assume that the CO molecule is oriented along the laboratory frame z axis, i.e., normal to the Ni surface, and hence the laboratory and molecular frames coincide. Equations (15) and (16) can be easily modified for cases in which the two frames do not coincide. In general, for a given orientation of the molecule and photon energy, the $\beta_{L,LM}$ of Eq. (16) must be evaluated only once, after which Eq. (15) can be used to readily obtain the ARPES spectra for any experimental configuration of electron collection and photon polarization.

III. CALCULATIONS

For the self-consistent field (SCF) wave function of NiCO we used a contracted segmented $[3s, 2p, 1d]$ Cartesian Gaussian basis derived from a primitive $(9s, 5p, 1d)$ basis¹⁸ on carbon and oxygen and an $[8s, 6p, 2d]$ set on the nickel contracted from a $(14s, 11p, 5d)$ basis.¹⁹ This basis set was augmented with diffuse s and p functions with exponents of 0.1 and 0.05 at the center of charge of the CO bond. These basis functions with smaller exponents were added in between the carbon and oxygen

nuclei so as to assure the correct behavior in the tail of the 5σ CO molecular orbital. Without such basis functions earlier studies²⁰ showed significant differences in the photoionization cross section obtained using identical continuum functions and a 5σ orbital expanded in a Slater basis or the standard valencelike Gaussian basis, e.g., $[4s, 3p]$. Details of the CO calculations have been given previously.²⁰ We take the CO bond distance to be 2.173 a.u. and the Ni—C bond distance to be 3.477 a.u., which are the lengths of these bonds in $\text{Ni}(\text{CO})_4$.²¹ We also choose the ground electronic state of NiCO to be a $^1\Sigma^+$ state with a Ni $3d^{10}$ configuration. We assume this configuration for the Ni atom because this is its configuration in the ground state of $\text{Ni}(\text{CO})_4$,²¹ and, furthermore, studies of the electronic structure of both NiN_2 and NiCO showed their ground states to be $^1\Sigma^+$ and characterized by a significant Ni $3d^{10}$ component in the wave function.¹³ With this choice, basis sets, and geometry, our SCF energy was -1618.7383 a.u.

The initial basis sets used in the solution of Eq. (8) for the photoelectron continuum orbitals of NiCO are shown in Table I. For these orbitals we used the procedure based on method B outlined above. The results presented here have not been iterated, since we found in previous work that iteration was often unnecessary in producing converged cross sections with method B. For the few checks we did perform, iteration showed no significant changes from the uniterated results. From

TABLE I. Gaussian basis sets used in obtaining the photoelectron orbitals for NiCO, defined as $\phi(r) = N(x - A_x)^l (y - A_y)^m (z - A_z)^n \exp(-\alpha |r - \mathbf{A}|^2)$.

Center (A)	l	m	n	Exponent (α)
$k\sigma$				
Ni	0	0	0	32.0, 16.0, 6.0, 2.0, 0.6, 0.2
	0	0	1	8.0, 2.0, 0.5
	0	0	2	2.0, 0.5
C	0	0	0	10.0, 4.0, 1.5, 0.5, 0.1
	0	0	1	1.0, 0.1
	0	0	2	1.0
O	0	0	0	10.0, 4.0, 1.5, 0.5, 0.1
	0	0	1	1.0, 0.1
	0	0	2	1.0
$k\pi$				
Ni	1	0	0	32.0, 16.0, 6.0, 2.0, 0.6, 0.2
	1	0	1	8.0, 2.0, 0.5
C	1	0	0	10.0, 4.0, 1.5, 0.5, 0.1
	1	0	1	1.0, 0.1
O	1	0	0	10.0, 4.0, 1.5, 0.5, 0.1
	1	0	1	1.0, 0.1
$k\delta$				
Ni	1	1	0	32.0, 16.0, 6.0, 2.0, 0.6, 0.2
C	1	1	0	10.0, 4.0, 1.5, 0.5, 0.1
O	1	1	0	10.0, 4.0, 1.5, 0.5, 0.1

our experience and such checks, the basis sets of Table I should provide reliable estimates of the photoionization cross section of NiCO. Several tests were also carried out to determine values of the truncation parameters of the partial wave expansions which would provide reasonably converged cross sections. As expected, our main concern here was the expansion parameters which would be adequate for the $1s$ orbital of the Ni atom. At the photoelectron kinetic energies in the studies, we found that the photoionization cross sections for the outer valence orbitals were insensitive to the actual convergence of the partial wave expansion of the $1s$ orbital. This, of course, assumes that the partial wave expansion of this orbital is scaled so that the orbital used in the numerical calculation is always renormalized to unity. Such a renormalization is also carried out for the other orbitals, including those for which the partial wave expansions are highly converged. For example, a partial wave expansion of $l_i^{\text{dir}}=58$ for the orbitals in the direct potential of NiCO^+ led to essentially the same photoionization cross sections as using $l_i^{\text{dir}}=29$, even though the normalizations for the 1σ orbital (essentially the $1s$ Ni orbital) were about 0.68 and 0.3, respectively.²⁰ In many of these calculations we consequently used the same choice of truncation parameters for the partial wave expansions as in our earlier studies of CO,²⁰ including $l_i^{\text{dir}}=29$. However, several checks on the convergence of the associated cross sections were made by doubling the partial wave expansions. Such studies indicated that the cross section we present here are converged to within 5–10%, which is appropriate for the present objectives.

All the cross sections presented here are obtained using the dipole-length approximation. As a check on the possible uncertainties in these cross sections arising from our use of approximate electronic wave functions, i.e., the Hartree-Fock form, we also obtained the cross sections in the dipole-velocity approximation. Although the cross sections obtained with the length and velocity forms do differ [e.g., in reference to Fig. 4, differential cross section (Mb/sr) for the 5σ peak at $\theta_k=0^\circ$ (length/velocity), 6.02/4.98; at $\theta_k=180^\circ$, 9.10/7.38; for the 4σ peak at $\theta_k=0^\circ$, 6.75/6.40; at $\theta_k=180^\circ$, 1.06/0.948], the conclusions we draw in this paper are independent of the actual form chosen.

The photon energies referred to in these studies assume the experimental values for the associated ionization potentials. For CO these are 19.7, 16.9, and 14.0 eV for the 4σ , 1π , and 5σ orbitals, respectively,⁸ while for NiCO we use the experimental values for CO adsorbed on Ni, i.e., 16.5, 11.9, and 13.5 eV.⁸ However, in comparing the spectra of CO and NiCO, we want to look at points in the spectra corresponding to the same photoelectron kinetic energy and not necessarily the same photon energy, since the former determines the photoelectron dynamics. Hence, in Figs. 1 and 3, the photoionization spectra for CO have been shifted down in photon energy by 3.2, 5.0, and 0.5 eV for the 4σ , 1π , and 5σ orbitals, respectively. Finally, although the 4σ , 1π , and 5σ levels of CO actually correspond to the 9σ , 3π , and 10σ orbitals in NiCO, in our discussion we will use the CO designations of 4σ , 1π , and 5σ .

IV. RESULTS AND DISCUSSIONS

In Figs. 1 and 2 we compare some of our calculated cross sections for CO and NiCO with the experimental data of Allyn *et al.*⁷ for adsorbed CO. The CO is assumed oriented perpendicular to the Ni surface with the carbon end down. Here, and elsewhere, the angles (θ_i, ϕ_i) are standard polar angles where θ is measured relative to the z axis, $\phi=0^\circ$ represents the positive x axis, and $\phi=90^\circ$ the positive y axis. In these experiments⁷ polarized light was used with $(\theta_i, \phi_i)=(45^\circ, 0^\circ)$ and the photoelectrons were collected normal to the surface, i.e., $(\theta_k, \phi_k)=(0^\circ, 0^\circ)$. The experimental data have been normalized by setting the peak value of the measured 4σ photoemission cross section to the calculated 4σ (NiCO) cross section. As expected, the " 4σ " cross sections change little in shape and magnitude in going from CO to NiCO. Why the calculated 4σ cross sections are shifted down from the experimental data will be discussed later. Recall, however that our calculated 4σ (CO) spectra are shifted down in energy by 3.2 eV for reasons discussed above.

Figures 1 and 2 also show that the calculated 5σ (CO) and 5σ (NiCO) cross sections seriously underestimate the magnitude of the measured values. The NiCO results are only a slight improvement over those of CO. Although the experimental data also include contributions from photoionization of the 1π level, its contribution is expected to be negligible for electron collection along the molecular axis.²² Calculations confirm this behavior. Why then do the experimental results show the 5σ cross section much larger than the 4σ cross section while the calculations do not? This problem is especially disturbing for the NiCO case in which the bonding CO 5σ orbital should be fairly well described due to inclusion of the Ni atom. Of the many possible reasons

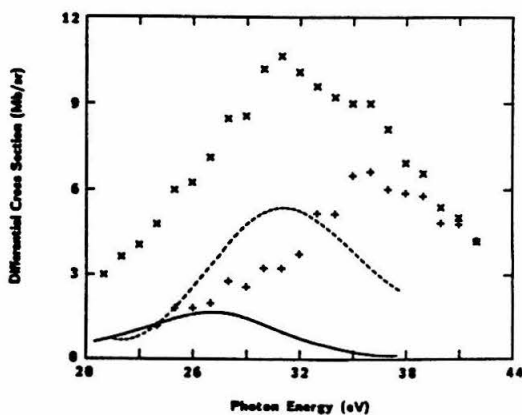


FIG. 1. Differential cross section vs photon energy for $(\theta_i, \phi_i)=(45^\circ, 0^\circ)$ and $(\theta_k, \phi_k)=(0^\circ, 0^\circ)$. Present results for CO: 4σ (---); 5σ (—). Experimental data of Allyn *et al.* (Ref. 7): 4σ (+ + +); $5\sigma+1\pi$ (x x x). See text for normalization of experimental data and energy scale for CO results.

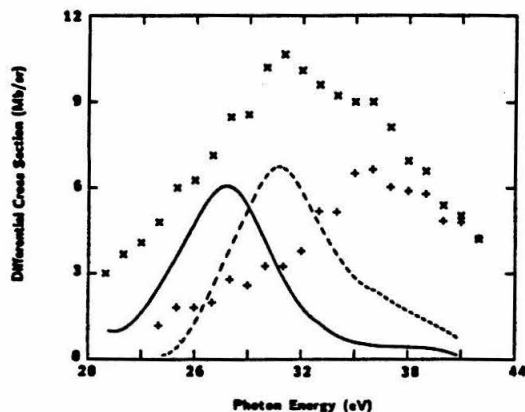


FIG. 2. Differential cross section vs photon energy for $(\theta_n, \phi_n) = (45^\circ, 0^\circ)$ and $(\theta_k, \phi_k) = (0^\circ, 0^\circ)$. Present results for NiCO: 4σ (---); 5σ (—). Experimental data of Allyn *et al.* (Ref. 7): 4σ (+++); $5\sigma + 1\pi$ (×××). See text for normalization of experimental data.

for the significant differences between theory and experiment we have assessed two within the limits of our triatomic model. The first involves the Ni—C bond length used in our calculations. This distance, 3.477 a.u., is that found in Ni(CO)₄.²¹ However, as noted by Kao and Messmer,¹³ low-energy electron diffraction studies of CO adsorbed on Ni[100] suggest a bond distance of 3.25–3.40 a.u. For the s^0d^{10} configuration, Kao and Messmer¹³ actually calculated a Ni—C bond length of 2.880 a.u. in NiCO, though they believe this value to be too short. To assess the influence of a shorter Ni—C bond distance on the 5σ cross sections in NiCO, we repeated our calculations on NiCO with a Ni—C distance of 3.251 a.u. These results are not shown but retain the same qualitative features of Fig. 2.

Some insight into this discrepancy between theory and experiment could also be obtained by considering the

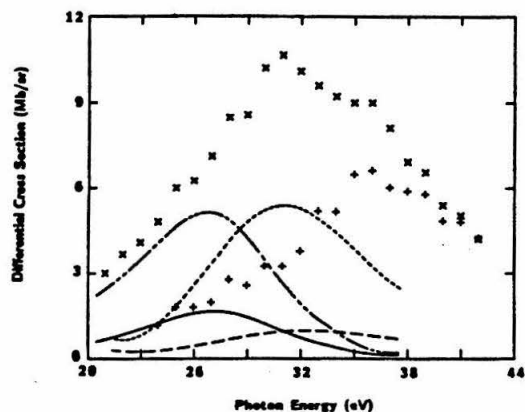


FIG. 3. See Fig. 1. Also shown are cross sections at $(\theta_k, \phi_k) = (180^\circ, 0^\circ)$ for CO: 4σ (---); 5σ (-·-·-).

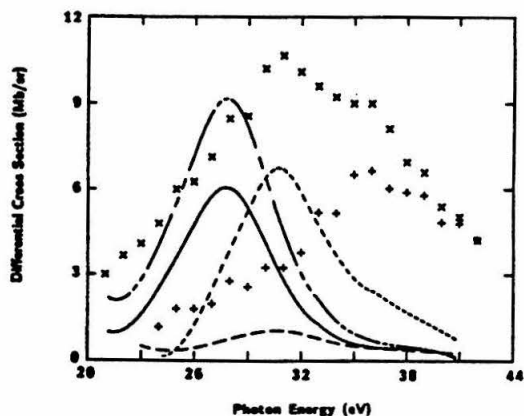


FIG. 4. See Fig. 2. Also shown are cross section at $(\theta_k, \phi_k) = (180^\circ, 0^\circ)$ for NiCO: 4σ (---); 5σ (-·-·-).

electrons photoejected downward from the adsorbed CO toward the surface. The theoretical results in Figs. 1 and 2 totally neglect these downward ejected electrons though, in reality, on an actual metal surface many of these electrons could be reflected back upward into the detector. In Figs. 3 and 4 we show the cross sections for these downward ejected electrons ($\theta_k = 180^\circ$) from CO and NiCO, respectively. For convenience, the results of Figs. 1 and 2 have also been included. Note that the cross section for downward ejected electrons from the “ 4σ ” orbital or either CO or NiCO is negligible relative to the upward ($\theta_k = 0^\circ$) flux. This result is consistent with the fact that the 4σ orbital is localized on the oxygen end of CO and thus points away from the surface.

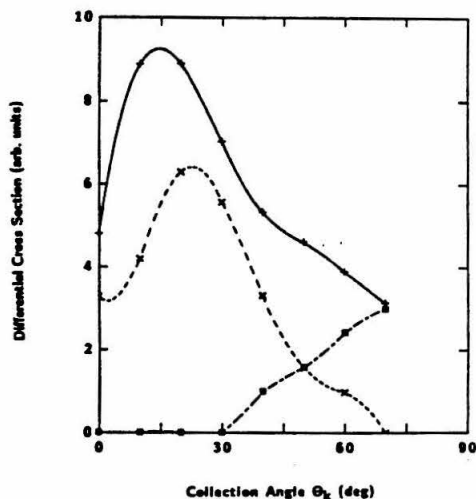


FIG. 5. Differential cross section vs the collection angle θ_k at $\phi_k = 0^\circ$ for unpolarized radiation. (See text.) Photon energy equals 40.8 eV. Experimental data of Williams *et al.* (Ref. 8): 5σ (—); 4σ (---); 1π (-·-·-).

However, the cross section for downward ejected electrons from the "5 σ " orbital of CO or NiCO is *greater* than the upward cross section. This result is consistent with the fact that the 5 σ orbital is located on the carbon end of CO and points directly toward the surface. Although with our simple NiCO model we cannot quantify the fraction of electrons reflected by the surface, our results suggest that these reflected electrons could be responsible for the large experimental 5 σ cross section. Note that even if all the downward CO electrons in Fig. 3 were reflected upward into the detector along with the $\theta_k=0$ electrons, our CO calculations would still not account for the large 5 σ cross section. Our NiCO calcula-

tion of Fig. 4 is more suggestive in this respect.

In addition to predicting the incorrect magnitude of the 5 σ peak in Fig. 2, the NiCO calculation does not account for the correct peak position or width. These latter discrepancies between the NiCO results and those of experiment are most likely due to relaxation effects.⁷ As stated earlier, our studies used the frozen-core approximation, in which the orbitals of the ion are constrained to be identical to those of the neutral molecule. The frozen-core approximation used here completely neglects any screening of the molecular ion seen by the photoelectron.²² Although this approximation may be appropriate for photoionization of gas-phase molecules, it can certainly be expected to work poorly for adsorbate

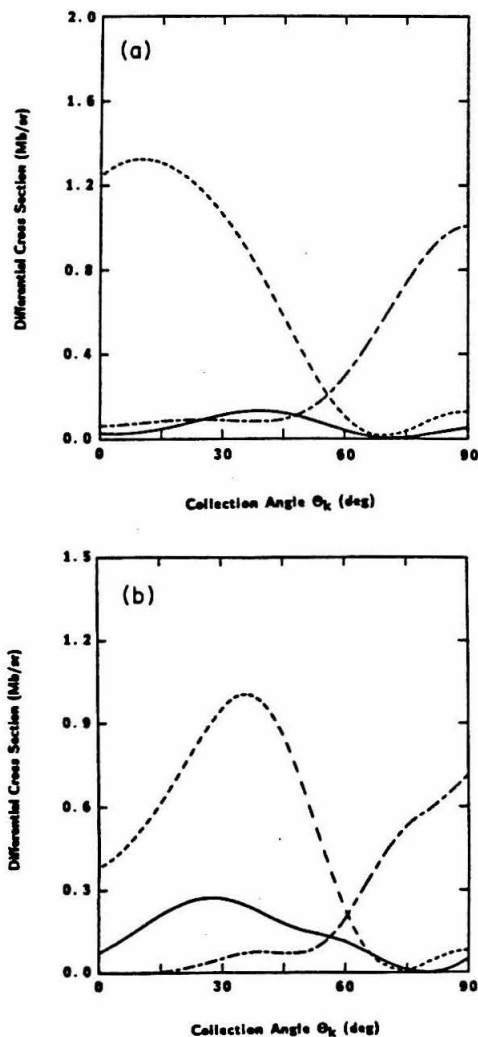


FIG. 6. Differential cross section vs the collection angle θ_k at $\phi_k=0^\circ$ for unpolarized radiation. (See text.) Photon energy equals 40.8 eV. 5 σ (—); 4 σ (---); 1 π (-·-·-). (a) Present results for CO; (b) present results for NiCO.

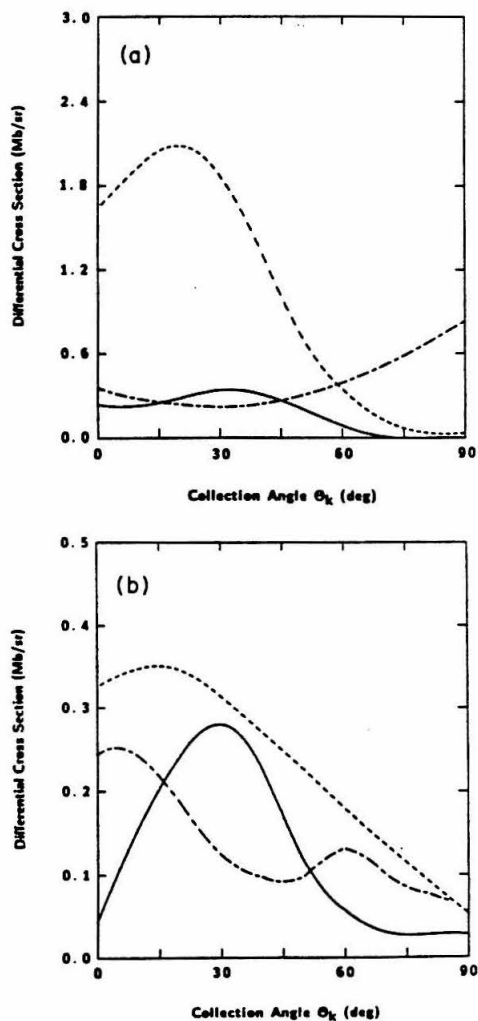


FIG. 7. Differential cross section vs the collection angle θ_k at $\phi_k=0^\circ$ for unpolarized radiation. (See text.) Photon energy equals 40.8 eV. 5 σ (—); 4 σ (---); 1 π (-·-·-). (a) Results of Ref. 5 for CO; (b) results of Ref. 5 for NiCO.

molecules on metals where electrons from the metal can very effectively screen and neutralize the adsorbate ion.

In addition to these energy-dependent studies, angle-resolved studies are an important test of our model for adsorbate photoemission. Figure 5 shows such data for CO on Ni[111].⁸ In this experiment, unpolarized He II (40.8 eV) radiation was used, and the photon incidence angle was held fixed at 45° from the surface normal. Here we treat unpolarized light as two orthogonal linearly polarized components which contribute independently to photoemission.¹⁰ One component is in the plane of incidence $(\theta_n, \phi_n) = (45^\circ, 0^\circ)$ and the other is perpendicular to this plane, i.e., $(\theta_n, \phi_n) = (90^\circ, 90^\circ)$. Photoelectron collection was in the incident plane $\phi_k = 0^\circ$. In Fig. 5 the emission intensities for the 4σ , 1π , and 5σ orbitals are shown as a function of the collection angle θ_k . These angular distributions agree qualitatively with the prediction by Grimley for photoemission from atomic p orbitals.²³

In Figs. 6(a) and 6(b), our results for photoionization from oriented CO and NiCO, respectively, are shown. Our CO results have not been corrected for the difference in ionization potentials between gas-phase and adsorbed CO as was done in the energy-dependent studies shown in Figs. 1 and 3. This allows for a more-direct comparison with the multiple-scattering calculations of Davenport.⁵ We do not consider surface-reflected electrons in these angular distributions since we cannot quantify this effect within our present model. Aside from an overall change of scale, our CO and NiCO results are very similar, with the 4σ peak shifted to slightly higher angles in the NiCO case. However, while the experimental results show the 5σ peak cross section greater in magnitude than that of the 4σ peak, both our CO and NiCO results show the 5σ peak far less in magnitude.

For comparison, Davenport's results⁵ for photoionization from oriented CO and NiCO are shown in Figs. 7(a) and 7(b). Davenport's CO results are similar to our CO and NiCO results. His NiCO results, on the other hand, show some significant differences from those of CO. Aside from an overall change of scale, the 5σ peak has increased in magnitude relative to the 4σ peak, but, still

in contrast to the experimental data, remains smaller. In addition, the NiCO 1π spectrum is very different from the CO results. Unfortunately, the experimental peak which Williams *et al.* assign as 1π might actually be substrate derived.¹¹

As a final note, our model does not include the contribution from backscattering of downward ejected electrons by adjacent surface atoms. Similarly, we exclude the effects of photon reflection²⁴⁻²⁶ and electron refraction²⁶ at the surface. These latter two contributions should not be very important in the experiments considered here. In all studies, the photon is incident at 45° from the surface normal, an angle at which reflection effects should be minimal,²⁴ especially at 40.8 eV where the angular studies are performed.²⁵ In the energy-dependent studies, collection is normal to the surface, where refraction effects should not be important.²⁷ We do not find refraction effects to be very important in the angular studies either (peaks are broadened and shifted to slightly higher angle),²⁷ and exclude them to make easier a direct comparison with the calculations of Davenport.⁵

In conclusion, we have performed *ab initio* calculations of angle-resolved photoelectron spectra from oriented, linear triatomic NiCO as a function of energy. For the orbitals not directly involved in bonding to the surface, we find that oriented CO provides a satisfactory model for CO adsorbed on Ni. However, for the 5σ orbital directly involved in bonding, oriented NiCO is better. The results of this cluster model cannot account for the large 5σ cross sections observed experimentally unless we consider the scattering of "downward" ejected photoelectrons into the detector. Our angular distributions for oriented CO agree reasonably well with those of the multiple-scattering model. However, our NiCO results do not.

ACKNOWLEDGMENTS

This work was supported by Grant No. CHE-85-21391 from the National Science Foundation. We also acknowledge use of the resources of the San Diego Supercomputer Center. One of us (R.L.D.) acknowledges support by the National Science Foundation.

*Present address: Institute for Defense Analyses, 1801 North Beauregard Street, Alexandria, VA 22311.

¹E. W. Plummer and T. Gustafsson, *Science* **198**, 165 (1977).

²D. A. Shirley, J. Stöhr, P. S. Wehner, R. S. Williams, and G. Apai, *Phys. Scr.* **16**, 398 (1977).

³N. V. Smith, *J. Phys. (Paris) Colloq.* **39**, C4-161 (1978).

⁴J. W. Davenport, *Phys. Rev. Lett.* **36**, 945 (1976).

⁵J. W. Davenport, *J. Vac. Sci. Technol.* **15**, 433 (1978).

⁶S. Wallace, D. Dill, and J. L. Dehmer, *Phys. Rev. B* **17**, 2004 (1978).

⁷C. L. Allyn, T. Gustafsson, and E. W. Plummer, *Chem. Phys. Lett.* **47**, 127 (1977).

⁸P. M. Williams, P. Butcher, J. Wood, and K. Jacobi, *Phys. Rev. B* **14**, 3215 (1976).

⁹R. J. Smith, J. Anderson, and G. J. Lapeyre, *Phys. Rev. Lett.* **37**, 1081 (1976).

¹⁰G. P. Apai, P. S. Wehner, R. S. Williams, J. Stöhr, and D. A. Shirley, *Phys. Rev. Lett.* **37**, 1497 (1976).

¹¹T. Gustafsson, *Surf. Sci.* **94**, 593 (1980).

¹²C. L. Allyn, T. Gustafsson, and E. W. Plummer, *Solid State Commun.* **28**, 85 (1978).

¹³C. M. Kao and R. P. Messmer, *Phys. Rev. B* **31**, 4835 (1985).

¹⁴H. J. Freund, R. P. Messmer, C. M. Kao, and E. W. Plummer, *Phys. Rev. B* **31**, 4848 (1985).

¹⁵See, for example, V. McKoy, T. A. Carlson, and R. R. Lucchese, *J. Phys. Chem.* **88**, 3188 (1984).

¹⁶M. E. Smith, R. R. Lucchese, and V. McKoy, *Phys. Rev. A* **29**, 1857 (1984).

- ¹⁷R. R. Lucchese, G. Raseev, and V. McKoy, *Phys. Rev. A* **25**, 2572 (1982).
- ¹⁸T. H. Dunning, Jr. and P. J. Hay, in *Modern Theoretical Chemistry 3*, edited by H. F. Schaefer III (Plenum, New York, 1977), p. 1.
- ¹⁹T. Smedley and W. A. Goddard III (unpublished).
- ²⁰R. R. Lucchese and V. McKoy, *Phys. Rev. A* **28**, 1382 (1983).
- ²¹A. B. Rives and R. F. Fenske, *J. Chem. Phys.* **75**, 1293 (1981).
- ²²D. L. Lynch and V. McKoy, *Phys. Rev. A* **30**, 1561 (1984);
D. L. Lynch, Ph. D. thesis, California Institute of Technology, 1986.
- ²³T. B. Grimley, *Discuss. Faraday Soc.* **58**, 7 (1974).
- ²⁴S. P. Weeks and E. W. Plummer, *Solid State Commun.* **21**, 695 (1977).
- ²⁵K. Jacobi, M. Scheffler, K. Kambe, and F. Forstmann, *Solid State Commun.* **22**, 17 (1977).
- ²⁶M. Scheffler, K. Kambe, and F. Forstmann, *Solid State Commun.* **25**, 93 (1978).
- ²⁷R. L. Dubs (unpublished).

**Chapter 9: Studies of NiN₂ as a Model for Photoemission from N₂
 Adsorbed on Nickel**

[The text of this chapter appeared in: R. L. Dubs and V. McKoy, Chem.
Phys. Lett. 142, 237 (1988).]

STUDIES OF NiN₂ AS A MODEL FOR PHOTOEMISSION FROM N₂ ADSORBED ON NICKEL [★]

Richard L. DUBS and Vincent McKOY

A.A. Noyes Laboratory of Chemical Physics, California Institute of Technology, Pasadena, CA 91125, USA

Received 10 August 1987; in final form 1 October 1987

We report a theoretical study of angle-resolved photoelectron spectra (ARPES) for the oriented, linear triatomic NiN₂. This study was motivated by the work of Horn et al. (Surface Sci. 118 (1982) 465), who studied ARPES spectra from N₂ adsorbed on Ni[110] and observed a resonance feature in the 2 δ_u cross section which is not present in the gas phase N₂ spectra. We confirm that this feature could be a result of symmetry breaking of the homonuclear N₂ orbitals by the surface. However, in this case we find that surface reflection of the emitted electrons cannot be ignored in interpretation of the experimental data.

1. Introduction

In the past ten years, angle-resolved photoelectron spectroscopy (ARPES) has evolved into a powerful probe of adsorbate-substrate interactions. Adsorbate orientation, orbital symmetry, and binding energy are all potentially accessible with this method [1-3]. Recently, Horn et al. [4] studied the adsorption of N₂ on Ni[110] with ARPES. They observed an apparent resonance in the adsorbate 2 δ_u cross section which is not observed in the gas phase spectrum [5] and which they attributed to symmetry breaking of the homonuclear N₂ orbitals by the surface [4].

We have investigated this observation by calculating ARPES spectra for the oriented, linear triatomic NiN₂. Such cluster models have been successful in reproducing a variety of spectroscopic properties of adsorbate-substrate systems [6,7]. We find that the resonance is indeed present in the 2 δ_u cross section, but is apparent only in electron flux emitted downward toward the Ni surface. This result is not entirely unexpected since the 2 δ_u orbital itself is pointed downward from the N₂ toward the Ni surface [4]. Our results suggest that if symmetry breaking is the explanation of this feature in the 2 δ_u photoionization cross section, surface reflection of

the photoelectrons cannot be ignored in interpreting the experimental data. Previously, we arrived at the same conclusion in studies of the photoionization of the 5 δ orbital of NiCO as a model for photoemission of adsorbed CO[8].

2. Calculations

The method used to calculate the photoionization cross sections for NiN₂ has been discussed previously in studies of NiCO [8]. The ground state of NiN₂ is assumed to be a ¹ Σ^+ state with a Ni 3d¹⁰ configuration [6,8]. As shown by Kao and Messmer [6], near the equilibrium internuclear distance this wavefunction has a significant admixture of the Ni 3d¹⁰ configuration. For the SCF wavefunction of NiN₂ we used a contracted segmented [3s, 2p, 1d] Cartesian Gaussian basis derived from a primitive (9s, 5p, 1d) basis [9] on each nitrogen and a [8s, 6p, 2d] set on the nickel contracted from a (14s, 11p, 5d) basis [8,10]. This basis was augmented with diffuse s and p functions with exponents of 0.1 and 0.05 at the center of the N₂ bond [8]. The N₂ bond distance was always taken as 1.1 Å, which is that of gas phase N₂ and has been used in other NiN₂ studies [6,11]. The Ni-N bond distance was taken as 1.64 Å [6] for all calculations except those of fig. 4 as explained later.

[★] Contribution No. 7634.

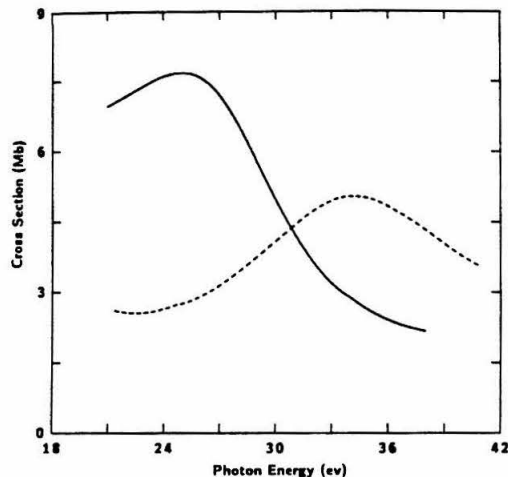


Fig. 1. Cross section versus photon energy for gas phase CO: 5σ , —; 4σ , ----.

The approximate experimental ionization potentials of 16.6 and 13.1 eV for the $2\tilde{\sigma}_u$ and $3\tilde{\sigma}_g$ orbitals, respectively, for N_2 adsorbed on Ni[110] were used in the calculations [4].

3. Background

3.1. Gas phase results

In figs. 1 and 2 we show the calculated cross sections for photoionization of gas phase CO [12] and N_2 [13], respectively. These two molecules are iso-electronic. The cross sections shown reproduce the relevant resonant features in the experimental cross sections [12,13]. Note that for the $3\sigma_g$ orbital of N_2 and for both the 4σ and 5σ orbitals of CO strong "resonant" enhancements are seen in these cross sections. The resonances are well known to arise from the $l=3$ partial wave component of the $k\sigma$ photoelectron wavefunction [14]. A dipole transition from an orbital such as the $3\sigma_g$ in N_2 must access odd partial waves in the continuum and therefore the $l=3$ resonance is present. CO is heteronuclear and dipole transitions from its 4σ and 5σ orbitals result in both even and odd partial waves in the continuum. However, a dipole transition from the ungerade orbital such as $2\sigma_u$ in N_2 must access only even partial waves

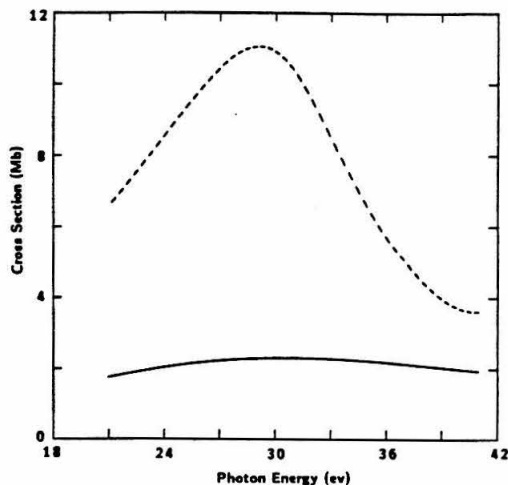


Fig. 2. Cross section versus photon energy for gas phase N_2 : $2\sigma_u$, —; $3\sigma_g$, ----.

in the continuum and in a one-electron approximation cannot have an $l=3$ component. For this reason, the cross section for the $2\sigma_u$ orbital of N_2 appears featureless as a function of energy.

3.2. N adsorbed on Ni[110]

Horn et al. [4] have determined that N_2 terminally bonds to a single Ni atom on the Ni[110] surface with its molecular axis perpendicular to the surface plane. Shown in fig. 3 are their experimental data for photoionization of the $3\tilde{\sigma}_g$ and $2\tilde{\sigma}_u$ orbitals of adsorbed N_2 . We retain the N_2 designation for the orbitals with the tilde designating adsorption. In the experiment, the electric vector of the light was 40° from the surface normal ($\theta_n=40^\circ$) and the electrons are collected along the normal ($\theta_k=0^\circ$) [4]. The resonance in the $3\tilde{\sigma}_g$ cross section is expected and is consistent with the gas phase results. However, the $2\tilde{\sigma}_u$ cross section shows a resonance as well. Horn et al. [4] suggested that this resonance is due to breaking of the homonuclear symmetry of N_2 , which removes the "g" or "u" character of the orbitals. A dipole transition from the $2\tilde{\sigma}_u$ orbital can then pick up some odd partial wave character in the continuum, i.e. the f-wave shape resonance. [4].

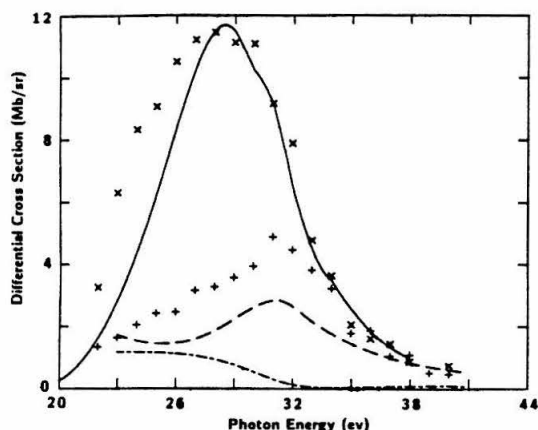


Fig. 3. Differential cross section versus photon energy at $(\theta_n, \phi_n) = (40^\circ, 0^\circ)$, $(\theta_k, \phi_k) = (0^\circ, 0^\circ)$. Present results for NiN_2 : $3\sigma_g$, —; $2\sigma_u$ ----. Experimental data of Horn et al. [4] for N_2 on Ni[110]: $3\sigma_g$, x; $2\sigma_u$, +. In addition, present results for NiN_2 at collection angle $(\theta_k, \phi_k) = (180^\circ, 0^\circ)$: $2\sigma_u$, ---.

4. Results

Fig. 3 shows our calculated photoemission cross sections for the oriented, molecular fragment NiN_2 . In these calculations the electric vector is also at 40° from the surface normal and photoelectrons are collected along the surface normal. The experimental data have been normalized to give best agreement to the calculated $3\sigma_g$ cross sections since this orbital points away from the Ni surface [4] and, therefore, the photoelectrons from this orbital should be least affected by the surface. Note that the calculation at $\theta_k = 0^\circ$ does not reproduce the resonance feature in the $2\sigma_u$ cross section. Obviously the removal of the homonuclear nature of the N_2 orbitals by the Ni atom is not apparent in our calculated cross sections at $\theta_k = 0^\circ$.

In fig. 3, we also include the cross section for photoemission from the $2\sigma_u$ orbital *downward* toward the surface ($\theta_k = 180^\circ$). The resonance structure is clearly seen in this curve. This result is not surprising given that the $2\sigma_u$ orbital itself points downward from the N_2 molecule toward the surface [4]. Our results suggest that if the symmetry-breaking explanation is correct, the experimentally observed resonance is *not* due to electrons emitted from the N_2 molecule di-

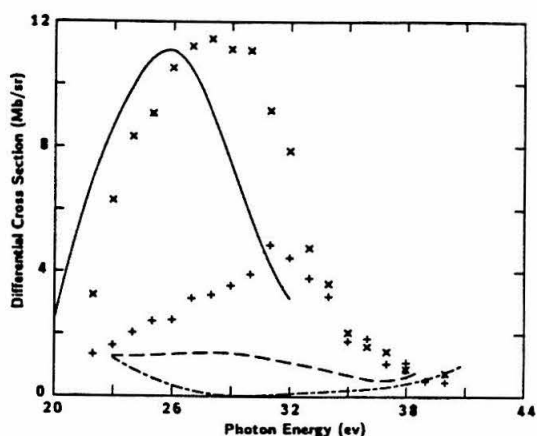


Fig. 4. Differential cross section versus photon energy. Same as fig. 3, but for a Ni-N distance of 2.0 Å.

rectly into the detector, but rather is due to electrons emitted downward from the $2\sigma_u$ end of the molecule and *reflected* by the surface into the detector. Previously, a similar argument was used in an attempt to explain the discrepancy in magnitude between theory and experiment for CO adsorbed on a Ni surface as modeled by oriented linear NiCO [8].

The calculations discussed above were all performed at a Ni-N bond distance of 1.64 Å [6]. Although a shorter bond distance would be expected to enhance the symmetry-breaking effect, theoretical calculations [6] indicate that 1.64 Å is as short as is physically reasonable. Hence, calculations at a shorter distance were not performed. However, in fig. 4 we show the same curves as in fig. 3 but for a bond distance of 2.0 Å [11]. Note the $2\sigma_u$ resonance is absent in both the upward and downward photoelectron flux. Apparently at this longer bond distance the Ni atom does not perturb the N_2 molecule enough to allow the resonant $l=3$ partial wave to contribute significantly to the $2\sigma_u$ cross section. This result suggests that experimental photoionization cross sections supplemented by calculations of the type presented here might be helpful in determining bond distances in adsorbate-substrate systems.

As a final note, an alternative to the symmetry-breaking explanation for the experimental $2\sigma_u$ resonance may be as follows. Recently Stephens and Dill [15] showed that interchannel continuum-continuum coupling in N_2 can cause the $3\sigma_g$ resonance

to manifest itself in the $2\sigma_u$ photoelectron angular distributions. This work stimulated further theoretical [16] and experimental [17,18] studies. The interchannel coupling effect in the photoionization of the $2\sigma_u$ orbital has been demonstrated experimentally in both asymmetry parameters [17] and vibrational branching ratios [18], although it appears to be practically washed out of the total cross section [16]. However, all these experiments are on gas phase molecules in which an average over molecular orientation is required. The experiment of Horn et al. [4], on the other hand, is on an oriented N_2 molecule with photoelectron collection along its molecular axis. This configuration is optimal for observation of a $\sigma \rightarrow k\sigma$ resonance. For this reason interchannel coupling cannot be ruled out as a possible explanation of the apparent resonant enhancement in the $2\sigma_u$ photoemission cross sections of adsorbed N_2 . Without an explicit calculation, however, it is difficult to estimate the magnitude of this contribution to the cross section.

Acknowledgement

This work was supported by Grant CHE-8521391 from the National Science Foundation. We also acknowledge use of the resources of the San Diego Supercomputer Center which is supported by the National Science Foundation.

References

- [1] E.W. Plummer and T. Gustafsson, *Science* 198 (1977) 165.
- [2] D.A. Shirley, J. Stöhr, P.S. Wehner, R.S. Williams and G. Apai, *Physica Scripta* 16 (1977) 398.
- [3] N.V. Smith, *J. Phys. (Paris)* 39 (1978) C4-161.
- [4] K. Horn, J. DiNardo, W. Eberhardt, H.-J. Freund and E.W. Plummer, *Surface Sci.* 118 (1982) 465.
- [5] E.W. Plummer, T. Gustafsson, W. Gudat and D.E. Eastman, *Phys. Rev. A* 15 (1977) 2339.
- [6] C.M. Kao and R.P. Messmer, *Phys. Rev. B* 31 (1985) 4835.
- [7] H.J. Freund, R.P. Messmer, C.M. Kao and E.W. Plummer, *Phys. Rev. B* 31 (1985) 4848.
- [8] R.L. Dubs, M.E. Smith and V. McKoy, *Phys. Rev. B*, submitted for publication.
- [9] T.H. Dunning Jr. and P.J. Hay, in: *Modern theoretical chemistry*, Vol. 3, ed. H.F. Schaefer III (Plenum Press, New York, 1977) p. 1.
- [10] T. Smedly and W.A. Goddard III, unpublished work.
- [11] K. Hermann, P.S. Bagus, C.R. Brundle and D. Menzel, *Phys. Rev. B* 24 (1981) 7025.
- [12] M.E. Smith, D.L. Lynch and V. McKoy, *J. Chem. Phys.* 85 (1986) 6455; D.L. Lynch, unpublished work.
- [13] R.R. Luchese, G. Raseev and V. McKoy, *Phys. Rev. A* 25 (1982) 2572.
- [14] J.L. Dehmer, in: *Resonances in electron-molecule scattering, van der Waals complexes, and reactive chemical dynamics*, ed. D.S. Truhlar (Am. Chem. Soc., Washington, 1984) p. 139.
- [15] J.A. Stephens and D. Dill, *Phys. Rev. A* 31 (1985) 1968.
- [16] B. Basden and R.R. Luchese, *Phys. Rev. A* 34 (1986) 5158.
- [17] S.H. Southwork, A.C. Parr, J.E. Hardis and J.L. Dehmer, *Phys. Rev. A* 33 (1986) 1020.
- [18] E.D. Poliakoff, M.-H. Ho, G.E. Leroi and M.G. White, *J. Chem. Phys.* 84 (1986) 4779.